INNOVATIVE SENSING WITH TAPERED U-SHAPED PLASTIC OPTICAL FIBERS: APPLICATIONS IN HUMIDITY AND FORMALDEHYDE DETECTION

SITI HALMA BINTI JOHARI

FACULTY OF ENGINEERING
UNIVERSITI MALAYA
KUALA LUMPUR

2024

INNOVATIVE SENSING WITH TAPERED U-SHAPED PLASTIC OPTICAL FIBERS: APPLICATIONS IN HUMIDITY AND FORMALDEHYDE DETECTION

SITI HALMA BINTI JOHARI

THESIS SUBMITTED IN FULFILMENT OF THE REQUIREMENTS FOR THE DEGREE OF DOCTOR OF PHILOSOPHY

FACULTY OF ENGINEERING
UNIVERSITI MALAYA
KUALA LUMPUR

2024

UNIVERSITI MALAYA

ORIGINAL LITERARY WORK DECLARATION

Name of Candidate: Siti Halma Binti Johari

Matric No: KVA180028/17055725/2

Name of Degree: Doctor of Philosophy

Title of Thesis: Innovative Sensing with Tapered U-Shaped Plastic Optical Fibers: Applications in Humidity and Formaldehyde Detection

Field of Study: Photonic (NEC 523: Electronics and Automation)

I do solemnly and sincerely declare that:

(1) I am the sole author/writer of this Work;
(2) This Work is original;
(3) Any use of any work in which copyright exists was done by way of fair dealing and for permitted purposes and any excerpt or extract from, or reference to or reproduction of any copyright work has been disclosed expressly and sufficiently and the title of the Work and its authorship have been acknowledged in this Work;
(4) I do not have any actual knowledge nor do I ought reasonably to know that the making of this work constitutes an infringement of any copyright work;
(5) I hereby assign all and every rights in the copyright to this Work to the Universiti Malaya ("UM"), who henceforth shall be owner of the copyright in this Work and that any reproduction or use in any form or by any means whatsoever is prohibited without the written consent of UM having been first had and obtained;
(6) I am fully aware that if in the course of making this Work I have infringed any copyright whether intentionally or otherwise, I may be subject to legal action or any other action as may be determined by UM.

Candidate's Signature Date: 14 NOVEMBER 2024

Subscribed and solemnly declared before,

Witness's Signature Date: 22 NOVEMBER 2024

Name:

Designation:

INNOVATIVE SENSING WITH TAPERED U-SHAPED PLASTIC OPTICAL FIBERS: APPLICATIONS IN HUMIDITY AND FORMALDEHYDE DETECTION

ABSTRACT

Precise humidity measurements are vital for many applications including food, agriculture, and electronic industries. Continuous exposure to formaldehyde may also cause injury to the central nervous, respiratory, blood and immunological systems. This thesis aims to develop a portable and workable sensing device by generating evanescent waves (EW) on a tapered U-shape plastic optical fiber (POF) coated with Zinc oxide (ZnO) nanorods and Hydroxyethyl cellulose / polyvinylidene fluoride (HEC/PVDF) for relative humidity (%RH) and formaldehyde vapor concentration sensing. The tapered POF was prepared using chemical and mechanical etching techniques. The %RH sensor was successfully developed and optimized using a tapered U-shaped POF coated with ZnO nanorods and HEC/PVDF as a sensing probe. With ZnO nanorods coating, the sensor performance was greatly improved as compared to the uncoated POF. Zinc oxide nanorods were synthesized using the hydrothermal method and grown for 12 hours on the tapered POF. For three source wavelengths of 470 nm, 530 nm and 645 nm, the output voltage of the sensor was found to be inversely proportional to %RH in the range of 35% to 90% RH. The proposed sensor produced the best sensitivity of 0.0231 V/%RH at 645 nm, with a slope linearity of 99.47% and fastest response and recovery times of 61 seconds and 68 seconds respectively. On the other hand, the HEC/PVDF based humidity sensor exhibited the highest sensitivity of 0.0733 V/%RH, with the smallest standard deviation of 0.0034 V when the LED's wavelength of 645 nm was used. The tapered U-shape POF coated with zinc oxide nanorods was also successfully evaluated at a wavelength of 645 nm for formaldehyde vapor sensing within a concentration range from

5% to 20%. The output voltage of 0.0958 V was observed, with the reduction of formaldehyde concentration from 20% to 0%. This was due to the more scattering effect of ZnO nanorods at 20% of formaldehyde concentration. The sensor response demonstrated an excellent linearity of 98.58% across all vapor concentrations. The sensitivity was measured to be -0.00543 V/%. This study showed that the proposed sensors were simple to fabricate, with the advantages of small size and good repeatability all of which are useful for %RH and formaldehyde sensing applications. The proposed sensor also has the potential to be used to detect air pollution produced, not just by formaldehyde vapor, but also by other dangerous or poisonous vapors or gases.

Keywords: Plastic optical fiber, taper, Zinc Oxide, Hydroxyethyl cellulose, Polyvinylidene fluoride, relative humidity sensor

PENDERIAAN INOVATIF DENGAN GENTIAN OPTIK PLASTIK TIRUS BERBENTUK U: APLIKASI DALAM KELEMBAPAN DAN FORMALDEHID

ABSTRAK

Pengukuran kelembapan yang jitu adalah penting untuk kebanyakan aplikasi seperti pemakanan, pertanian dan industri elektronik. Pendedahan kepada formaldehid secara berterusan juga menyebabkan kecederaan pada sistem saraf, penafasan, darah, dan sistem imunologi. Tesis ini bertujuan membangun peranti penderia boleh alih yang menghasilkan gelombang evanesen pada gentian optik plastik (POF) tirus berbentuk U yang disalut nanorods zink oksida (ZnO) dan Hydroxyethyl cellulose / polyvinylidene fluoride (HEC/PVDF) untuk mengesan kelembapan relative (%RH) dan konsentrasi wap formaldehid. POF tirus dibangun menggunakan teknik mekanikal dan punaran kimia. Penderia %RH telah berjaya dibangun dan optimumkan menggunakan POF tirus berbentuk U bersalut ZnO dan HEC/PVDF sebagai alat penderia. Penderia yang bersalut ZnO menunjuk prestasi lebih baik berbanding POF tirus tanpa salutan. Kaedah hidroterma sintesis selama 12 jam digunakan untuk pertumbuhan ZnO pada POF tirus. Voltan keluaran penderia berkadar songsang terhadap %RH antara 35% hingga 90%RH bagi tiga sumber panjang gelombang iaitu 470 nm, 530 nm dan 645 nm. Penderia yang dicadang ini telah menghasilkan sensitiviti terbaik iaitu 0.0231 V/%RH pada panjang gelombang 645 nm dengan kelinearan 99.47% serta masa tindak balas dan masa pemulihan terpantas iaitu masing-masing 61 s dan 68 s. Selain itu, pada panjang gelombang 645 nm, penderia kelembapan bagi HEC/PVDF mempamerkan sensitiviti tertinggi iaitu 0.0733 V/%RH dengan sisihan piawai terendah iaitu 0.0034 V. POF tirus berbentuk U yang bersalut ZnO juga berjaya diukur pada panjang gelombang 645 nm untuk mengesan kepekatan wap formaldehid antara 5% hingga 20%. Pengurangan voltan keluaran adalah sebanyak 0.0958 V kepada pengurangan kepekatan formaldehid antara 20% to 0%. Ini kerana terdapat banyak kesan pergerakan cahaya oleh nanorod ZnO ketika

kepekatan formaldehid pada 20%. Kelinearan yang cemerlang iaitu 98.58% dipamerkan pada setiap kepekatan wap formaldehid. Sensitiviti penderia yang diukur adalah -0.00543 V/%. Cadangan penderia dalam kajian ini menunjukkan ia mudah bentuk dengan kelebihannya yang bersaiz kecil dan kebolehulangan yang baik, di mana ia berguna untuk mengesan %RH dan formaldehid. Cadangan penderia ini juga sesuai untuk mengesan pencemaran udara dan bukan sekadar wap formaldehid, tetapi juga wap dan gas yang berbahaya dan beracun.

Keywords: Gentian optik plastik, tirus, Zink Oksida, Hydroxyethyl cellulose, Polyvinylidene fluoride, pengesan kelembapan relatif

ACKNOWLEDGEMENTS

I would like to express my gratitude to Allah for giving me the strength, fortitude, and health to accomplish this research thesis. Without the grace and blessing of HIM, this thesis would have been impossible to complete. I would like to express my special appreciation to my supervisor, Prof. Ir. Dr. Sulaiman Wadi Harun, for his great supervision and support. His vast knowledge in the field and his continuous guidance gave me inspiration and confidence throughout my research journey. I am also indebted to my co-supervisor, Dr. Hazli Rafis Abdul Rahim, for his invaluable ideas and motivation in strategizing my research work. His expertise was instrumental in facilitating my research work when facing any difficulty.

I also owe my gratitude to all members of the University of Malaya photonics laboratory for their brilliant ideas, real support, and sincere help all of which made the research atmosphere less stressful and pleasurable to work in. A special thanks to my optical sensor lab mates for providing constructive feedback on my work, and supporting me in better understanding and expanding my ideas.

Above all, I would like to express my heart-felt gratitude to my family members, especially my beloved parents, Johari Sahid and Sufiah Saad, for their encouragement and prayers all the way through this journey. Not to forget, my dearest husband, Muhamat Nosrul Omar, for the love and sacrifice during this tough journey. Also, thanks to my son, Muhammad Nasr Mateen, for being understanding of my work.

Last but not least, I would like to thank Universiti Teknikal Malaysia Melaka (UTeM) and the Ministry of Higher Education Malaysia (MOHE) for providing financial aid for my PhD program under SLAB/SLAI scholarship.

TABLE OF CONTENTS

LIST OF FIGURES

LIST OF TABLES

LIST OF SYMBOLS AND ABBREVIATIONS

SYMBOLS

N	:	Refractive index
n_1	:	Refractive index of medium 1
n_2	:	Refractive index of medium 2
no	:	Outer environment
θ_i	:	Incident angle
θ_2	:	Refractive angle
θ_a	:	Acceptance angle
θ_c	:	Critical angle
λ	:	Wavelength
R	:	Radius
η_{EF}	:	Fraction of power
C	:	Speed of light in vacuum
^oC	:	Degree celsius
V	:	Speed of light inside the material
V	:	V-number
d_p	:	Penetration depth
C	:	Concentration of the formaldehyde vapor
V_o	:	Output voltage
M	:	Molecular weight
Ps	:	Saturated pressure
Pv	:	Partial pressure
V	:	Volume of the chamber
γH	:	Hysteresis

ABBREVIATIONS

CYTOP	:	Amorphous Fluorinated Polymer
EDX	:	Energy Dispersive X-ray
EMI	:	Electromagnetic Interference
EW	:	Evanescent wave
FESEM	:	Field Emission Scanning Electron
GO	:	Graphene Oxide
HEC	:	Hydroxyethyl Cellulose
IMZI	:	Inline Mach-Zehnder Interferometer
LED	:	Light-Emitting Diode
MMF	:	Multimode Fiber
MR	:	Maximum Repeatability
NA	:	Numerical Aperture
PC	:	Polycarbonate
PE	:	Polyethylene
PMMA	:	Polymethylmethacrylate
POF	:	Plastic Optical Fiber
PS	:	Polystyrene
PVA	:	Polyvinyl Alcohol
PVDF	:	Polyvinylidene Fluoride
RH	:	Relative Humidity
SMF	:	Single Mode Fiber
TIR	:	Total Internal Reflection
ZnO	:	Zinc Oxide

CHAPTER 1: INTRODUCTION

1.1 General Background

In recent years, as our society has become more technologically adept, the need for information in all aspects of everyday life has grown. Sensor device technology and its detection methods play a significant role in the data collection process (Venketeswaran et al., 2022). A sensor is a device that responds to a certain stimulus by generating a functional output in response to a change in certain intrinsic properties. Physical quantities such as certain chemical and biological substances, chemical vapors, temperature or pressure are examples of stimuli (Naresh & Lee, 2021). A sensor devices output signal, known as the measurand, normally takes the form of voltage, resistance, or other metric and fluctuates in response to changes in physical parameters. In general, sensors are grouped into six classes based on how they convert energy: optical, mechanical, thermal, magnetic, electronic and electrochemical sensors (Patel et al., 2020). Recent advances in optical fiber technology have increased research interest in optical sensors owing to the benefits of light over electrical devices (Paul et al., 2024). For information transport, optical systems typically require a smaller medium than magnetic or electronic systems.

This thesis reports the development of small-sized and portable optical fiber sensors based on evanescent wave (EW) interaction. The generation of the EW through the tapered fiber is physically modified using a chemical and mechanical etching technique. Then, the tapered plastic optical fibers (POFs) were coated with zinc oxide (ZnO) and hydroxyethyl cellulose/polyvinylidene fluoride (HEC/PVDF) material and bent into a U-shaped structure to enhance the generation of evanescent waves. An auxiliary performance of the proposed sensor is also reported in this thesis through a formaldehyde sensing application.

1.2 Problem Statement and Motivation

Optical fibers have been utilized over the years for various applications including telecommunication, fiber laser and sensors. To date, many research works have been committed to the development of various optical fiber sensors, and these works have expanded to examine many new applications; such as monitoring humidity, chemical compounds, gases, vapors, biological signals, etc. (Yumei Zhang et al., 2022; Zhao et al., 2020). Compared with conventional electrical sensors, optical fiber-based sensors are cheap and more suited to be employed in explosive or hazardous environments, or places where electromagnetic interference (EMI) immunity is required. They also offer the possibility of multiplexing many different sensors (strain, pressure, temperature, displacement, humidity and acceleration) into the same optical fiber, thus reducing the need for multiple cabling required in traditional electrical-based sensors (Venketeswaran et al., 2022).

A variation of fiber, namely tapered optical fibers, have also attracted considerable interest in recent years, as they exhibit several interesting properties (Syuhada et al., 2020). They have a large evanescent field that travels along the cladding, which can be manipulated for the particular sensing application. For instance, Syuhada et al. successfully used a tapered optical fiber incorporating graphene oxide (GO) and a polyvinyl alcohol (PVA) composite film for humidity sensing. The sensor operation relied on the modulation of transmitted light intensity, which was induced by variations of the refractive index (RI) of the sensitive material coating. In other work, a simple optical fiber relative humidity sensor was demonstrated using a dumbbell-shaped inline Mach-Zehnder interferometer (IMZI) as a probe (Asiah Lokman et al., 2015). The humidity sensor here was constructed by coating the tapered waist region of the IMZI with ZnO nanowires. The water absorbed from the ambience changes the RI of the coating materials, that subsequently converts the lossy fiber into a light guide. Humidity sensing

has also been demonstrated using a tapered optical fiber with agarose gel (Bariain et al., 2000).

Accurate humidity measurements are crucial for a variety of industrial sectors, such as food, agriculture, and electronics. However, depending on the level of sophistication required, commercially available humidity sensors can be inaccurate and irresponsive. They are susceptible to EMI and have a limited range of operation. Accurate humidity sensors for real-time measurement are needed for quality and safety control within these industries. However, previously developed fiber optic sensors are based on single mode fiber, with the light source used normally costly. Therefore, development of a low-cost humidity sensor with a low-cost optical probe and light source is very much required. In view of this, a new optical humidity sensor using POF is explored in this study. The POF has many advantages such as lower cost, ease of handling and immunity from EMI. On the other hand, there is also increasing interest in nanomaterials such as ZnO for sensing applications due to their huge advantages in electrical and optical properties. ZnO is an n-type oxide semiconductor material which is often applied in the development of humidity sensors due to its high thermal and chemical stability, low cost, large specific surface area and high electrical conductivity (H. A. Zain et al., 2020).

This research work is motivated by the growing attention in POF and nanomaterials, such as ZnO, for sensing applications. The extensive utilization of nanostructured ZnO in many fields, such as solar cells, sensors for gas, field emission devices, photovoltaic panels, and humidity devices, has garnered considerable interest. (Oprea et al., 2014). This is attributed to inherent advantages including abundant surface morphology, thermal stability, quality chemicals and superior electrical properties. All these features of ZnO are very useful for constructing an advanced sensing system with high sensitivity. A POF type sensor probe can be easily fabricated by coating a cladding layer on the plastic fiber

core. This thesis aims to demonstrate a tapered U-shape POF coated with a sensitive material for humidity and formaldehyde vapor sensing. In this work, ZnO nanorods are used as a sensitive material for both humidity and formaldehyde vapor sensing at room temperature. When exposed to humid air or formaldehyde vapor, the ZnO produces a POF structure change from leaky to guided. Then the light intensity passing through the sensor probe varies remarkably, depending on the relative humidity level or formaldehyde concentration. In addition to zinc oxide, HEC/PVDF is also deposited on the tapered U-shape POF for humidity sensing. The refractive index of the deposited HEC/PVDF coating changes when it swells after absorbing water molecules from the environment.

1.3 Hypothesis

1. ZnO nanorods and HEC/PVDF act as changeable refractive index materials which enhance the evanescent field between POF and sensitive material.
2. Voltage difference of the U-shaped tapered POF coated with ZnO nanorods is higher than the HEC/PVDF coated.
3. The proposed structure shows a linear output power decay with higher sensitivity result for ZnO coating.
4. A tapered U-shape POF is a simple and workable structure for sensing applications.

1.4 Objectives of the Study

The main goal of the study is to develop a portable and workable sensing device by generating the evanescent wave on the tapered U-shape POF coated with ZnO nanorods and HEC/PVDF. To achieve this, the following objectives have been outlined:

1. To fabricate a tapered U-shape POF coated with ZnO nanorods (or HEC/PVDF) for humidity and formaldehyde vapor concentration sensing.
2. To optically characterize and optimize the sensing performance by controlling the POF waist with different LED wavelengths regarding humidity and formaldehyde vapor concentrations sensing.
3. To evaluate the RH sensor using a tapered U-shape POF coated with ZnO nanorods
4. To evaluate the formaldehyde vapor concentration sensor using a tapered U-shape POF coated with ZnO nanorods.

1.5 Organization of the Study

This thesis comprises six chapters providing an experimental study on a tapered U-shape POF for sensing applications. The current chapter briefly introduces the background, problem statement, motivation, hypothesis and objectives of this study. **Chapter 2** presents a literature review pertaining to research works comprising of basic theories of the optical fiber technology and its types, POF structures and its properties as well as various explanations of the fabrication techniques. This chapter also presents comprehensive information on the ideas of evanescence and the propagation of light in the POF. It also elaborates about the ZnO nanostructures, hydrothermal synthesis method, global applications of the ZnO, HEC/PVDF, sol-gel immersion method and applications of the HEC/PVDF. At the end of this chapter, recent works on humidity and formaldehyde sensors will be reviewed.

Chapter 3 explains the details of the fabrication process of the tapered POF using chemical and mechanical etching techniques, and the preparation of the ZnO coating. ZnO nanorods were synthesized using hydrothermal methods and then coated onto a tapered POF before bending it to form a U-shape for sensing applications. The preparation of HEC/PVDF coated onto a tapered U-shape POF is also described in this chapter.

Chapter 4 demonstrates a RH sensor using a prepared tapered U-shape POF coated with zinc oxide nanorods as a probe. The ZnO nanorods were synthesized using hydrothermal methods, and then coated onto the tapered POF. The proposed sensor is exposed to humidity concentration levels ranging from 35 %RH to 90 %RH in order to analyze the sensor performances. This chapter also describes and investigates the humidity sensing performance with the tapered U-shape POF coated with HEC/PVDF.

Chapter 5 describes the application of a tapered U-shape POF coated with ZnO nanorods for formaldehyde vapor sensing. The sensor performance is evaluated using an LED wavelength of 645 nm for formaldehyde vapor sensing, within a concentration range from 5% to 20%. Finally, **chapter 6** concludes the outcome of this research work, and provides some recommendations for future works of the proposed sensor.

1.6 Limitations of the Study

Given the predominant focus of this study on the tapered POFs, it is imperative to exercise caution when handling these fibers. The occurrence of breaking during fiber preparation might be attributed to the fragility of the narrow-tapered waist diameter in fibers when the chemical and mechanical etching technique is applied. This is because it uses acetone, a liquid solvent that can dissolve plastic, and also involved is uncontrolled physical pressure through sandpaper to get the desired fiber waist diameter. Thus, the taper transition areas of the fiber are expected to have small differences. However, the

utilization of the fiber waist area to a certain extent could make the tapered U-shaped POF enhance its sensitivity to variations in refractive index and its interactions with the external environment across various wavelengths. Due to the thermal limitations of POF (< 100 ˚C), it is essential to consider the impact of temperature on the physical properties of the fiber during the synthesis process and in sensing applications.

CHAPTER 2: LITERATURE REVIEW

2.1 Introduction

It is now over 50 years since the thought that optical fibers could be applied for measurement and sensing first emerged (Culshaw & Kersey, 2008). Early works on optical fiber sensors were based on bifurcated fiber bundles, which consisted of transmitting and receiving fibers. The transmitting fiber was used to illuminate a surface while the receiving fiber was used to capture the reflection light from this surface (Yasin et al., 2020). After suitable calibration, the received signal can give a very precise indication of the relative position of the end and the reflecting surface. Optical fiber sensors continued to be researched, since they were offering excellent performance especially in non-contact sensing applications (Ballato & Gibson, 2021). Up to date various approaches have been proposed and developed to measure various measurands; including medical (Griffiths & Robinson, 1999; Udd et al., 1994), natural structures (Udd et al., 1994), chemical (Stewart et al., 1997) and biological species (Ferguson et al., 1996; Healey et al., 1997; Wolfbeis, 2004), environmental conditions (Jiang et al., 2013; Zepp et al., 1987) and many other physical parameters (Udd & Spillman Jr, 2011).

Optical fiber based sensors have obtained significant attention in recent years; since they offer many advantages over other sensing technologies which include immunity to EMI, compactness, lightweight, multiplexing capability, high sensitivity, etc. (Azman, 2022). Laser light is commonly used for optical sensing, and it incurs a relatively high cost posing several problems such as fluctuations, non-representation and low intensity. Therefore, this method has typically been improved using visible light. Researchers have recently integrated nanotechnology with optical technology to upgrade the sensor performance to be fast, inexpensive, highly sensitive and have a wide range of sensing.

This chapter provides a comprehensive literature review of optical fiber sensors. First, the optical fiber, plastic optical fiber and tapered optical fibers are introduced. Then, the chapter discusses optical fiber sensors including the ZnO nanostructures and HEC/PVDF materials, which are widely used as a coating material especially for humidity sensing. The importance of humidity and formaldehyde are also discussed in this chapter.

2.2 Optical Fibers

Generally, optical fiber is a long, flexible, cylindrical waveguide which can transport light in either the visible or infrared regions of the electromagnetic spectrum, depending on the core material. The two most important components of optical fibers are the core and the cladding. A plastic or buffer coating is also applied around the cladding structure to protect the fiber from breaking and improve its robustness. Several bare fibers are placed together in one cable, protected by an outside covering (called the jacket) for optical communication applications. Figure 2.1 shows the parts of an optical fiber, including the jacket.

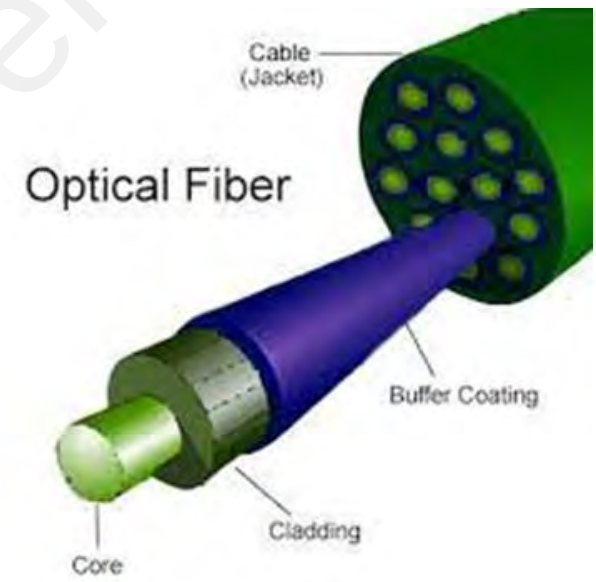

Figure 2.1: The parts of optical fiber (Memon et al., 2017)

It is well recognized that there must be a variation in the RI sandwiched between the core and cladding material in order to guide optical waves. The core, which is the axial part of the optical fiber, is the area of the fiber where the light is transmitted. Doping elements are used to modify the fiber refractive index, thereby changing the light velocity through the fiber. The cladding, on the other hand, is the layer that surrounds the core completely. The cladding refractive index must of course be less than the core to enable light inside the core to strike the core-cladding interface at a bouncing angle, hence confining it inside the core by total internal reflection (TIR) (Amiri et al., 2018; Prabu & Malavika, 2019). Figure 2.2 shows that any light travelling at an incident angle (θi) larger than the critical angle (θc) will be fully reflected internally into the medium from which it originated. This TIR concept can also be applied in any other waveguide medium, such as plastic optical fiber.

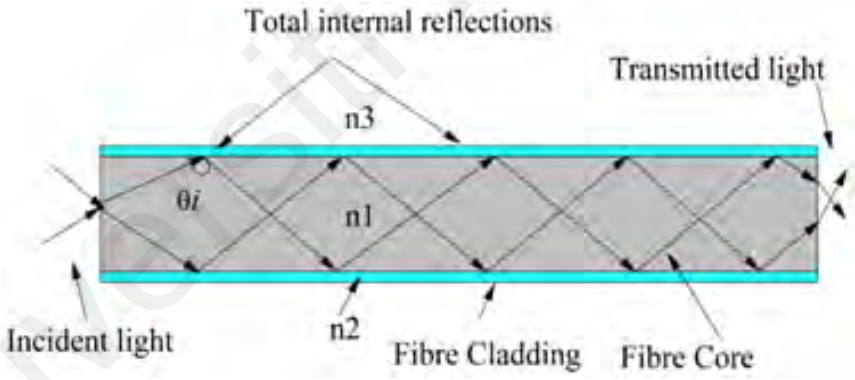

Figure 2.2:Total internal reflection phenomenon (Memon et al., 2017)

Optical fibers may be classified into two main categories: single mode and multimode, as seen in Figure 2.3. Multimode fibers (MMF) possess a core that is bigger in size compared to single mode fibers (SMF), allowing the transmission of several modes of light. The increased core diameter of MMFs enables the use of more affordable optical transmitters, such as light-emitting diodes (LEDs) and connections.

SMFs, on the other hand, have a much smaller diameter than MMFs and allow only a single mode (called the fundamental mode) to pass through them. SMFs are designed to maintain the spatial and spectral integrity of each optical signal over longer distances and allow more data to be transmitted. Alternately, SMFs are made to keep the integrity of optical signals over longer distances causing distortion. This makes it possible to send more data. Due to the capability to send high data rates with low intrinsic losses, SMFs are the best way to send data for numerous uses (Jeunhomme, 1983).

SMFs are often used for transmitting data over long distances and for applications requiring high bandwidth. MMF primarily applies to shorter transmission lengths, often not greater than 2 km. It is commonly employed for private data networks, on-site communications, and parallel-optic applications.

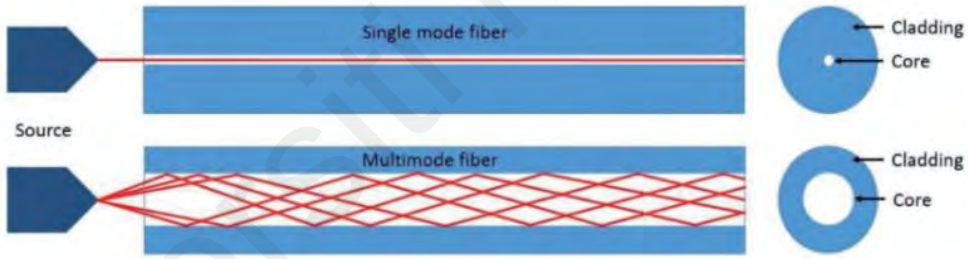

Figure 2.3: Multimode vs single mode fiber (Imani & Cuellar, 2020)

Optical fiber typically consists of three major components; a central core of refractive index n_1, a cladding with refractive index n_2 $(n_2 < n_1)$ and a buffer coating, as shown in Figure 2.4. The buffer maintains the mechanical robustness of the fiber, thereby reducing bending effects (Chin et al., 2010). When light is transmitted at the entry of the core, there is a portion of light from the beam reflected into the surrounding medium, with the other portion propagated into the fiber according to Snell's law. Light propagation uses the basic

concepts of transmission, reflection, and refraction. Equation (2.1) shows the relationship between the incident angle and the refractive angle between the two mediums.

$$n_1 sin\theta_1 = n_2 sin\theta_2 \tag{2.1}$$

The light propagation inside the core of an optical fiber is based on the TIR. The presence of TIR is crucial for the propagation of light inside the central region of an optical fiber. It requires the incident angle at the core/cladding boundary to be greater than a critical value θ_c with the condition that $n_2 < n_1$. If θ_2 is set at 90°, the previous equation can be used to obtain the critical angle (θ_c) as follows:

$$\sin(\theta_c) = \frac{n_2}{n_1} \tag{2.2}$$

As shown in Figure 2.4, incident light at angles of less than θ_c are refracted from the core into the cladding, and thus propagate out from the fiber.

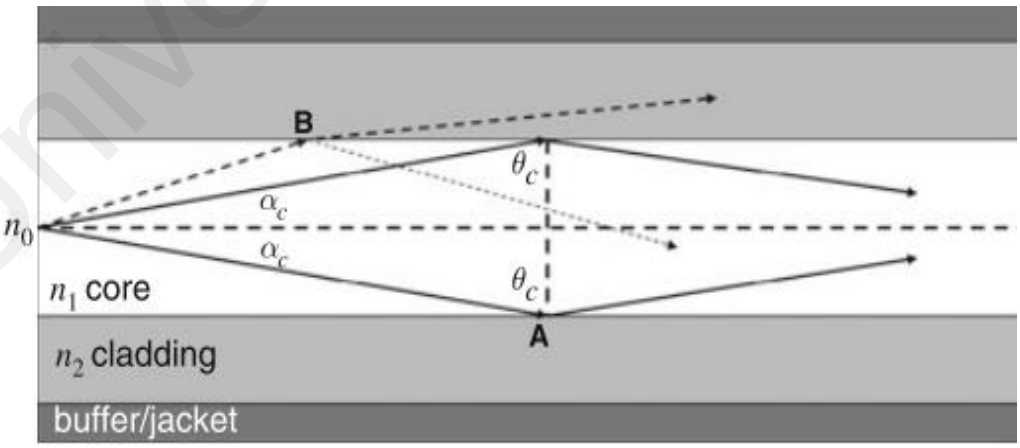

Figure 2.4: Light propagation inside optical fiber structures, which comprises of core, cladding and buffer/jacket (Chin et al., 2010)

The maximum incident angle that allows the light ray entering the fiber and propagating in the core is defined as the acceptance angle (θ_a). It is commonly related to a numerical aperture (NA) which is given by:

$$NA = \sin\theta_a = \sqrt{n_1^2 - n_2^2} \tag{2.3}$$

Based on the above equation, *NA* can be represented in terms of refractive index of core (n_1) and cladding (n_2). However, the value also relies on the refractive index of the outer environment (n_o), which is air ($n = 1$) (Chin et al., 2010). A fiber with a higher value of *NA* enables a larger incident light to enter the fiber. Incoming light with a smaller incident angle would travel closer to the central axis of the fiber (low order modes), while a larger incident angle would travel at longer path-lengths (higher order modes). Due to the longer distance travelled at higher order modes, greater transmission losses could be observed for MMFs as compared to SMFs.

2.3 Plastic Optical Fiber

Plastic or polymer optical fiber (POF) is a type of optical fiber made from plastic materials rather than the traditional silica glass. It has the same construction as silica optical fibers with a core, cladding and sometimes a jacket. POF is typically made from polymethylmethacrylate (PMMA) or other plastic materials with suitable optical properties such as amorphous fluorinated polymer (CYTOP), polystyrene (PS) and polycarbonate (PC) (Domingues & Radwan, 2017). The plastic cladding has a refractive index lower than the core. POF generally has a larger core diameter compared to glass optical fibers. The core size of POF is typically ranges from 0.5 mm to 1 mm, making it easier to handle and connect. In some cases, the core diameter is 100 times larger than the conventional silica fiber. POF has a relatively high numerical aperture, which means it

can accept light at greater angles compared to silica optical fibers. This property allows for easier coupling of light sources and connectors. However, it typically has higher attenuation (signal loss) compared to glass optical fibers. Figure 2.5 shows a structure of a plastic optical fiber is a step-index multimode POF (Mitsubishi Rayon GH-4001). This fiber has an outer diameter of 1.0 mm, and a cladding thickness of 0.01 mm. The refractive indices of the core and the cladding are 1.490 and 1.402, respectively, and the numerical aperture (NA) is about 0.504. The materials of the core and the cladding are poly (methyl methacrylate) (PMMA) and fluorinated polymer, respectively, and the jacket is made of polyethylene (PE) (Yoo et al., 2011).

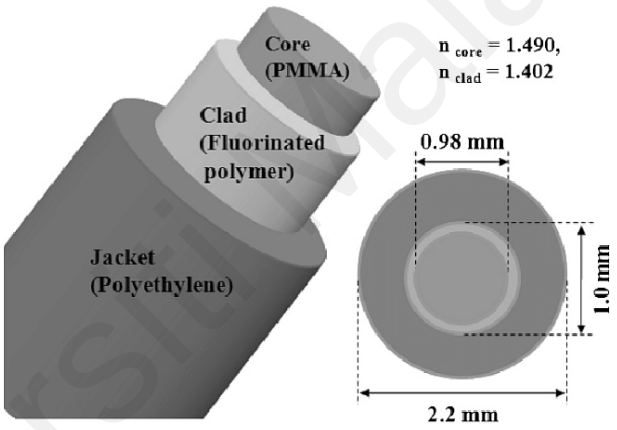

Figure 2.5: A typical structure of a POF (Yoo et al., 2011)

The major advantage of POFs relies on their robustness and flexibility, in terms of ductile behavior, and their high elastic strain limits (Soge et al., 2021). For example, PMMA has an elastic limit of around 10%, as compared to 1–3% for silica. The lesser known advantages of POFs are their increased sensitivity to strain (strain-optic coefficient) and their potential negative thermo-optic coefficient. Compared to silica fibers, they can bend more without affecting signal transmission, making them suitable for applications where flexibility is important. POFs are primarily used for short-range data communication and illumination purposes. They are also preferable for use in

industrial environments where resistance to EMI is crucial. They can be used for factory automation, control systems, and sensor networks. In short, POF serves as a cost-effective and efficient solution for short-range optical communication and sensing applications, especially in environments where the flexibility and easy installation of plastic fibers are advantageous (Ghaffar et al., 2021).

2.4 Tapered Optical Fiber

A simple method for the preparation of an optical fiber probe for sensing applications is based on tapering the fiber. This provides capture of the evanescent wave (EW) of the mode travelling through the tapered location where it refers to the portion of light that travels through the fiber but extends slightly beyond the core into the cladding, thus allowing communication with the surrounding medium enabling the determination of measurands such as humidity and refractive index. A tapered optical fiber is an optical fiber which has been deliberately tapered down to a smaller diameter along a certain section of its length. This tapering down process alters the geometry of the fiber, causing it to transition gradually from a large to a smaller diameter, as shown in Figure 2.6.

Figure 2.6: A schematic diagram of a tapered optical fiber (D. Wang et al., 2021).

The tapered fiber waveguide optical characteristics are affected by the contours of the conical tapering sections, the tapered waist diameter and by the refractive index of the adjacent medium (Korposh et al., 2019). The amount of power in the EW, and therefore

in the interaction with the surrounding medium, increases as the fiber becomes thinner and also with decreasing difference between the refractive index of the fiber and its surroundings (Harun et al., 2013). This is because when the cladding is removed, the evanescent wave enters the surrounding area and is strong enough to excite molecules near the core. Subsequently, the ratio of power in the EW mode to the power in the core increases, and the penetration depth is determined by the surrounding refractive index. Equation (2.4) presents the penetration depth formulation (Ahmad & Hench, 2005).

$$d_p = \frac{\lambda}{2\pi\sqrt{(n^2{}_{core} sin^2\theta_i - n^2{}_{clad})}} \tag{2.4}$$

Initially, these tapered fibers were used in the advancement of directional couplers, where more than two tapers were joined together, so as to allow effective light coupling between fibers (Bilodeau et al., 1988). Tapered optical fibers typically are very useful for sensor development including compactness, flexibility and large evanescent fields. They exhibit unique properties, mainly due to their geometry. The lowered diameter of the tapered section increases the intensity of the evanescent field, thus allowing for strong interactions with surrounding media or coatings. Tapered fibers can also couple light between different modes of the fiber to enable mode conversion and manipulation. These properties give rise to many applications in different fields including evanescent wave sensing. In this application, tapered fibers are used to detect changes in refractive index at the fiber surface, which is useful in bio and chemical sensing. Regarding the tapered optical fiber coated with a interactive material, the waveguide characteristics are influenced by the optical width (which is a product of refractive index and the geometrical thickness) of the coating. The versatility of these types of fibers renders them valuable tools for a wide range of applications across photonics, sensing, telecommunications and other scientific/technological fields. The choice of taper profile, materials and fabrication

methods enables tailoring their properties to specific application requirements. The construction of the tapered optical fibers is commonly obtained by heating a short location of the fiber, whilst simultaneously stretching both fiber ends, as illustrated in Figure 2.7.

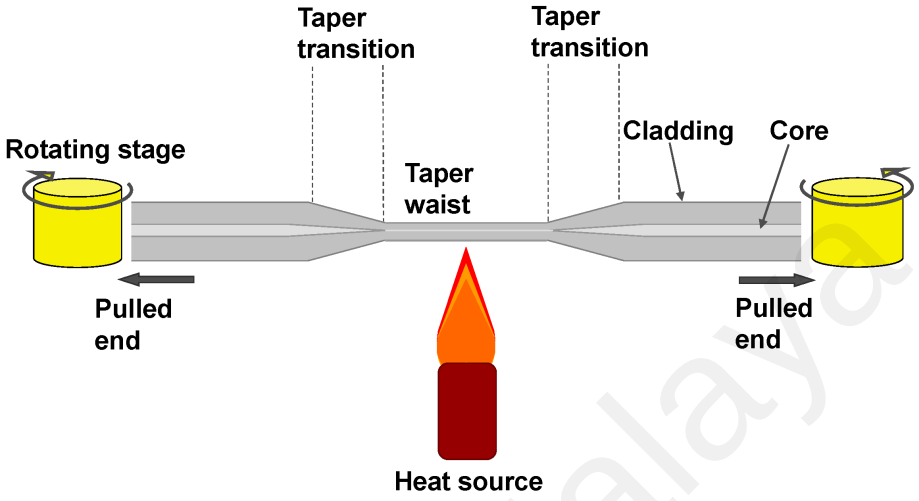

Figure 2.7: Fabrication of tapered optical fibers using a flame as a heat source (Korposh et al., 2019).

Commonly, a gas burner flame heat source is used, and/or an arc discharge or high-power laser radiation. For the SMF case, an important function of the cladding is to minimize the interference of the electric field of the propagating mode into the surrounding medium. During this tapering method, both the core and cladding widths are decreased by the same ratio. Light is then coupled from the fundamental mode of the un-tapered fiber to modes of the tapered section allowing it to interact with the surrounding medium. Another method to achieve the interface of the light propagating inside the fiber with the surrounding medium is to decrease the cladding diameter of the fiber, whilst maintaining the diameter of the core. This was done by a combination of polishing, chemical or focused ion beam etching (Korposh et al., 2019). The chemical etching is prepared by using acetone as an etchant solvent, and the mechanical etching technique is prepared mechanically by using sand paper and aluminum oxide polishing film (Mulyanti

et al., 2017). As opposed to the previous method, mode coupling between the fundamental and higher order modes is eliminated, since the refractive index of core is retained.

2.5 Recent Developments in Tapered Fibers Technology and Theoretical Models

Recent advancements in tapered fiber technology have significantly enhanced their application in optical sensing, with improvements in sensitivity, integration and real time monitoring capabilities. These advancements are driven by innovations in fabrication techniques and theoretical models that optimize the performance of tapered fibers in various sensing environments. The following sections detail these advancements and theoretical models.

Regarding fabrication techniques, recent methods involve the use of plasmonic microheaters and structural bending, which allow for the creation of ultra compact fiber tapers without the need for traditional flame-based techniques. This approach enables precise control over the tapering process, facilitating the production of micro-nano fibers with abrupt taper and ultra-short transition regions (Jia et al., 2023; Yang, 2023). For applications in sensing, tapered fibers are increasingly used in biosensing, environmental monitoring and industrial surveillance due to their high sensitivity and ease of integration. These fibers can detect changes in refractive index and other environmental parameters, making them versatile tools in various fields (Ban & Lian, 2024).

Regarding geometrical optics theory, the performance of taper fiber sensors is heavily influenced by the taper angle, length and radii. Theoretical models emphasize the importance of these parameters, showing that as the taper radius decreases, the taper ratio increases, therefore enhancing sensitivity. The penetration depth and sensitivity are also affected by the incidence angle and wavelength (Raghuwanshi et al., 2023). Furthermore, studies on material and geometric effects have shown that the shape and material used in

the taper significantly impacts on the formation of evanescent waves, which are crucial for sensing. Different taper structures, such as linear, concave and convex, have been analyzed using simulation software to optimize their detection potential (Adouane et al., 2023).

While advancements in tapered fiber technology have improved their application in sensing, challenges remain in optimizing the fabrication process and theoretical models to further enhance performance. The integration of new materials and geometries continues to be a promising area for future research, potentially leading to even more sensitive and versatile fiber sensors.

2.6 Optical Fiber Sensors

A sensor is widely developed to improve the healthcare system, to use in food, and water quality monitoring, and to assist the industry to manufacture standard products. The sensors market is still dominated by electronic sensors; however, they suffer from many limitations including susceptibility to EMI, limited sensing range, complex calibration and physical components that can degrade over time due to factors like mechanical stress, temperature variations and chemical exposure (Sabri et al., 2013). These limitations, along with the necessity for remote monitoring/sensing, have directed researcher attention towards utilizing optical fiber sensors.

Optical fiber sensors are cutting-edge devices which use photons as the signal carrier instead of the electron, thus making the device immune to EMI. These sensors also exploit the unique properties of light to enable accurate and efficient measurement of various physical and chemical parameters. They are built upon the principle of utilizing changes in light propagation within a specially designed optical fiber to detect and quantify changes in their surroundings. Light is injected into the core and guided through total

internal reflection, ensuring minimal signal loss over long distances. The key innovation lies in manipulating this guided light to interact with the external environment in a way that enables the sensor to respond to changes.

Various mechanisms are employed to make optical fiber sensors sensitive to specific parameters. One common type is the intensity-based sensor, where changes in the parameter being measured alter the intensity of the light transmitted through the fiber. These changes can be detected using photodetectors and analyzed to infer the parameter value. Another type is the phase-based sensor, where shifts in the phase of the light are used to measure the parameter of interest.

Optical fiber sensors offer several advantages over traditional sensing technologies. They are immune to EMI, making them suitable for use in environments with high levels of electromagnetic noise. Additionally, their small size, flexibility and ability to be remotely operated allow them to be easily integrated into complex systems and hard-to-reach areas. Their high sensitivity and fast response times further enhance their utility in real-time monitoring applications. Furthermore, they are resilient in harsh environments such as high humidity, high temperature, and dangerous atmospheres with high concentration of explosive and corrosive gases (nuclear plants, oil rigs, oil/gas pipeline), due to their robust materials and mechanical properties. In addition, optical fiber sensors can independently and simultaneously measure more than one parameter in real-time and continuously.

These sensors have a wide range of applications. In structural health monitoring, they can be embedded within materials to assess temperature, strain, and stress changes, facilitating in the early detection of potential failures. In healthcare, optical fiber sensors are used for minimally invasive procedures, such as monitoring vital signs and diagnosing conditions within the body. Environmental monitoring benefits from their ability to detect

pollutants, gases, and other hazardous substances in real time. As researchers continue to refine and expand their capabilities, optical fiber sensors are likely to contribute even more significantly to the advancement of various fields, pushing the boundaries of what is possible in measurement and monitoring.

2.7 Innovative Geometries in POF Sensors

An important aspect of POF technology is their geometry which improves both sensitivity and functionality. All this will have influence on how light travels inside the fiber, in most cases the EW coupling with the surroundings is enhanced. Investigations have been made employing various configurations especially straight, twisted, bent, and looped fibers to enhance their performance in various detections. These configurations utilize the physical properties of POFs to design sensors with better sensitivity and response time, hence facilitating their application in various fields. Straight structure incorporating a tapered POF coated with ZnO nanorods was examined, which was a relative humidity sensor. It utilized a tapering process to enhance the sensor's performance by increasing the evanescent wave interaction with the external medium. The sensor shows sensitivity of 0.295 %/mV and a linearity slope of 98.38%, with detection limit of 0.7133 % (Harith et al., 2020).

Humidity measurement at various locations has been made possible owing to the development of a twin point humidity sensor incorporating twisted and bent POFs. This configuration involves two twisted fibers, which are subsequently bent at precise radii in order to increase light coupling between the fibers. The sensor is found to respond linearly to variation of humidity from 30% to 80% within the humidity range (Hussian et al., 2024). Macro and micro bending when applied in conjunction with POFs yields a very high value of sensitivity. Removal of the outer coating and external circular macro and localized micro bends leads to the POF sensor becoming 10 times more sensitive than

configurations devoid of micro bends. This arrangement makes it possible to very satisfactorily determine changes in the humidity level by monitoring changes in the normalized power (Kuswanto et al., 2022). A loop-shaped POF that is tapered with zinc oxide nanorods are coated on it employs the evanescent wave in the detection of humidity. This configuration has a very robust sensitivity and repeatability performance, which is enhanced due to the increase interaction of fibers and the environment as a result of the coating and the loop (Hisam et al., 2022).

In this work, liquid level sensing through U-shaped fibers is presented and tested. The scattering optical losses are minimized by the bent U-shape to the fiberglass tube. This configuration takes advantage of the fact that the levels of the liquid change, and so do the levels of intensity of light directed through the fiber. Afterwards, the light is recorded and measured. U-bent constructions have been successfully employed with very high degree of sensitivity, and has been reported that sensitivity of 1.4 and 3.3 mV/mm is noted for varying liquid heights. Such sensitivity makes it possible to gauge the liquid levels in real time and in diverse environments including industrial processes and environmental monitoring systems (Waluyo et al., 2022). A newly designed U-shaped plastic optical fiber sensor with optimized polyimide and graphene oxide coatings exhibits better temperature independence in humidity sensing with a sensitivity of 0.17×10^{-2} %RH over a wide temperature range (Zhong et al., 2020). Additionally, the detection of the iron content in supplements has also been reported in the U-bent design. Here, the bending deformation of the fiber alters its refractive index, which in turn changes light transmission thereby enabling its use in applications with high chemical analysis requirements (Ashraf et al., 2022).

In another application, straight, decladded optical fibers with a carbon nanotube-doped chitosan coating provide a fast-response sensor best suited for breath and voice

monitoring. Its linear response within a dynamic range of ~70-97% RH and also its fast response times (100 ms) point out its potential in real-time respiratory applications (Mohan & Negi, 2024). Taken together, these studies put forward the transformative potential of advanced materials and innovative fiber designs in developing highly sensitive, stable, and versatile optical sensors. On a related note, research into sodium polyacrylate-derived photonic sensors has seen the creation of a weakly coupled flexible sensor for use in bionic skin. Through the strain amplification under a tapered fiber structure, this sensor has high sensitivity to humidity (0.19 dB/%RH) and temperature (0.29 dB/°C), making it especially apt for use within wearable health monitoring systems (Li et al., 2024).

To summarize, the bending of POFs is an improvement in their performance, which increases the scope of their applications. For example, in industry monitoring, environment protection and biomedical sensing.

2.8 Zinc Oxide Nanorods Structure

Zinc Oxide (ZnO) nanorods are a type of nanomaterial with a unique structure. They are used as important functional material due to its wide bandgap of 3.4 eV and large exciton binding energy (60 meV) at room temperature. They have strong pyroelectric and piezoelectric properties due to the large electromechanical coupling and non-existence of a center of symmetry in the ZnO wurtzite structure (Baruah & Dutta, 2009). The ZnO nanorods structure that can be described using the wurtzite structure model. The wurtzite structure is a common crystal structure that's frequently observed in various semiconductors, including ZnO.

Figure 2.8 shows the wurtzite crystalline structure of the ZnO nanorods, with lattice parameters a and c equal to 3.2495 Å and 5.2062 Å, respectively (Borysiewicz, 2019).

The lattice is described as two intertwined hexagonal closely packed Zn and O lattices, arranged in such a way that each Zn^{2+} ion is coordinated by four O^{2-} ions in a tetrahedral arrangement. Likewise, each O^{2-} ion is coordinated by four Zn^{2+} ions in the same way (Wang, 2004). These properties make it a suitable candidate for numerous applications such as converter, photocatalyst, hydrogen production and sensor (Kołodziejczak-Radzimska & Jesionowski, 2014). Additionally, it has found promising applications in field-effect transistors, solar cells, photodetectors and gas sensors (Kind et al., 2002). It also attracts considerable attention among other metal oxide semiconductors due to its versatile construction, wide range of shapes and surface chemistry (Hussain et al., 2014).

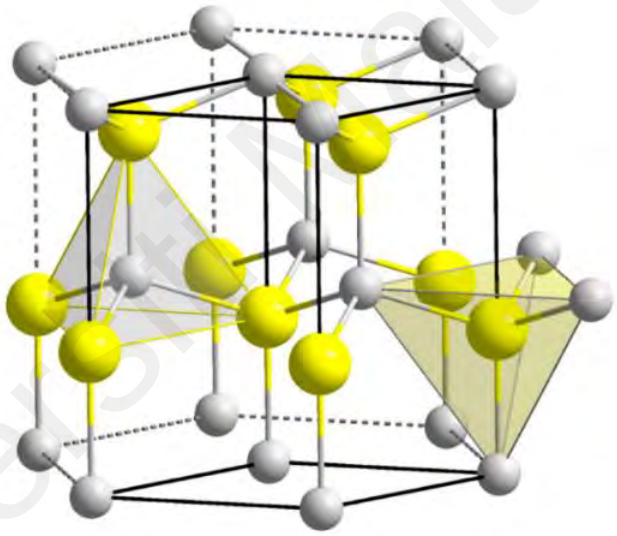

Figure 2.8: The wurtzite structure model of ZnO, Zn in yellow, O in grey, the tetrahedral coordination is shown for both types of atoms (Borysiewicz, 2019).

ZnO can be grown in several forms; including nanoflowers (Miles et al., 2015), snowflakes (Jing et al., 2012), nanowires (Shan et al., 2008) and nanorods (Dedova et al., 2007), as illustrated in Figure 2.9. ZnO nanorods are a type of one-dimensional nanostructure composed of ZnO material. Nanorods are elongated structures with diameters in the nanometre range, and their lengths are significantly larger than their diameters. ZnO nanorods have attracted significant attention, due to their unique properties and potential applications in various fields. They exhibit excellent

conductivity, due to their good electron mobility, which causes an effective separation of holes and electrons and decreases resistance (Zhu & Zeng, 2017). Chemical reactions between the adsorbed oxygen molecules and the surface creates a large number of adsorbed oxygen species which accelerate the sensing reaction (Navale et al., 2017).

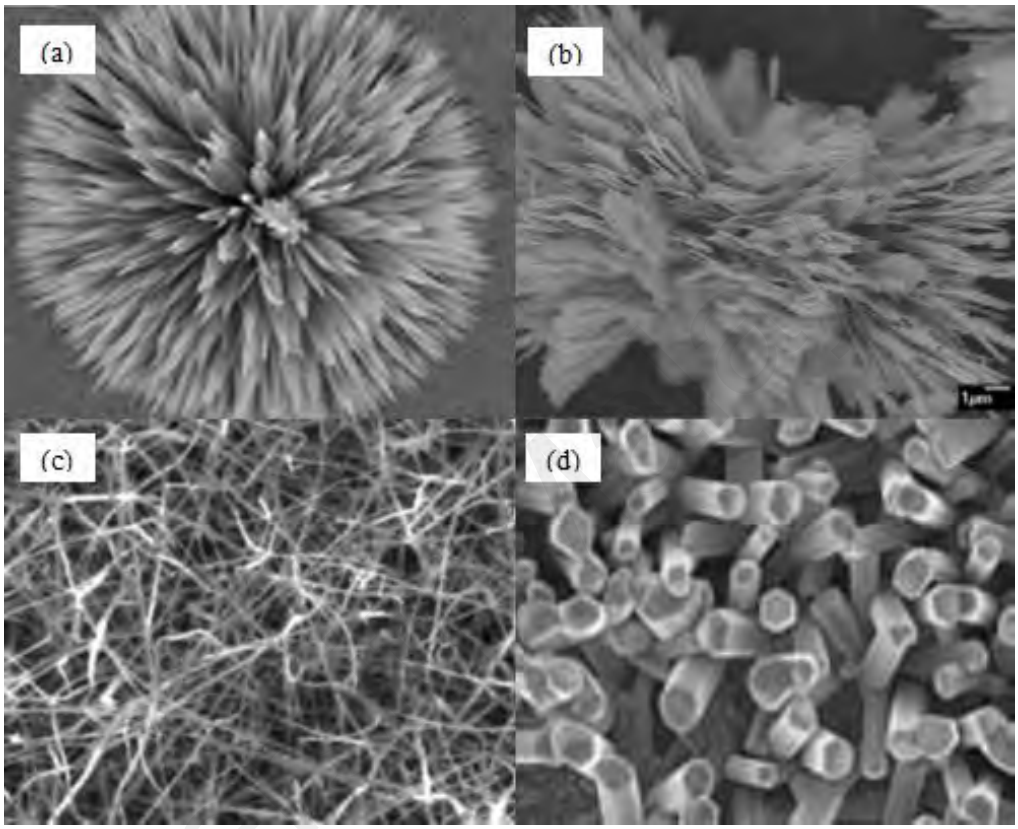

Figure 2.9: Examples of zinc oxide structure; (a) nanoflowers (Miles et al., 2015), (b) snowflakes (Jing et al., 2012), (c) nanowires (Shan et al., 2008) and (d) nanorods (Dedova et al., 2007)

ZnO nanorods possess several interesting properties which make them valuable for various technological applications across fields such as electronics, photonics, energy, sensing and biomedicine. They have a high surface-to-volume ratio, making them suitable for applications requiring surface interactions such as sensors and catalysts. ZnO is a wide-bandgap semiconductor with excellent optical properties. Nanorods can be used to fabricate light-emitting diodes (LEDs), photodetectors and laser devices. ZnO nanorods

can also catalyse chemical reactions under light illumination, making them useful for applications such as in pollutant degradation and water purification. ZnO nanorods can be incorporated into flexible and transparent electronic devices due to their unique structural and electronic properties. In addition, they can be integrated into nanoscale electronic devices due to their semiconducting properties. ZnO nanorods have many potentials for biomedical applications, and have been explored for drug delivery, bioimaging and antibacterial applications. Currently, researchers continue to explore novel synthesis techniques and applications to harness the potential of these nanomaterials.

2.8.1 Synthesis of Zinc Oxide Nanorods via Hydrothermal Method

ZnO nanorods can be synthesized using various methods; including chemical vapor deposition (CVD), electrodeposition and hydrothermal growth. In the CVD process, ZnO nanorods are grown by reacting to a zinc precursor with an oxygen source at high temperatures. Catalysts or templates may be used to control the growth direction. Electrochemical methods can be used to deposit the ZnO nanorods onto conductive substrates. Compared to the CVD process and electrodeposition, hydrothermal technique is a preferred method of synthesis due to its basic growth state. This method involves growing nanorods from a solution of zinc salts and a base at elevated temperatures and pressures. The growth is guided using seed crystals or specific substrates. Hydrothermal methods use alcohol as a substance to accelerate the nucleation and development compared with water. Also, it is an eco-friendly technique as it does not require any extra organic solvents or technique like calcination and grinding (Baruah et al., 2012).

Hydrothermal synthesis techniques exhibit several benefits such as simplicity, low temperatures (between 60 and 100 ^{o}C), larger output and a more manageable method. The crystal can be grown in various forms which rely on the configuration of the initial

mixture and the method pressure and temperature. It therefore provides a highly pure material with a large level of crystallinity (Polsongkram et al., 2008). This technique is grounded on solution phase synthesis, and carried out in aqueous solution under low growth temperatures below 100 ˚C. It is a preferable fusion process to gas phase synthesis due to its simplicity, low cost and tolerable growth conditions (Baruah & Dutta, 2009).

Figure 2.10 shows the various process steps followed for the synthesis of ZnO nanorods on an alloy substrate using a simple solution growth-assisted hydrothermal method (Gaddam et al., 2015). The cleaned alloy substrate is deposited with approximately a 100nm ZnO seed layer, via DC reactive magnetron sputtering, before the growth process. Here, an aqueous solution consisting of an equal amount of zinc nitrate hexahydrate (Zn $(NO_3)_2.6H_2O$) and hexamethylenetetramine (HMTA, $C_6H_{12}N_4$) at a concentration of 25 mM is prepared. The ZnO film coated substrate was placed over the surface of the solution (about 60 ml) in a screw reagent bottle. Subsequently, the ZnO coated substrates were maintained at growth temperature for 4 hours duration, by keeping the closed bottle inside a hot air oven. The growth process of the ZnO nanorods involves the following chemical reactions:

1. Decomposition reaction: $(CH_2)_6N_4 + 6H_2O \leftrightarrow 4NH_3 + 6HCHO$
2. Hydroxyl supply reaction: $NH_3 + H_2O \leftrightarrow NH_4^+ + OH^-$
3. Supersaturation reaction: $Zn^{2+} + 2OH \leftrightarrow Zn\ (OH)_2g$
4. ZnO nanorod growth reaction: $Zn(OH)_2 \leftrightarrow ZnO + H_2O$

Figure 2.10: Schematic diagram of the procedure for the synthesis of ZnO nanorods using hydrothermally method (Gaddam et al., 2015).

After the growth process, the formation of white colored nanostructured films was observed over the substrates. Figure 2.11 shows the FESEM images for the ZnO nanorods, which were grown using the hydrothermal method at different growth temperatures. This confirms that the orientation of the ZnO nanorods were relatively vertical to the substrate, while the average length and diameter of the ZnO nanorods increased with an increase in growth temperature. This indicates that the growth temperature has a major effect on the morphology in terms of the length and diameter of the nanorods.

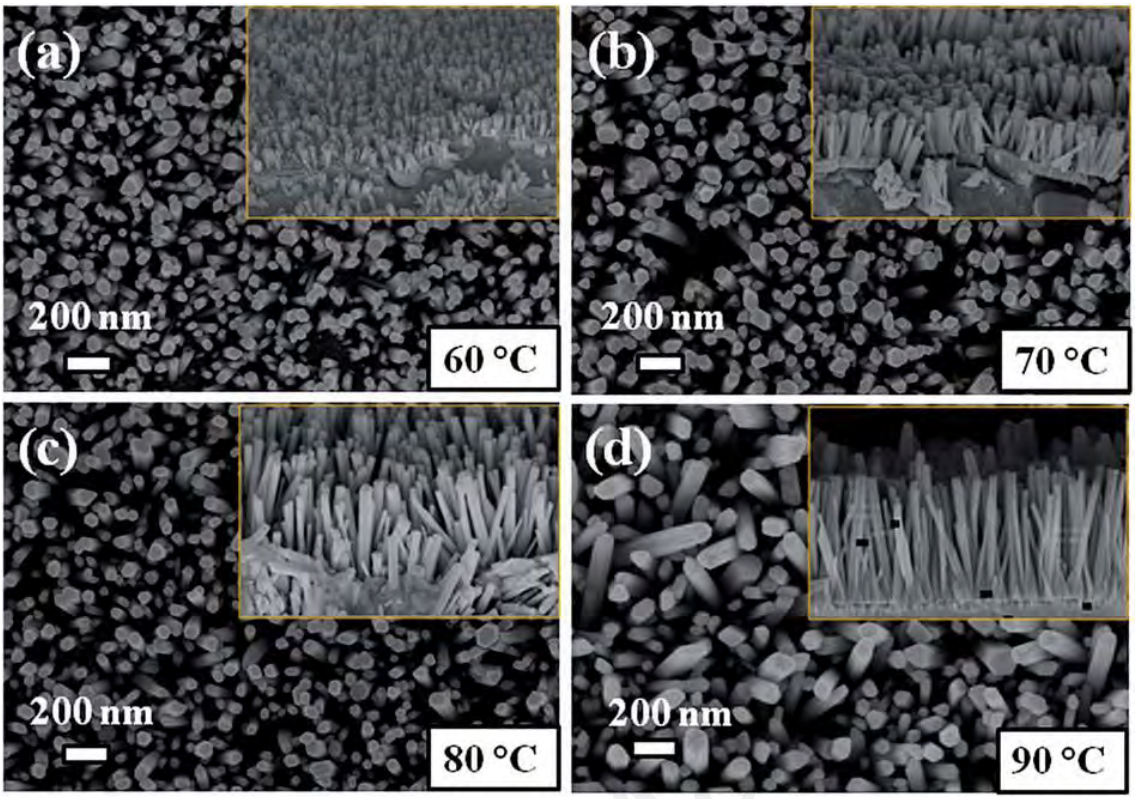

Figure 2.11: FESEM images for the ZnO nanorods, which were grown using the hydrothermal method at different growth temperatures of (a) 60 °C, (b) 70 °C, (c) 80 °C, and (d) 90 °C (Gaddam et al., 2015). The inset figures show the corresponding cross-sectional images.

2.9 Hydroxyethyl Cellulose / Polyvinylidene Fluoride (HEC/PVDF)

A HEC/PVDF composite is a material that combines two different polymers: hydroxyethyl cellulose (HEC) and polyvinylidene fluoride (PVDF). The structures of HEC and PVDF are shown in Figures 2.12 (a) and (b), respectively. Each of these polymers contributes its own set of properties to the composite, resulting in a combination of characteristics that can be tailored for specific applications including sensing. HEC is a water-soluble polymer derived from cellulose, which is a natural polymer found in plant cell walls. It is often used in a variety of applications due to its biocompatibility, film-forming properties and high water-absorbing capacity. On the other hand, PVDF is a fluoropolymer known for its excellent chemical resistance, thermal stability, mechanical

strength and electrical properties. It is often used in piezoelectric devices, sensors, membranes and outdoor coatings.

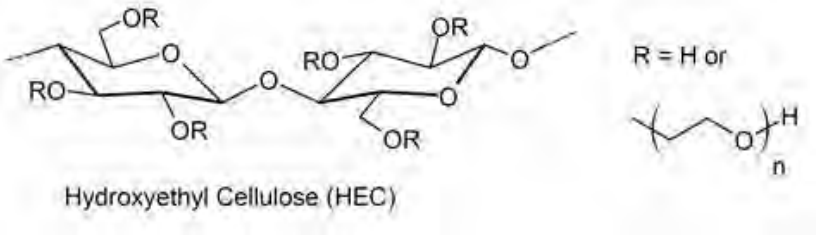

(a)

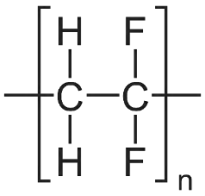

(b)

Figure 2.12: Structures of (a) HEC and (b) PVDF

The combination of HEC and PVDF in a composite material can lead to synergistic effects that harness the strengths of both polymers. In this study, the HEC/PVDF composite is used for humidity sensing due to its superior water absorption characteristics. A tapered POF is coated with a HEC/PVDF polymer mix for use in a relative humidity sensor. In response to an external stimulus, the optical properties of the coated tapered fiber change. In the hydrates condition, the fiber and composite function as a refractive index cladding, allowing for increased light transmission. The HEC/PVDF composite-coated sensor improves the humidity sensor sensitivity by allowing more light to pass through the tapered fiber, due to its ability to swell in a humid environment (Jiao et al., 2018). The sol-gel immersion method was utilized in this study to coat taper POF with HEC/PVDF composite because it is greener and safer owing to the fire-retardant behavior of its components (Peng et al., 2018). Figure 2.13 shows the sample of the

polymer composite solution, which was obtained by blending HEC and PVDF and its microscopic image (A Lokman et al., 2015).

Figure 2.13: Image of HEC/PVDF solution and its microscopic image (A Lokman et al., 2015).

2.10 Humidity Sensors

Humidity impacts on our lifestyles in many ways due to its special attributes. Researchers are therefore continually developing new humidity sensors to have rapid response, good stability, high linearity, long-term durability and exceptionally low hysteresis. The term “humidity” describes the quantity of water vapor in a gas. Various approaches can be used to measure humidity; the two most widely used are absolute humidity and relative humidity. Absolute humidity is a measure of the amount of water vapor in each volume. Whereas relative humidity (abbreviated as RH) is defined as the ratio of the amount of moisture content of air to the maximum (saturated) moisture level that the air can hold at a same given temperature and pressure of the gas. Temperature

does have a direct effect on the relative humidity and hence it is a relative measurement. The RH measurement is expressed as a percentage and determined by the expression:

$$RH\% = (P_V / P_S) \times 100 \quad (2.5)$$

where P_V is the actual partial pressure of moisture content in air and P_S is the saturated pressure of moist air at the same given temperature (both in Bar or KPa).

Drying products (such as paper, paint, matches, leather), food products (such as milk, cereal, tea, and bakery items) and manufacturing products (such as plywood, abrasives, pharmaceutical powders, gum, and tablets) are all affected by the amount of water vapor in the air. They therefore require humidity control. Humidity detection is also crucial in agriculture for soil relative humidity monitoring and crop protection. Respiratory equipment, incubators, sterilizers, biological products and pharmaceutical processing also require precise humidity control. Since water vapor is the key agent in both climate and weather, surface humidity measurements are essential for meteorological forecasting and analysis, hydrology, climate research, environmental science and aviation services. Figure 2.14 summarizes some of the application areas of humidity sensors.

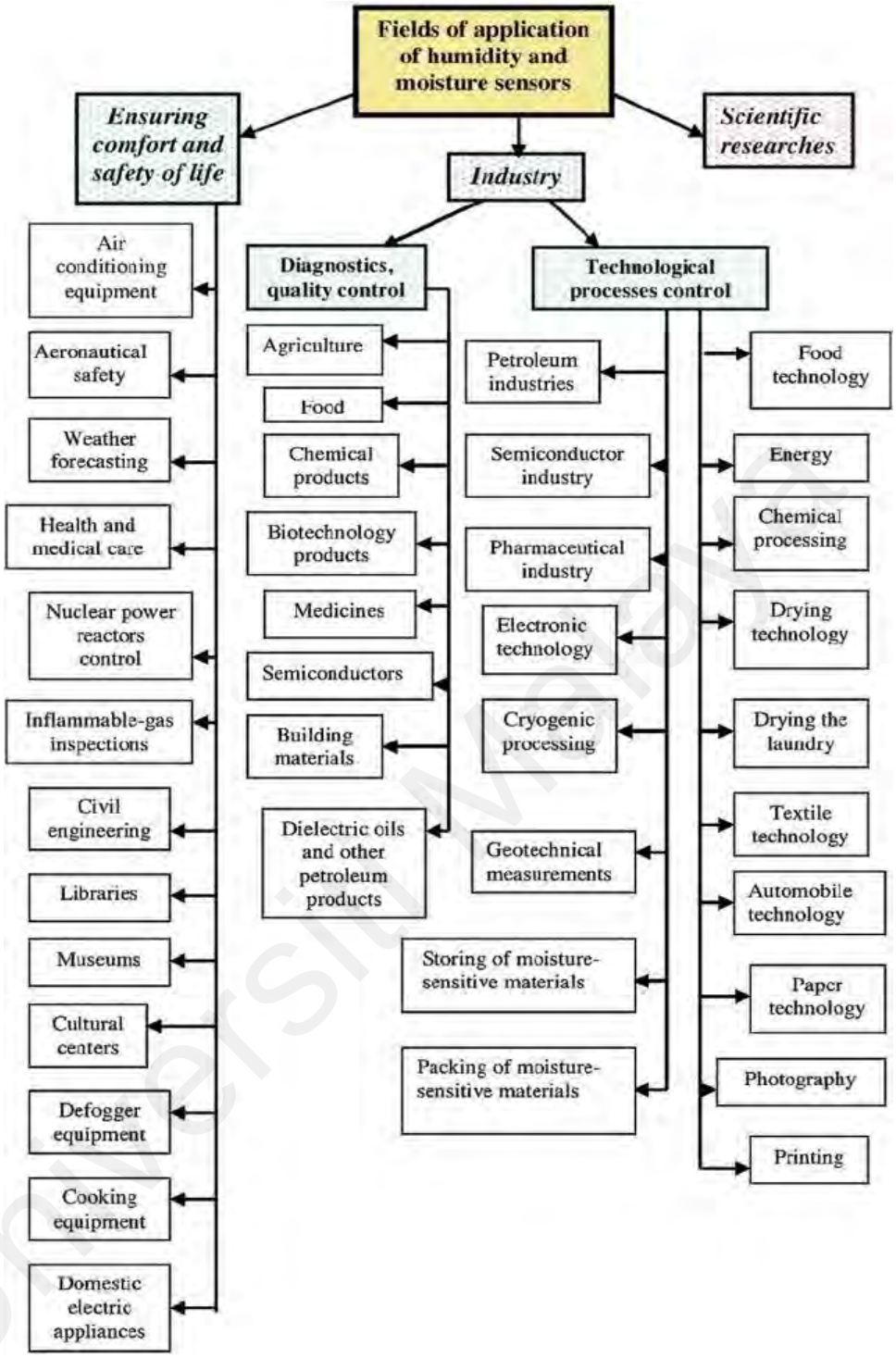

Figure 2.14: Applications of humidity sensors (Tulliani et al., 2019)

Advancement in humidity sensor systems requires the improvement of sensing elements, sensing mechanisms, structure or probe design and fabrication technologies. These days, many humidity sensors are made of a variety of different materials and are reported to operate on several different principles. To date, various types of humidity

sensors have been reported previously, including optical/optoelectronic/photonic/optoelectronic (Sikarwar & Yadav, 2015), resistive (Hammouche et al., 2021), quartz crystal microbalance (QCM) (Rianjanu et al., 2020), and capacitive (Fauzi et al., 2021). Among those sensors, optical-based humidity sensors are typically more sensitive, and offer a broader range of capabilities. However, they are often bulkier and more expensive (Chen et al., 2017) due to the conversion between light and electricity. Optical humidity sensors can rely on a multitude of parameters such as transmitted power, phase, frequency and wavelength. The former is the simplest approach and is employed for low-end humidity measurement applications, where high accuracy is not a stringent requirement.

Among the optical sensors, optical fiber-based humidity sensors are currently receiving the most attention, especially for applications in environmental monitoring and control. By leveraging the unique properties of optical fibers, this technology offers precise and reliable measurements of humidity levels in various environments. Unlike traditional humidity sensors, optical fiber sensors provide several distinct advantages that make them well-suited for a range of applications. As previously mentioned, they are immune to EMI and thus they are particularly valuable in industrial settings where electromagnetic noise is prevalent.

The working principle of optical fiber humidity sensors often involves the use of a humidity-sensitive material that undergoes changes in its optical characteristics in response to variations in humidity levels. This material is typically coated onto the exterior of the fiber or integrated into the fiber itself. As humidity levels change, the material refractive index or other optical characteristics shift, causing changes in the transmitted light. These changes are then detected and analysed to determine the humidity level. Optical fiber humidity sensors offer high sensitivity, enabling them to detect even

subtle changes in humidity. This is especially important in applications where maintaining specific humidity levels is crucial such as in controlled environments like laboratories, cleanrooms and manufacturing facilities. Additionally, these sensors are capable of real-time monitoring, providing continuous updates on humidity conditions and enabling timely interventions if necessary.

The ability to deploy this sensor in challenging environments is another notable advantage. Because optical fibers are thin, flexible and resistant to harsh conditions, they can be placed in locations that are difficult to access or are subject to extreme temperatures, pressures or chemical exposure. This flexibility allows for accurate humidity measurements in diverse scenarios; including in industrial processes, agriculture and even remote environmental monitoring. In the development of new sensors, many works have been focused on developing new functional materials for novelty and performance improvement in terms of sensitivity, specificity and response time. It can be seen that a great variety of materials have been explored for various sensing mechanisms.

2.11 Formaldehyde Sensors

Formalin is a commercial formaldehyde product, which is prepared as an aqueous solution containing 37 to 50 percent formaldehyde by weight. It is a clear, colorless liquid with a pungent smell. Formalin is used as a disinfectant and preservative in medical laboratories and mortuaries. However, in some cases, there are also misuses that adds formalin to food products as a cheap way to extend their shelf life and prevent spoilage. Formalin is highly toxic and can cause severe health problems if ingested. The use of formalin in food products is illegal in most countries, and its misuse has gained a significant concern by food safety authorities (Hoffmann et al., 2019; Rakha et al., 2022). In other research, formaldehyde contamination can cause toxic effects to the lungs, brain and heart (Arzuk et al., 2021; Bernardini et al., 2022).

The detection of formaldehyde is a critical area of research due to the severe health implications associated with its exposure. Previous studies have proposed and demonstrated various formaldehyde detection methods. The detection of formaldehyde in gaseous form, which construction materials and other sources can emit, has been reported (Du et al., 2023; Fang et al., 2021; Kuk et al., 2023). Other methods, such as chromatography and mass spectroscopy, have also been proposed (Faria et al., 2022; Nie et al., 2023). Both chemical-based or chromatography and mass spectroscopy detection methods are very accurate, but they need pre-preparation of sample and take a long time in measurement.

Due to this drawback, fiber-optic sensors are preferable for this application, since their methods are simpler and they have resistance to EMI. In addition, due to the advantages of mechanical strength and low-cost fabrication, much work has been done in formaldehyde detection based on fiber sensors. More recently, optical fiber sensors have shown promising performance in the detection of formaldehyde in different applications, where designs are tailored for specific environments. Darder et al. employed 3D printing filaments to realize an evanescent wave plastic optical fiber (POF) sensor (Darder et al., 2022). This simplified the manufacturing process and reduced the detection limits for airborne formaldehyde by fivefold, with respect to traditional POFs. This innovation makes 3D-printed POF sensors highly competitive in environmental monitoring due to their enhanced sensitivity and cost efficiency. In other work, they used the colorimetric reaction of Leuco Fuchsin-doped Nafion® cladding of a POF sensor to achieve a 0.03 ppm detection limit for workplace environments, meeting the standards for occupational safety (del Mar Darder et al., 2022).

In the control of food quality, Veríssimo et al. created an optical fiber sensor with a polyoxometalate coating for formaldehyde detection in milk, with detection limits of 0.2

mg/L (Veríssimo et al., 2020). The presented sensor exhibited reliable quantifications, similar to those obtained with conventional spectrophotometric methods. It was efficient to detect milk adulteration. Moreover, Saracoglu & Hayber used a bent plastic optical fiber sensor for the measurement of refractive index changes caused by preservatives such as formaldehyde in milk, which showed high linearity and sensitivity up to 14.3% (Saracoglu & Hayber, 2016).

These studies have elegant, high-performance enhancements of fiber optic sensors for the detection of formaldehyde, mainly through innovative coatings and fiber shapes tailored to specific sensing environments.

2.12 Arduino as Data Acquisition Platform for Sensing Device

The growing demand for flexibility, portability, cost reduction and real time monitoring has led to a need for miniature and compact devices that can be used for testing and measuring purpose. Consequently, Arduino has become a popular open-source microcontroller platform that can be used for a wide range of projects, including data acquisition from sensing devices. Data acquisition refers to the process of collecting information or data from various sensors or sources in the real world and converting it into a form that can be used for analysis, monitoring or control purposes. Arduino is a versatile platform for building data acquisition systems due to its ease of use, affordability and rich ecosystem of libraries and hardware components. Using Arduino as a data acquisition platform for sensing devices therefore offers a cost-effective and customizable solution for a wide range of applications; from environmental monitoring to industrial automation to scientific experiments. The Arduino community and extensive documentation also make it relatively easy to find support and resources when building a data acquisition system.

2.13 Characteristic of POF Sensor

A sensor of high quality will be observed in a linear format, whereby Equation (2.6) is employed to depict a linear correlation between two variables:

$$y = mx + c \tag{2.6}$$

where the sensor output dependant variable is y, the input independent variable is x, the slope of the line is m and c is the y-intercept. This classic linear equation can be used to estimate the sensitivity, linearity and resolution of a sensor.

The slope (m), usually obtained from the resulting best-fit line, represents the sensitivity of the sensor. This is normally estimated by performing linear regression analysis on the sensor output (y) against the input parameter (x) data points. The units of sensitivity depend on the specific input and output units.

Stability is typically calculated by monitoring the sensor output signal over time to determine the maximum allowable drift or change. Additionally, hysteresis in sensor measurement is also considered to investigate the maximum difference in sensor output for the same input value when approaching it from increasing and decreasing input condition. The hysteresis can be calculated as Equation (2.7), where ΔVmax is the maximum voltage variance at a certain humidity level and VFS is the full-scale output of voltage (Parangusan et al., 2020).

$$\gamma H = \pm (\Delta Vmax/VFS)100\%) \tag{2.7}$$

2.14 Summary

From the literature review, it can be summarized that plastic optical fiber can offer many advantages, particularly in terms of flexibility and capability, to perform sensing applications. Also modification of the POF by performing tapering, coating with a sensitive material and bending the fiber can enhance the sensitivity. The tapering process, which is a chemical and mechanical etching technique, is simple and easy to fabricate with minimum cost of tools. Although tapered fiber technology is gradually improving with time, certain obstacles continue to remain in the optimization of the processes of fabrication and material properties to achieve a desired level of performance. More theoretical studies and developments are needed to respond to these challenges, and fully exploit the capabilities of tapered fibers in different applications. Also from the review, the hydrothermal coating method has green environment advantages. In addition, the bending method applied to the POF will lead to a better sensor by providing more interaction with the environment.

CHAPTER 3: PREPARATION OF TAPERED PLASTIC OPTICAL FIBER COATED WITH ZINC OXIDE AND HEC/PVDF

3.1 Introduction

Plastic optical fibers (POFs) have recently attracted a significant research interest due to their inherent benefits; such as large diameter, high numerical aperture, lower attenuation in the visible areas, ease of manufacturing and excellent mechanical strength (M Batumalay et al., 2014; Teng et al., 2016). Furthermore, POF is flexible and smooth and has a lower softening temperature therefore allowing flexibility and tapering. This leads to POF-based humidity sensors providing viable alternatives to traditional technologies because of the current emphasis on intensity modulation technology and cost-effective solutions. The RI of the coating changes in response to the humidity level as a result of evanescent absorption as light scatters across the sensor location. Consequently, the brightness of the emitted light is altered (Malathy Batumalay et al., 2014; Fuke et al., 2010; Vijayan et al., 2008). To improve the environmental effect of the refractive index, fiber cladding is often eliminated using several methods, such as chemical or mechanical etching (Mulyanti et al., 2017) as well as heat pulling methods (Rahman et al., 2011). This ensures that the tapered section can be coated with sensitive materials, such as metal oxides (Divagar et al., 2018; Rajan et al., 2010) and non metal materials such as polymer.

Among various metal oxide materials, ZnO is widely used for sensing applications such as detecting gas concentration, humidity levels, temperature and pressure. ZnO has several advantageous properties that make it suitable for these purposes; such as possessing water insolubility, having high chemical and photo stability and the ability to absorb a wide range of radiation. These properties also make ZnO a popular material in the photonics field where it can be used for light emission, modulation and detection. In the previous chapter, we discussed the hydrothermal synthesis techniques for preparing

ZnO nanomaterials, which have several benefits over other methods. The advantages include ease, lower temperatures (ranging from 60 to 100 °C), enhanced productivity, and a more manageable procedure. The hydrothermal synthesis techniques can also produce ZnO nanomaterials with various shapes, sizes, and structures, which can affect their sensing and photonic performance.

HEC/PVDF is a composite which is cheap and also stable. It has been commonly used as a coating material to improve the refractive index fiber sensor sensitivity (Zain et al., 2021). For instance, it improves the relative humidity sensitivity due to its absorbing properties which enhances its capability to absorb water. The sensor sensitivity to relative humidity changes in the air is improved by the HEC/PVDF gel coating absorbing water which alters the coating refractive index.

In this chapter, tapered POFs were fabricated using both chemical and mechanical etching techniques to provide precise control. Consequently, the diameter of the tapered location is easier to control. Then, the nanorods were synthesized using hydrothermal methods and then coated onto a tapered POF before being bent into a radius of 3 cm for sensing applications. The preparation of POF and the growing of ZnO nanorods on POF via hydrothermal synthesis process are presented. The preparation of HEC/PVDF coated tapered POF using sol-gel immersion method is also described in this chapter.

3.2 Tapered POF Preparation using a Chemical and Mechanical Etching Technique

The ease of controlling the tapered region renders chemical and mechanical etching of POF very popular among researchers. This method involves the employment of acetone, de-ionized (DI) water, as well as sandpaper to polish the targeted area. Several samples with different waist diameter have been prepared for characterization and optimization

investigation. The POF used consists of polymethylmethacrylate (PMMA) as the core and fluorinated polymers as the cladding. In this work, a standard multimode model SH4001 Super Eska POF fiber (from Mitsubishi Chemical Co., Japan) was used; the diameter was 1000 µm, the core refractive index 1.492 and the cladding refractive index was 1.402. Initially, a cutter blade was employed to cut the fiber jacket from the center of the fiber with a 3 cm length, as depicted in Figure 3.1 (a). This was followed by an unclad process using acetone solution. The fluorinated polymers were cleaned using acetone with a Kimwipes tissue, resulting milky white surface appearing around the fiber is shown in Figure 3.1 (b). This milky white surface was then continuously removed with Kimwipes tissue and neutralized with DI water. Finally, sandpaper of 1000 grit and 7000 grit (Figure 3.1 (c)) was used in the polishing process to remove a portion of the core. Micrometers (Figure 3.1 (d)) were frequently used to obtain the desired diameter of the tapered fiber. The surface of the polished POF was then gently wiped with ethyl acetate solution to remove the microparticles produced by sand paper before the final cleaning process repeated several times with DI water.

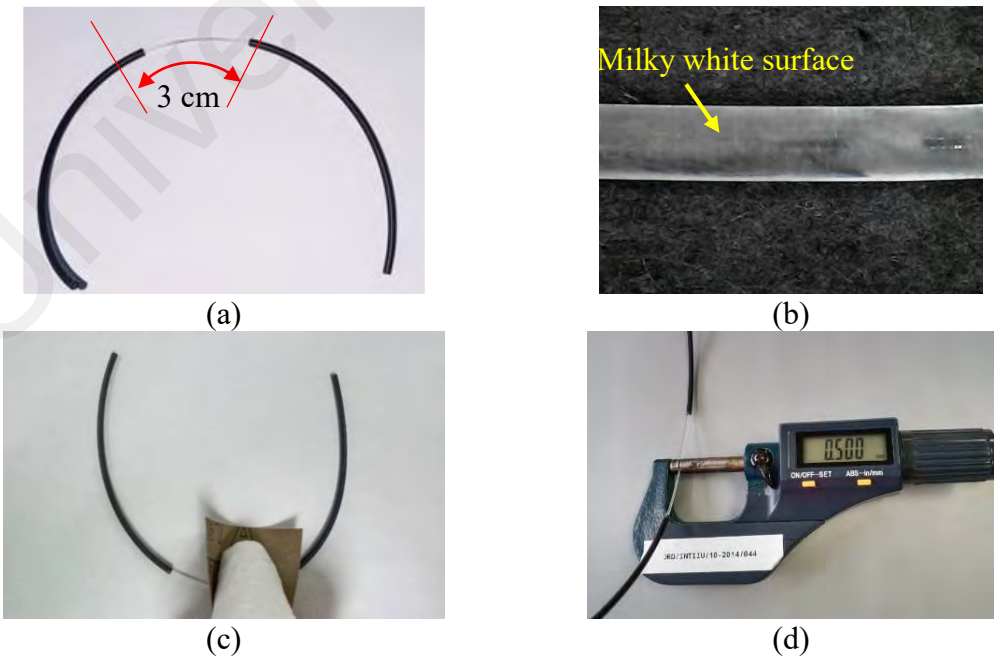

Figure 3.1: (a) Removal of fiber jacket (b) Milky white surface of POF (c) Polishing POF using sandpaper (d) Monitoring POF waist diameter using micrometers

Figure. 3.2 shows the microscopic picture of the original uncladd fiber with a diameter of 1000 um and the tapered fiber with 600 µm, 550 µm, 500 µm and 450 µm diameter. These images were captured by using microscopes with 5 times magnification. This technique is capable of producing a tapered POF with good reproducibility, despite being basic, cheap, harmless and only requiring minimum handling. Furthermore, the polishing process is gradual, and is a simple process to monitor the waist diameter physically.

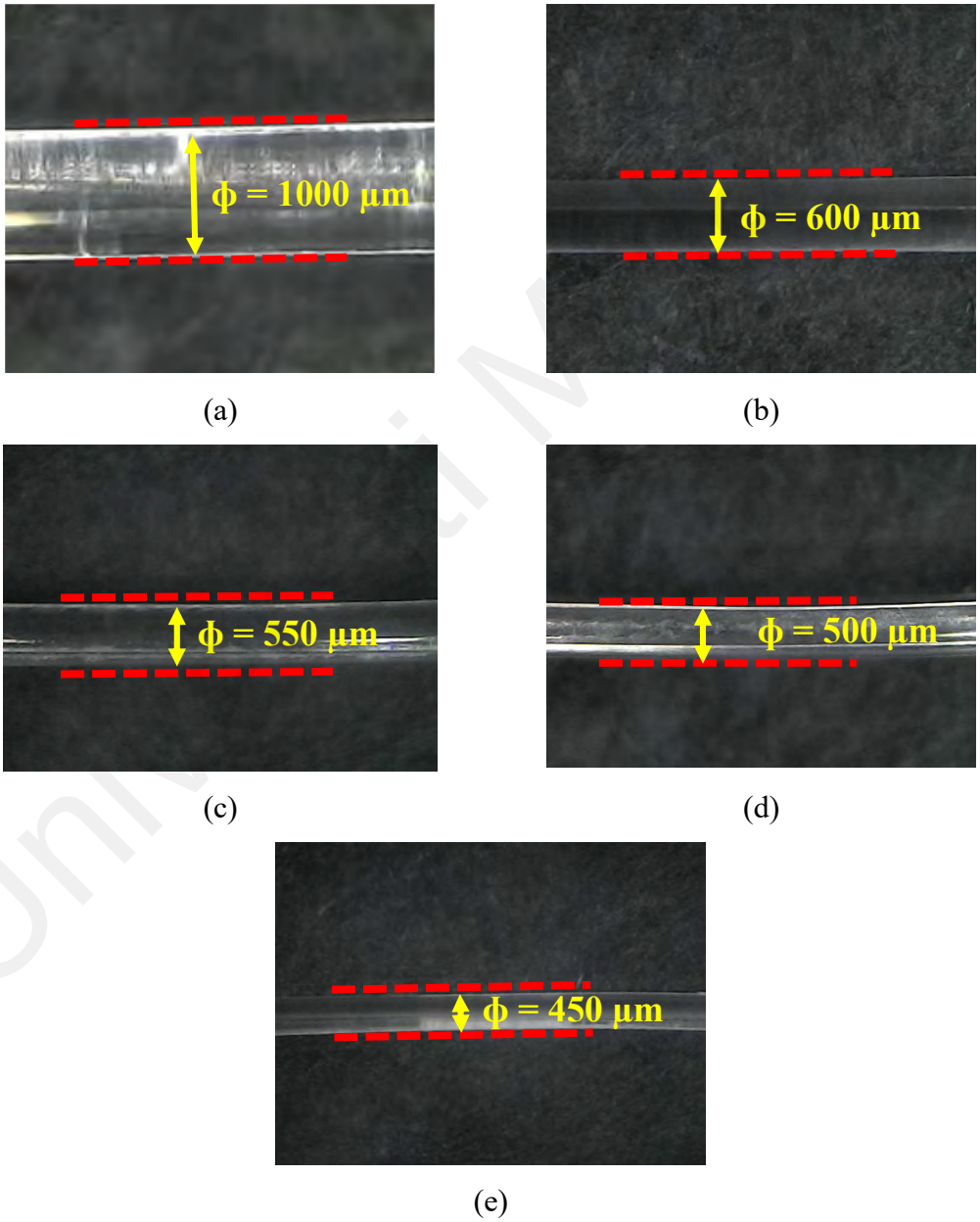

Figure 3.2: (a) Un-tapered POF with diameter of 1000 µm and tapered POF with (b) 600 µm (c) 550 µm (d) 500 µm (e) 450 µm diameter

3.3 Using the Hydrothermal Method to Grow Nanorods on the POF

The nanorod growth consists of two processes: seeding and growth process, as shown in Figure 3.3.

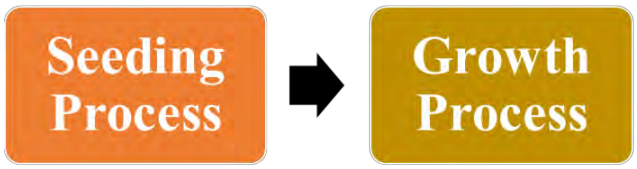

Figure 3.3: Hydrothermal synthesis procedures on the POF

3.4 Seeding Process

Figure 3.4 shows the process performed on the tapered POF. The reason for the seeding process is to create nucleation centres for the nanorod growth. The synthesis was achieved in the same way as done in work before (Fallah et al., 2013; Rahim, Manjunath, et al., 2016). The technique is extremely dependent on the uniformity, length, diameter, density of the solution, POF core surface action, the creation of the nucleation site on the POF core and on the annealing of the nanorods. The procedure consists of four primary steps; production of the seeding solution, POF core action, forming nucleation site on the POF core and annealing.

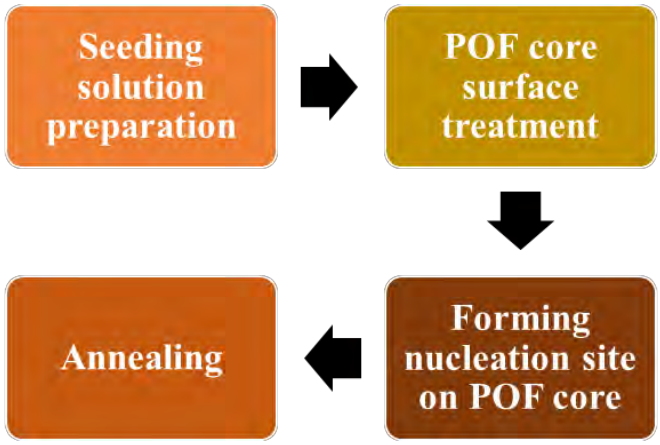

Figure 3.4: Seeding procedure on the POF

Initially, two sets of solutions were prepared; ZnO nanoparticles solution and pH control solution. The first solution was synthesised by dissolving 0.0044 g of zinc acetate dihydrate [$Zn(O_2CCH_3)_2.2H_2O$] (from Friendemann Schmidt, Germany) with 20 ml of unadulterated ethanol [C_2H_5OH] (from HmbG Chemical, Germany) to make a 0.001 M solution using constant stirring for 30 minutes at 50˚C. After the solution was cooled down to ambient temperature, it was then further diluted by adding another 20 ml of pure ethanol to produce 40 ml of ZnO nanoparticle solution, as shown in Figure 3.5.

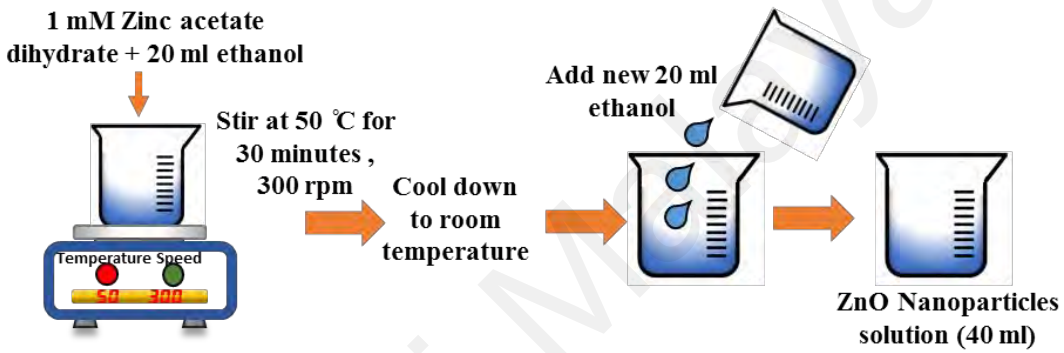

Figure 3.5: Preparation of the ZnO nanoparticles solution

For the pH control solution, aliquots of 0.0003g of sodium hydroxide pellets [NaOH] (from Friendemann Schmidt Chemical, Germany) were dissolved into 20 ml of pure ethanol to form a 0.001 M solution using constant stirring for 30 minutes at 50˚C, as shown in Figure 3.6. This control solution was deemed as essential to determine the ZnO properties via the hydrothermal process. The growth of the nanorods improves when the pH of the ZnO nanoparticles solution increases to alkaline. It has also been shown that the pH value could affect the nuclei and environment of the ZnO growth (Zhang et al., 2004).

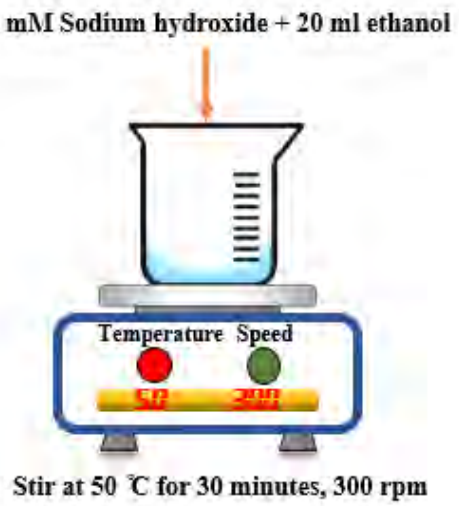

Figure 3.6: Preparation of the pH control solution

The pH control solution was dropped on the nanoparticles after 10 minutes. This was achieved using a dropping and stirring technique, where the ZnO nanoparticles solution was stirred slowly for every single 1 ml pH control solution drop using a pipet for around 1 minute, as shown in Figure 3.7. Then the process was repeated 20 times until the pH increased from ~4 to ~9. This step was crucial to provide more hydroxyl ions (OH^-) in the seeding solution (Baruah & Dutta, 2009). The mixture was maintained in an ultrasonic water bath at 60 ºC for 3 hours until a change in colour of the solution from clear to milky became noticeable.

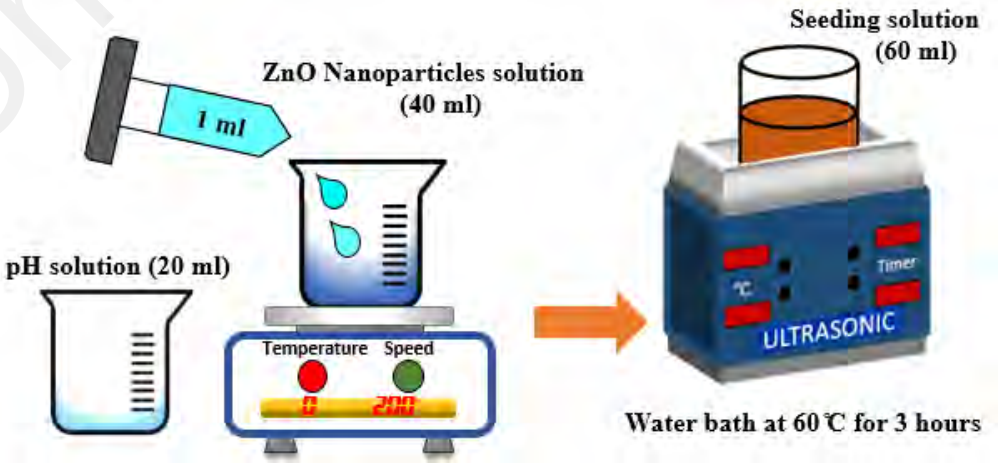

Figure 3.7: Drop and stir technique for alkaline process to prepare seeding solution

Figure 3.8 depicts the process of POF surface treatment in which the exposed core was dipped in a 1:10 mixture of Tween 80 and DI water. Next, the fibers were then exposed to air for 2 hours to dry. Figure 3.9 (a) shows the procedure of forming nucleation sites on the tapered POF. Firstly, the POFs are given slow stirring for 30 minutes. This was then followed by annealing the samples under 70 ˚C for 3 hours, as shown in Figure 3.9 (b) (M. Lokman et al., 2016).

Figure 3.8: POF surface treatment process

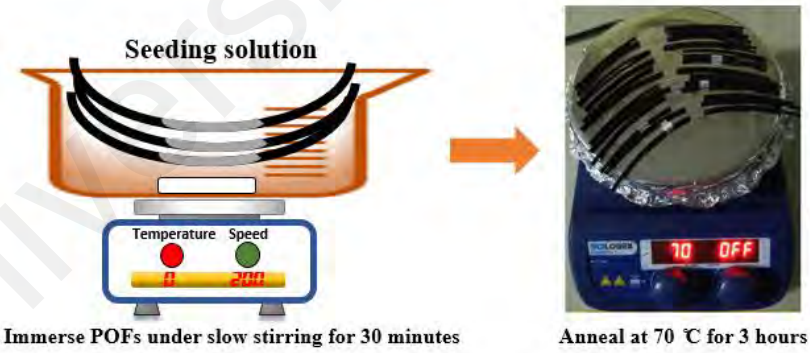

Figure 3.9: Forming nucleation site on POF core and annealing process

3.5 Growth Process

ZnO growth was performed following the seeding process. Subsequently, 1.4875 g of zinc nitrate hexahydrate [$Zn(NO_3)_2 \cdot 6H_2O$] (from Sigma-Aldrich, Germany) and 0.7 g of hexamethylenetetramine [$(CH_2)_6N_4$] (from Sigma-Aldrich, Germany) were both

dissolved in 500 ml of DI water to form 0.01 M solutions, as depicted in Figure 3.10. The synthesis solution was replaced every 5 hours with a new solution in order to maintain a continuous growth of ZnO nanorods on the tapered POF. The ZnO nanorods were grown for 12 hours on the tapered POF which was rinsed with DI water several times after it naturally cooled down to room temperature. The seeded tapered POFs were placed in the mixture then heated in an oven at 90 °C, as shown in Figure 3.11 (a). The techniques used in this process are similar to the methods reported by Jali et al.,2021 and Rahim et al., 2016 (M. H. Jali, M. A. M. Johari, et al., 2021; Rahim, Lokman, et al., 2016). Finally, both ends of tapered POFs were inserted in plastic holder with a fixed radius of 3 cm in order to obtain a permanent U-shape, as shown in Figure 3.11 (b).

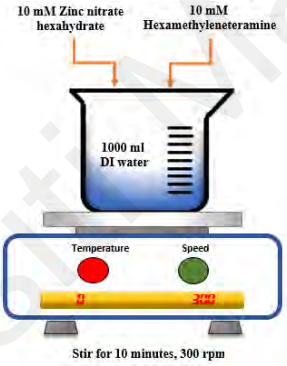

Figure 3.10: Preparation of 10 mM ZnO growth solution

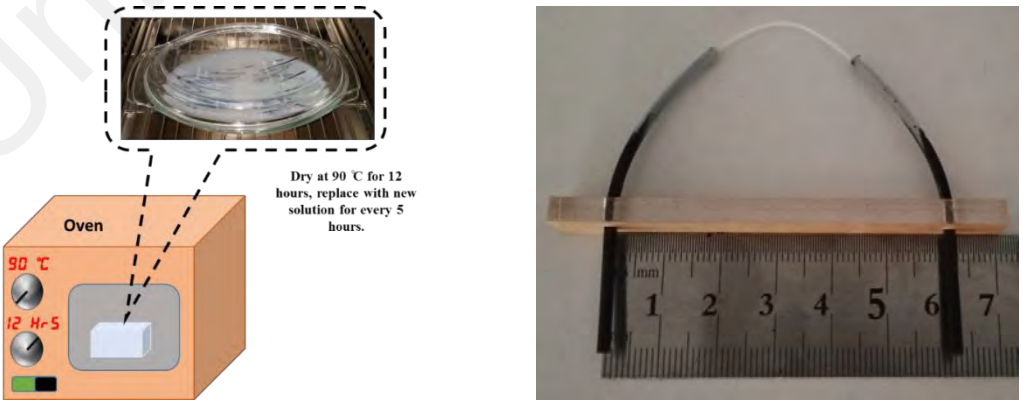

(a) (b)

Figure 3.11: ZnO nanorods growth procedure; (a) Seeded POF immerse in growth solutions and put in oven, (b) ZnO nanorods coated POF bend into U-shaped

3.6 ZnO Nanorods Characterization via FESEM

The morphology of the ZnO nanorods was performed utilising a Field Emission Scanning Electron Microscopy (FESEM), which was the Hitachi model 3400N, to observe the growth on the tapered POF surfaces. Figure 3.12 shows the FESEM images of the ZnO nanorods, which were grown on tapered U-shaped POF. From these images, the morphologies obtained confirmed that the structure of ZnO nanorods is based on the rod structure, and consists of many superfine nanorods on the fiber. The magnification was set at 100k x to clearly observe the ZnO structures coated on the fiber. An energy dispersive X-ray (EDX) method, with an operating voltage of 10 keV, was then carried out on the POF to identify the chemical elements. An EDX elemental analysis revealed that the topcoat layer covering the tapered U-shaped POF consisted of zinc (79.02%) and oxygen (20.98%), which verified that the sensing material for relative humidity sensing is ZnO. This is shown Figure 3.13.

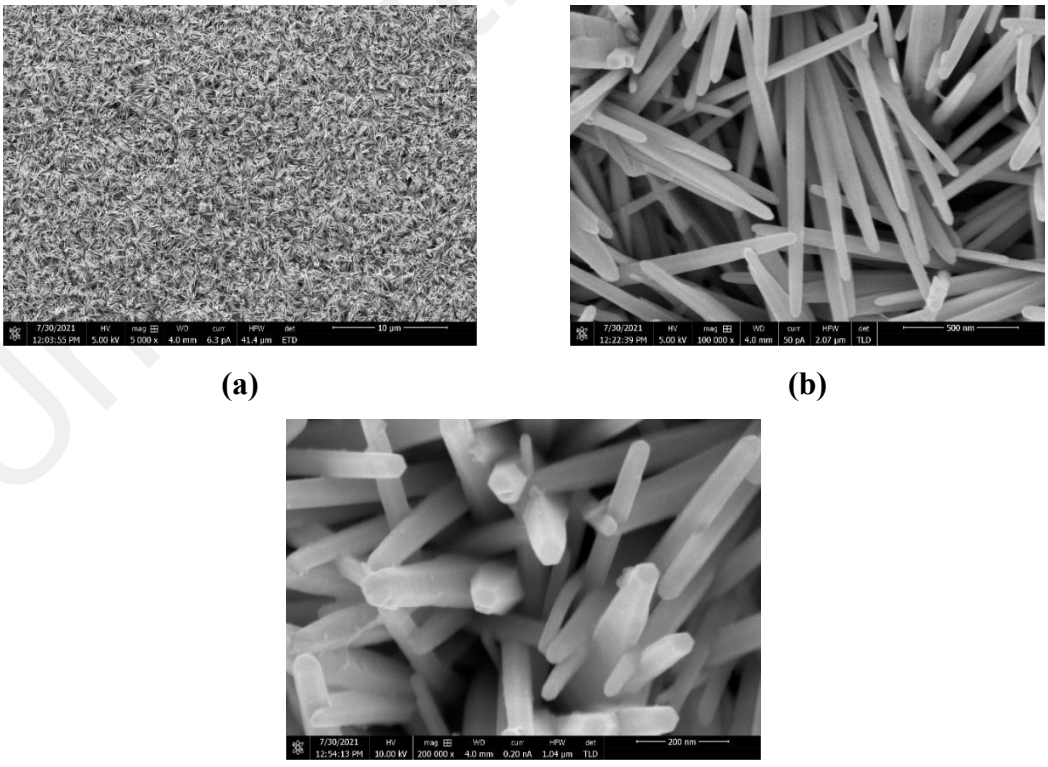

(a) **(b)**

(c)

Figure 3.12: The FESEM images of the ZnO nanorods coated onto the POF with magnification of (a) 5k x (b)100k x and (c)200k x.

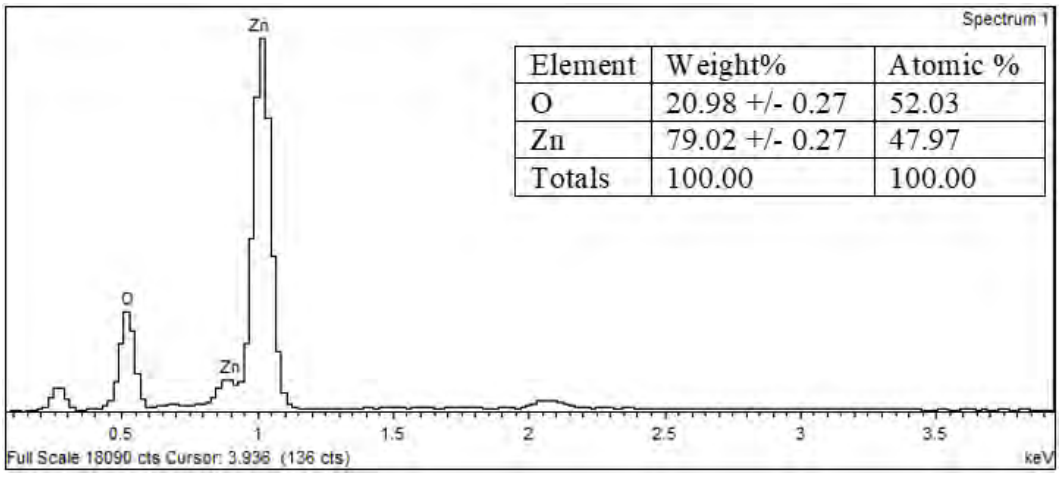

Figure 3.13: EDX elemental analysis of the ZnO nanorods coated onto the POF revealing samples consist only of zinc and oxygen.

3.7 Preparation of HEC/PVDF

The preparation of HEC/PVDF consisted of two steps. Initially, 1 gm of PVDF (Mw = 275,000) was dissolved into 120 mL of dimethyl formamide (DMF). The solution was then placed inside an ultrasonic bath set at 90ºC for 5 hours. After the solution had cooled down to room temperature, 4 g of hydroxyethyl cellulose (HEC) was added into the solution and stirred for 10 hours at 300 rpm, in order to have a completely homogenous solution. Once finished, the mixture was deposited on the fiber tapered area using a syringe, then the sample was left to dry for 48 hours (Batumalay et al., 2013; A Lokman et al., 2015; Zain et al., 2021). This technique is also known as the sol-gel immersion method. Figure 3.14 shows the process of preparing HEC/PVDF solution and sample coating.

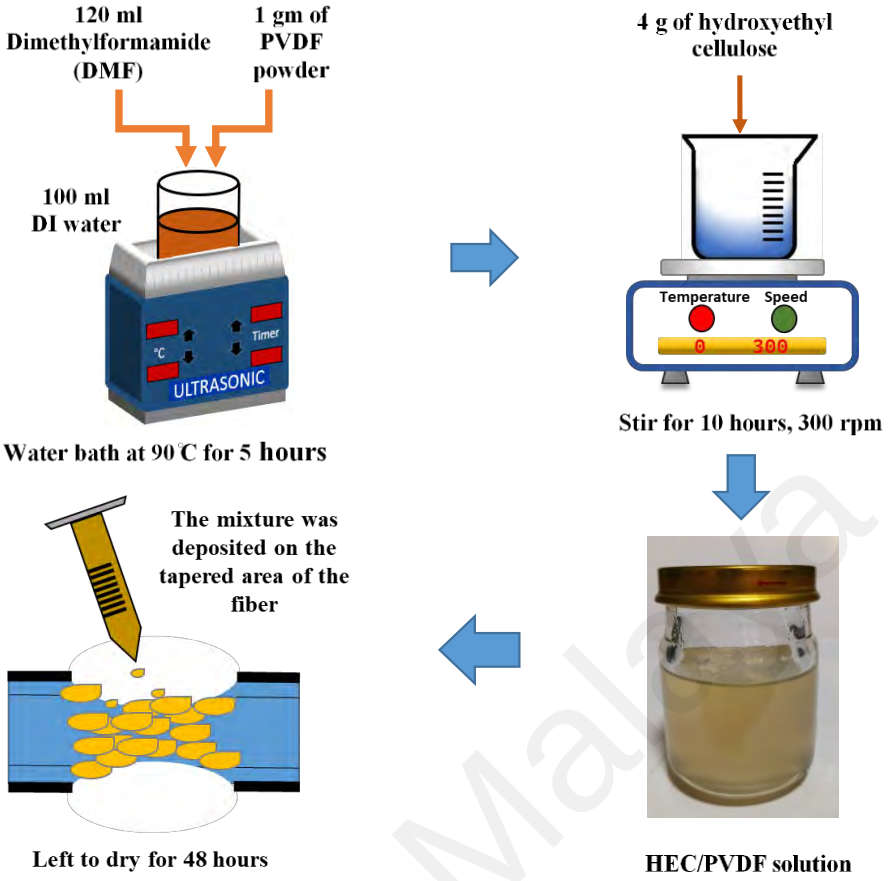

Figure 3.14: Preparation of HEC/PVDF solution and coating process

3.8 HEC/PVDF Characterization via FESEM

FESEM was used to observe the morphology of the prepared polymer membranes. Figure 3.15 shows the surface morphology of HEC/PVDF coated on the optical fiber at different magnifications. The surface morphology exhibited several white dots, showing the presence of HEC/PVDF gel therefore corroborating the results of prior investigation (Batumalay et al., 2013; Zuo et al., 2014). Besides being observed through FESEM image, EDX was performed in order to find the chemical composition from the coated material. In accordance with Figure 3.16, the EDX elemental analysis consists of carbon, oxygen, fluoride, natrium and chlorine. Comparable analyses have previously revealed these constituents as reported by Zou et al., 2014 (Zuo et al., 2014).

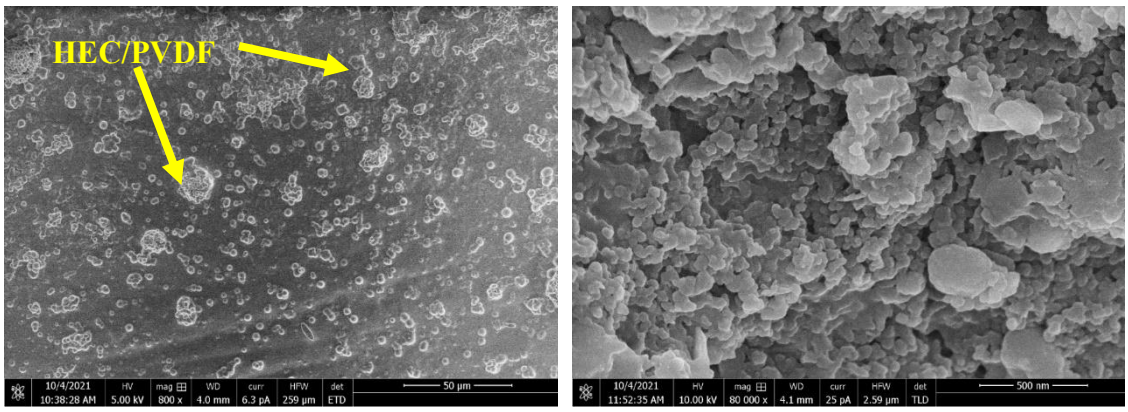

(a) (b)

Figure 3.15: FESEM image of HEC/PVDF at different magnifications (a) 800 x (b) 80,000 x

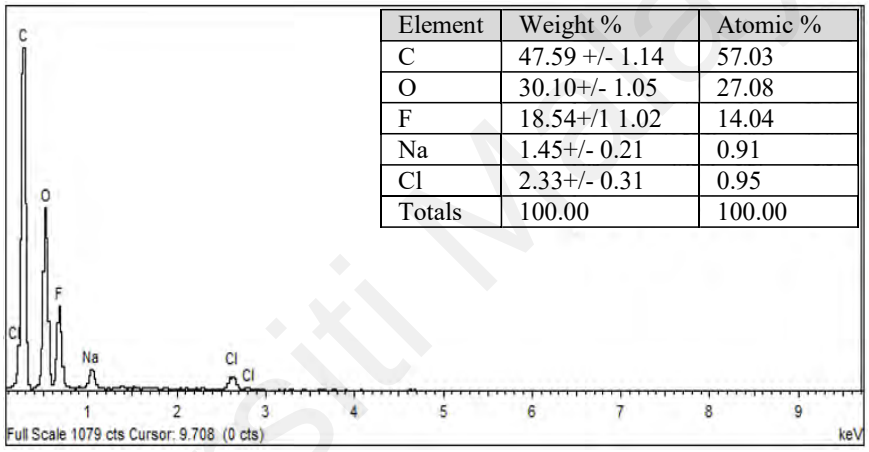

Element	Weight %	Atomic %
C	47.59 +/- 1.14	57.03
O	30.10+/- 1.05	27.08
F	18.54+/1 1.02	14.04
Na	1.45+/- 0.21	0.91
Cl	2.33+/- 0.31	0.95
Totals	100.00	100.00

Figure 3.16: EDX element of HEC/PVDF

3.9 Summary

A tapered U-shaped POF was successfully fabricated using chemical and mechanical etching processes. The fabrication process involved two main steps: etching and coating. First, the POF was etched using a combination of chemical and mechanical methods to reduce its diameter. Acetone and DI water were used as the chemical etchants, while sandpaper was used to polish the surface of the fiber. The etching process enhanced the evanescent wave interaction between the fiber core and the surrounding medium.

Second, the etched POF was coated with two different materials which are ZnO nanorods and HEC/PVDF composite. ZnO nanorods were synthesized using a

hydrothermal method with a seeding approach and followed by the growth of nanorods. HEC/PVDF composite was prepared using a sol-gel immersion method, which involved the dissolution of HEC and PVDF in dimethylformamide and the immersion of the fiber in the solution. ZnO nanorods and HEC/PVDF composite acted as an inner cladding that will use to improve the stability and repeatability of the sensor. The coating process will increase the sensitivity and resolution of the sensor by modulating the light transmission in the fiber.

CHAPTER 4: HUMIDITY SENSING

4.1 Introduction

The monitoring of humidity levels is an essential activity in industrial control, agricultural, health and safety, as well as meeting environmental requirements of sensitive materials and machines (N. Wang et al., 2021; Yu et al., 2020). Commercially available humidity sensors, using changes in electrical conductivity or capacitive properties, are actually insensitive at high humidity levels where the accumulation of water droplets or dew could cause charge leakage affecting the sensing system (Yusof, Harun, et al., 2019). Subsequently, optical fiber-based humidity sensors have become very popular due to low-cost development, promising fast response, small size and immunity to EMI (X. Zhou et al., 2018). Fiber optic sensors have previously been used to sense humidity using various techniques. For instance, loop resonator based RH sensors have been able to achieve a sensitivity as high as 0.2053 dBm/%RH. However, they showed sensitivity to changes in their looped touching region (Jali, Rahim, Johari, Hamid, et al., 2019). Micro-ball (Mallik et al., 2016), and micro-bottle (Md Johari et al., 2018) resonators have also been used to detect RH, but extra care should always be taken to ensure the resonators are positioned properly to facilitate the correct coupling of light. Additionally, there is also increasing interest in nanostructure materials to be used for sensing applicationn mainly due to their huge advantages in electrical and optical properties. This growing activity amongst researchers is motivated by advances in humidity sensor technology based on nanostructure materials including advantages of small size, immunity against electromagnetic waves, rapid response and recovery time and high sensitivity (Saeed Azad et al., 2017; Hernaez, Acevedo, Mayes, & Melendi-Espina, 2019). There have been significant numbers of studies on optical RH sensors based on nanostructure materials; such as ZnO (Irawati et al., 2017), tungsten disulfide (WS_2) (Luo et al., 2016), tin oxide (SnO_2) (Ascorbe et al., 2016), titanium dioxide (TiO_2) (Faruki et al., 2016),

polyethylenimine (PEI) and graphene oxide (GO) (Hernaez, Acevedo, Mayes, Melendi-Espina, et al., 2019). Among them, ZnO has been widely used for RH sensing, as it possesses a high refractive index material (RI = 2.008). Here, the surface adsorption of water molecules onto the ZnO leads to changes in the optical properties of ZnO (Chakrabarti et al., 2020). By using an optical fiber for RH sensing, the complex RI can be modified by coating the optical fiber with the nanostructure material (M. Q. Lokman, H. R. B. A. Rahim, et al., 2016).

In recent years, POF sensors have been used extensively for measuring RH, since they offer many advantages; such as large diameter, high numerical aperture, excellent mechanical strength and ease of mass production (Guo et al., 2019). Considering all these advantages, researchers often modify the fiber by tapering or bending the POF to create a strong evanescent wave for sensing purposes. With specific attention being on intensity modulation schemes and low-cost solutions, POF-based RH sensors now offer valuable alternatives to traditional technologies. When light scatters through the sensing region, the RI of the coating varies with the humidity level, due to evanescent absorption. Resultingly, the intensity of the output light is changed (Malathy Batumalay et al., 2014; Fuke et al., 2010). In order to improve the environmental impact of the refractive index, the optical fiber cladding was removed using chemical and mechanical etching (Mulyanti et al., 2017), heat pulling methods (Rahman et al., 2011), and a tapered section was coated with metal oxides (Divagar et al., 2018; Rajan et al., 2010).

Previously, researchers have also demonstrated relative humidity sensing using a straight POF (Saeed Azad et al., 2017; Corres et al., 2007; Harith et al., 2015; Liu et al., 2012) and U-shape POF (Guo et al., 2019; Jagtap et al., 2018). Jindal et al. found that a U-shape POF showed better performance in RH sensing when compared with a straight POF (Jindal et al., 2002). In other work, the U-shape POF was tapered in order to enhance

the sensitivity of various sensors (Beres et al., 2011; Punjabi et al., 2015; Tan et al., 2020; Wandermur et al., 2014). However, there are no previous reports of any work done on tapered U-shaped POFs coated with ZnO nanorods or HEC/PVDF for RH sensing. In this chapter, a RH sensor is demonstrated using a tapered U-shape POF probe coated with zinc oxide nanorods and using HEC/PVDF as a transducer.

4.2 Humidity Sensing using a Tapered U-shape POF Coated with ZnO Nanorods.

In this section, a RH sensor is demonstrated using a tapered U-shape POF coated with zinc oxide nanorods as the probe. The ZnO nanorods were synthesized using hydrothermal methods, and then coated onto a tapered POF, as described in the previous chapter. ZnO possesses distinctive optical and electrical properties; such as thermal stability, high electrical conductivity together with a high exciting binding energy (60 meV), a large bandgap energy (3.37 eV) and reactive surfaces for chemisorption of molecular water at ambient temperature (Kulkarni & Shirsa, 2015). ZnO nanorods have particularly shown good response to humidity in the literature (S Azad et al., 2017; Harith et al., 2020; Yusof et al., 2018). One of the main features of ZnO nanorods is that their effective RI changes during exposure to humidity, thus causing higher light scattering loss via the nanorod structure. This effect contributes to changes in the light transmission, and increases the sensitivity to humidity (Yusof, Harun, et al., 2019). By combining the bending and tapered POF geometry into a U-shape, the sensitivity of the sensor is further improved. U-shape gives better perfomance because this design allows for a larger evanescent field at the core-cladding interface, leading to better light interaction with the surrounding medium (Maseer et al., 2023).

4.2.1 Effect of the Light Source Wavelength on the Humidity Sensing Performance

In order to change the amount of coupled light into the cladding, the evanescent field of the sensor is modified by altering the RI of the coating material. A major factor in the sensing is the depth of penetration of the evanescent wave, which relies on both RIs of core and coating (Elosua et al., 2017). In the past, metal oxides were used as the sensing material; since they are heat resistant, possess high resistance to their surroundings and chemical degradation. ZnO is a useful material for sensing applications due to its numerous available synthesis processes, fast chemical adsorption and electronic features. O_2 can easily adsorb into the metallic oxide, making oxygen ions by capturing conduction band electrons. This results in a reduction in the material conductivity (Peterson & Sawyer, 2021). O_2 also exhibits some interesting properties; such as room temperature ferromagnetism, piezoelectric behaviour, chemical sensing properties and huge magneto-optic (Rahim, Manjunath, et al., 2016). The variations in the electrical conductivity of the material allow the optical detection of the ZnO nanorods for humidity measurements. This is caused by the absorption of molecules of water and variations in the effective surrounding RI (Harith et al., 2015; Salah et al., 2014). The complex refractive index varies as the electrical conductivity of the ZnO nanostructures. This has been shown to affect the optical scattering features of incident light on the ZnO nanorods (M. Lokman et al., 2016).

In this sub-section, an evanescent wave based %RH sensor response for three different wavelengths of LED (470, 530 and 645 nm) in an Arduino platform is reported. These wavelengths were chosen based on a need to achieve cost-effective equipment and uncomplicated sensor system (Orfanakis et al., 2021). ZnO nanorods were grown on the tapered POF, via the hydrothermal method, and then bent into a U-shape, as described in the previous chapter. A photodetector detects the scattered light from the nanorods, while

the Arduino platform performs signal processing and calibration. For the first time to our knowledge, the %RH sensor has been successfully realized by combining the benefits of tapered POF coated with ZnO via the hydrothermal method in a U-shaped structure. The proposed sensor produces higher penetration depth, which increases the evanescent power in the surrounding medium and enhances the sensitivity.

4.2.1.1 Experimental Setup

To obtain the permanent U-shape of the proposed sensor, both ends of the POF were inserted into a plastic holder with a fixed radius of 3 cm, as shown in Figure 4.1. The POF diameter was tapered and polished to reduce the diameters from 600 µm to 450 µm.

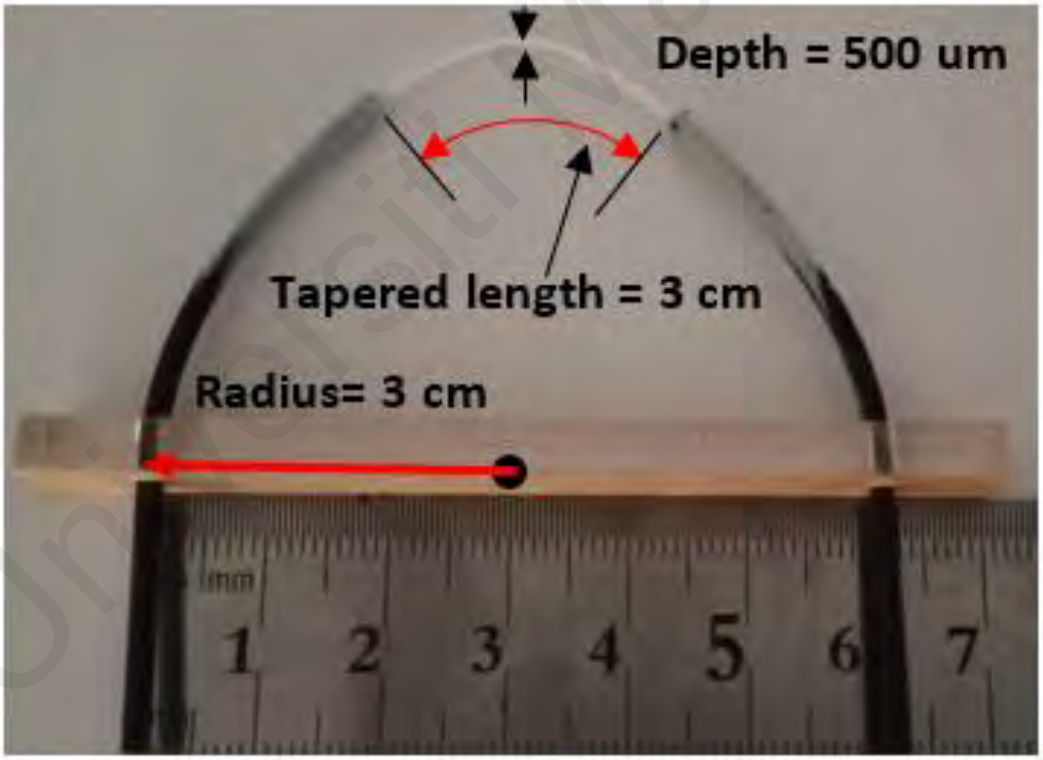

Figure 4.1: The prepared sensor probe based on a tapered U-shaped POF coated with Zinc Oxide nanorods.

Then, the experiments were carried out by placing the U-shaped POF inside a sealed chamber with dimensions of 0.13 m x 0.9 m x 0.6 m. Figure 4.2 (a) shows the

experimental setup for humidity sensing. The experiments were started by placing silica gel in the chamber to lower the RH level to 35%, and then replaced by wet tissues to raise the RH level to 90%. A temperature and humidity meter (Model UT333S, Uni-Trend Technology, China) was fixed into the chamber to serve as a reference of the actual humidity level.

During exposure of the sensor to relative humidity, the temperature inside the controlled chamber was kept constant at 24 ºC. LEDs (from Industrial Fiber Optics, USA) with wavelengths of 470, 530 and 645 nm were used as the light source. A phototransistor (Model IF-D92, Industrial Fiber Optics, USA) was used to detect the output light intensity in voltage form. The output from the phototransistor was then amplified and sent to a computer for recording and analysis. Additionally, there existed an option to check the output voltage using a liquid crystal displays (LCD).

This output voltage was recorded for every 5% RH level starting from 35% to 90% RH and repeated three times to verify the reliability of the sensors. Then, the average output voltage was recorded at all waist diameters (450 μm, 500 μm, 550 μm and 600 μm) at three different wavelengths (470 nm, 530 nm and 645 nm) to find the optimized waist diameter which produced the higher sensitivity. The stability of the optimized sensor was then tested by recording the output voltage for a prolonged period of 180 s. In addition, the response and recovery times for the sensing response were also measured by exposing the sensor device into the chamber at 40% RH and 90% RH repeatedly. The actual image of the experimental setup (without the controlled chamber) is shown in Figure 4.2 (b).

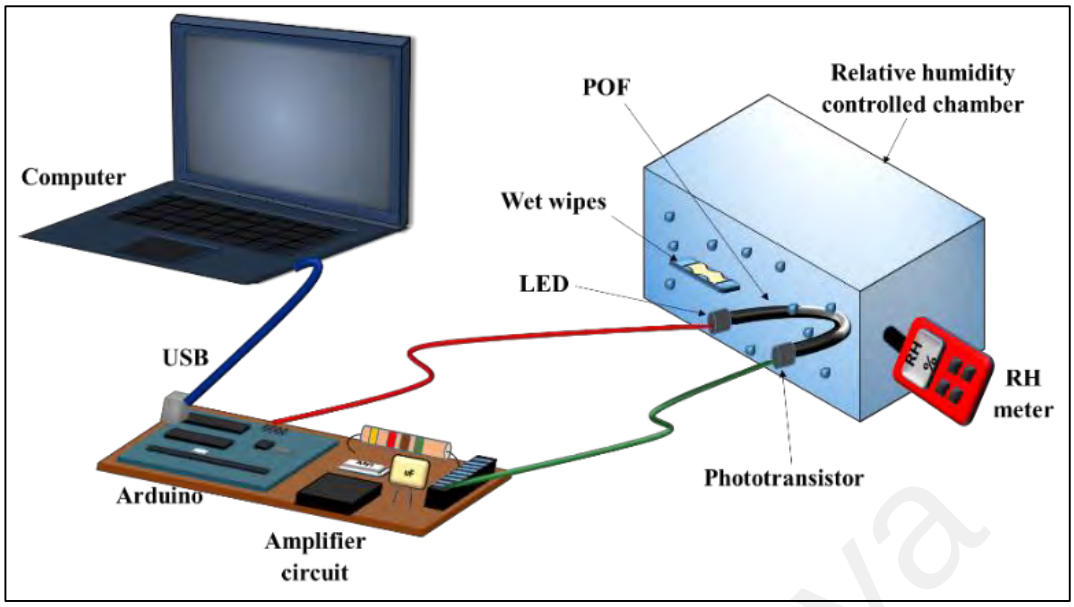

(a)

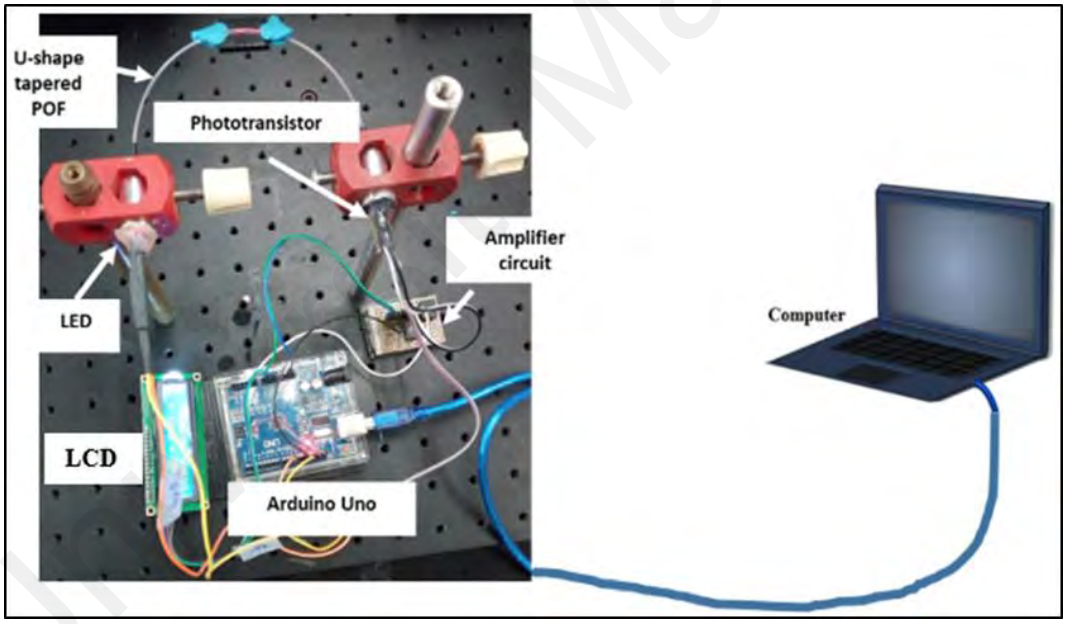

(b)

Figure 4.2: The experimental setup for humidity sensing (a) schematic diagram (b) the actual image showing the Arduino platform and amplifier circuit.

4.2.1.2 Results and Discussion

The humidity sensing responses of four waist diameters at three different wavelengths of light source, used in conjunction tapered U-shaped POF coated with ZnO nanorods sensor probe, was firstly obtained. Figure 4.3 shows the trendline graph, which was recorded as the humidity is changed from 35% to 90 %RH.

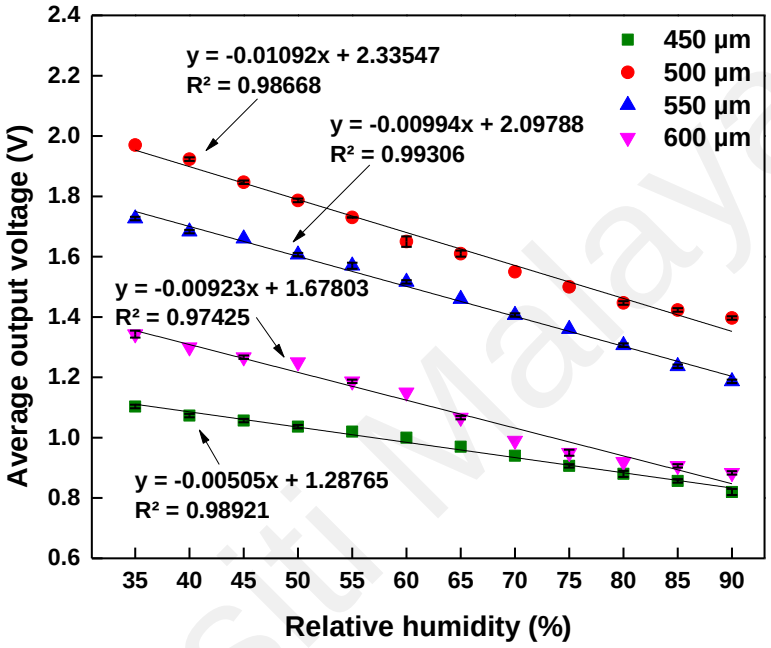

(a)

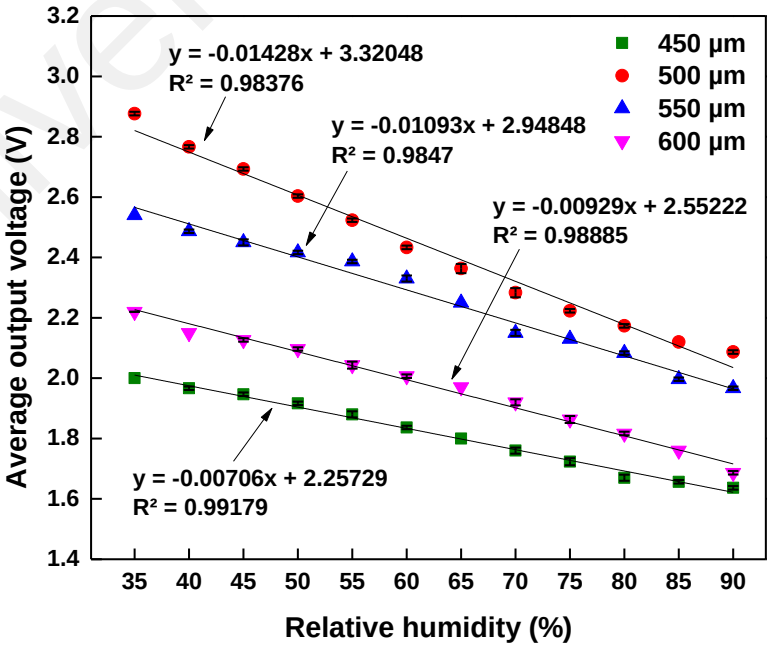

(b)

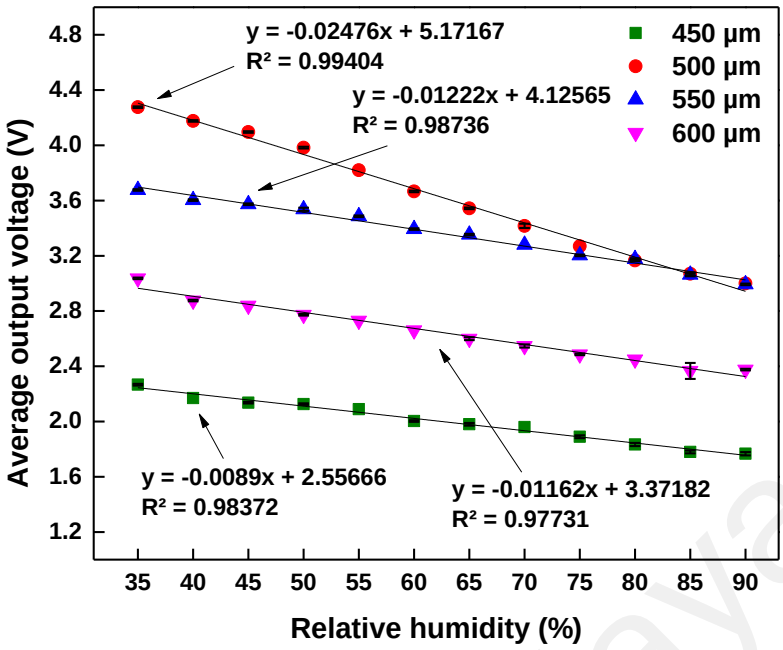

(c)

Figure 4.3: Trendline graph for wavelength (a) 470 nm (b) 530 nm (c) 645 nm

The average output voltage during forward measurement for three wavelengths decreased linearly with the increment of RH levels. This was due to the addition of water molecules which changed the refractive index of the ZnO nanorods. Also, larger leakage and light absorption within the ZnO nanorods structures occured. As a result, the intensity of the light significantly reduced because of massive light absorption into the ZnO nanorods medium when the %RH increased (M. H. Jali, M. A. M. Johari, et al., 2021). Figure 4.4 displays an overview of the sensitivity of four different fiber diameters at three distinct wavelengths. From the graph, waist diameters of 500 µm at 470 nm, 530 nm and 645 nm wavelength exhibit higher sensitivities which are 0.0109 V/%RH, 0.0143 V/%RH and 0.0248 V/%RH, respectively.

Furthermore, the 645 nm wavelength presented the highest sensitivity over the other two wavelengths. A similar result was also reported by Lokman et al. (M. Q. Lokman, H. R. Bin Abdul Rahim, et al., 2016) where a red LED (610 - 700 nm) observed the highest sensitivity as compared to green (500 - 570 nm) and blue (450 - 500 nm) LED for

humidity sensing. This result agrees with Equation (2.4), which states that light with a longer wavelength would travel further into the surrounding medium due to its interaction with the tapering region. Thus, the wavelength of 645 nm gave the strongest EW and resulted in the highest sensitivity.

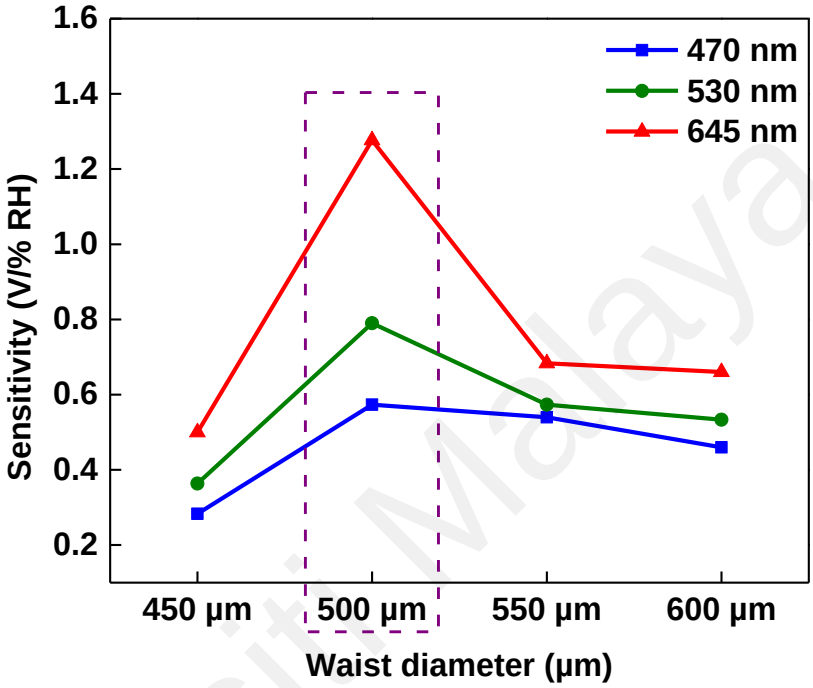

Figure 4.4: Optimized waist diameters at wavelengths of 470 nm, 530 nm and 645 nm

Figure 4.5 shows the repeatability properties of the 500 µm tapered U-shaped POF for three wavelengths (470, 530, and 645 nm) with different levels of humidity. The output voltages were measured three times between 35% to 90% RH. A reduction in voltage levels was observed as the RH level increased across all wavelengths. From the figure, it can also be observed that all wavelengths produced consistent results. The highest sensing response when tested with a 645 nm wavelength of light source showed the output voltage drops for 1.28 V from 4.28 V to 3.00 V. This was then followed by wavelengths of 530 nm and 470 nm which the amount of voltage drops was recorded as 0.79 V and 0.57 V, respectively.

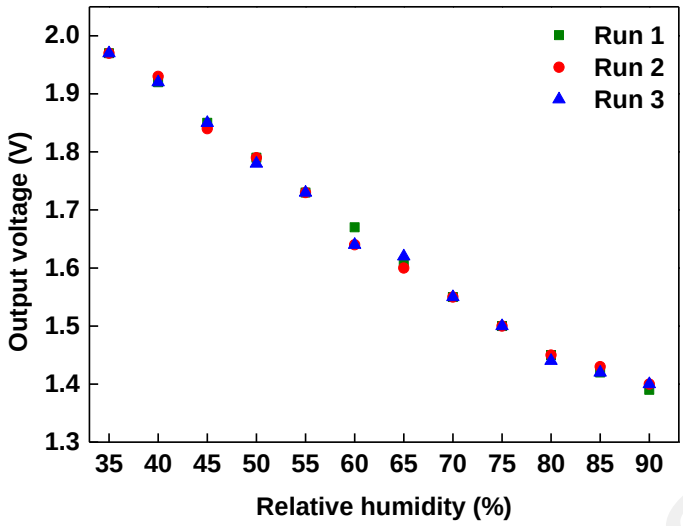

(a)

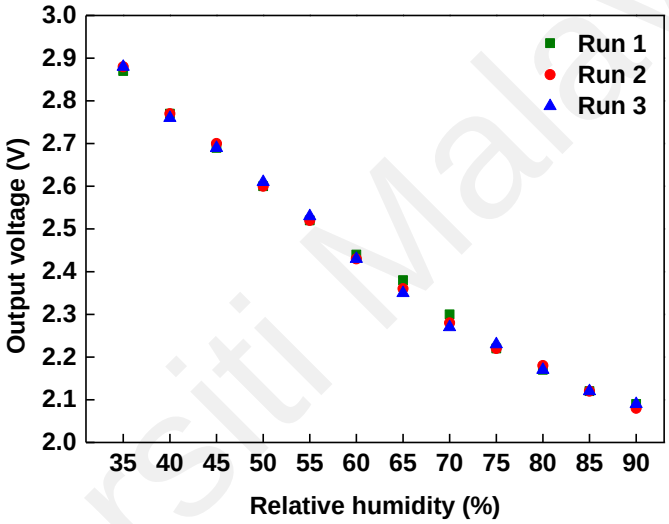

(b)

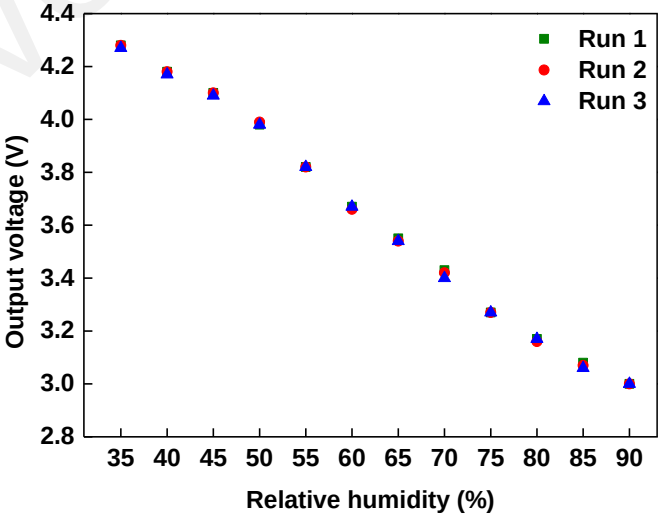

(c)

Figure 4.5: Sensing repeatability properties of U-shaped POF coated with zinc oxide nanorods probe at different LED wavelengths of (a) 470 nm (b) 530 nm and (c) 645 nm

The sensors were also tested for voltage stability by exposure to ambient %RH (55 %RH) at 24 ºC, where the output voltages were recorded continuously for 180 s. Figure 4.6 displays the output voltage stability for three different LED wavelengths. It was observed that the proposed sensor exhibits consistent output voltage, which shows good stability and durability of the sensor for all three wavelength sources.

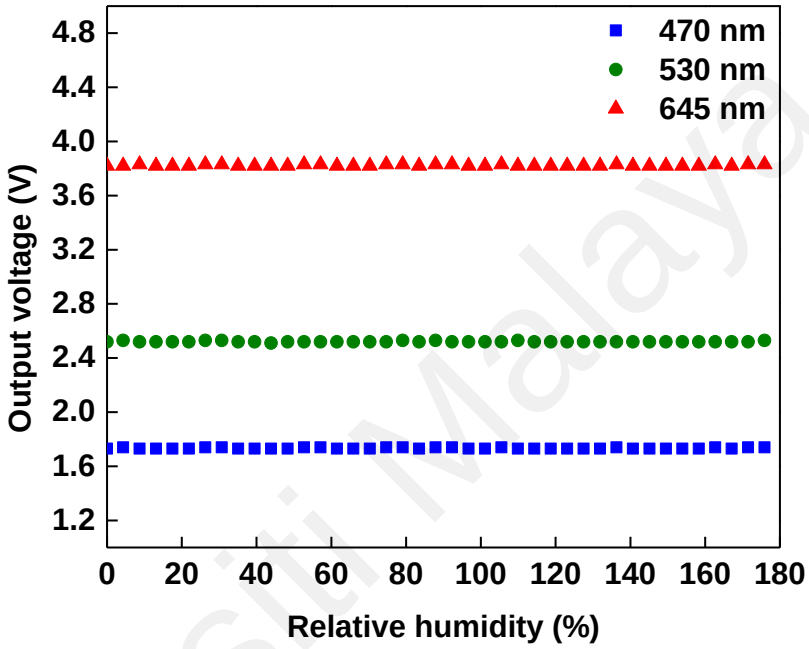

Figure 4.6: Output voltage stability at three different LED wavelengths.

Hysterisis curves of the sensing response at three different wavelengths are displayed in Figure 4.7. These sensing responses were seen when the fiber was alternately subjected to a desorption and absorption process of RH in the range of 35% to 90 % RH and vice versa inside the controlled chamber. The humidity hysteresis was calculated using Equation (2.7) (Parangusan et al., 2020). The wavelength at 645 nm produced higher reliability and measurement consistency due to a maximum percentage of hysterisis of only 2.1% compared to 470 nm (3.04%) and 530 nm (4.16%). This similar phenomenon was also reported by (M. H. Jali, H. R. A. Rahim, et al., 2021) which indicates that a narrower hysteresis is obtained when the sensor results exhibit higher reliability and measurement consistency.

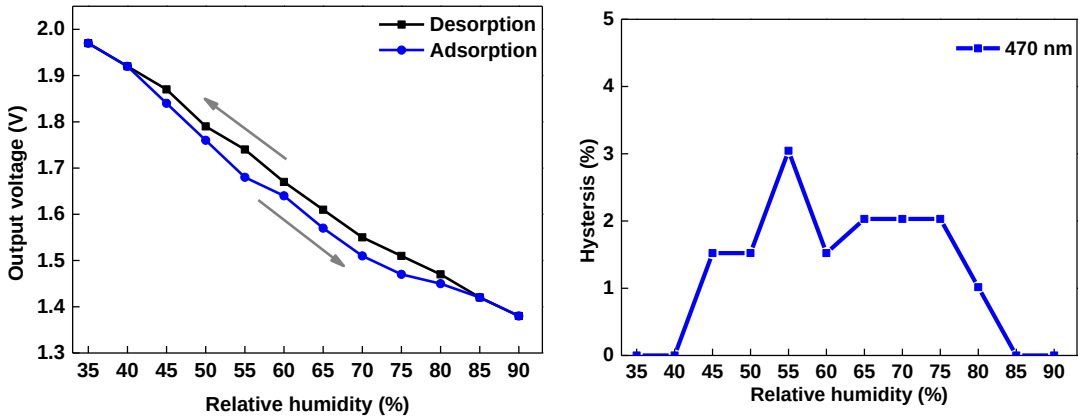

(a)

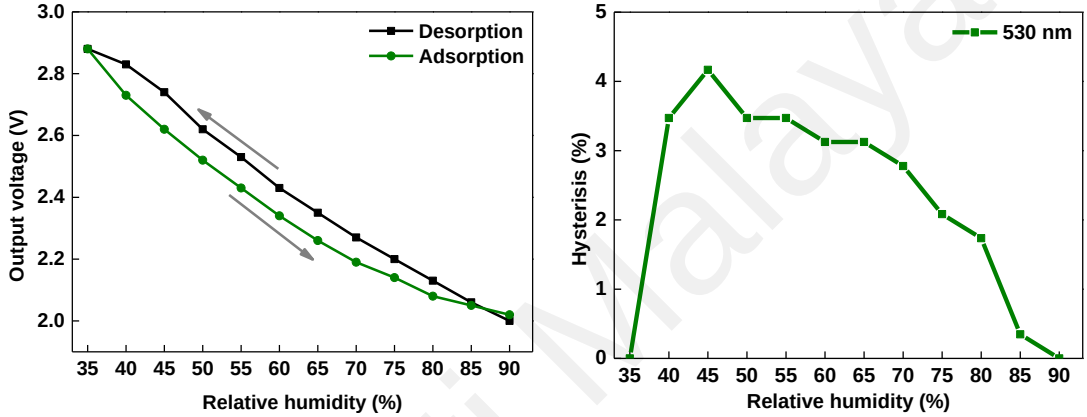

(b)

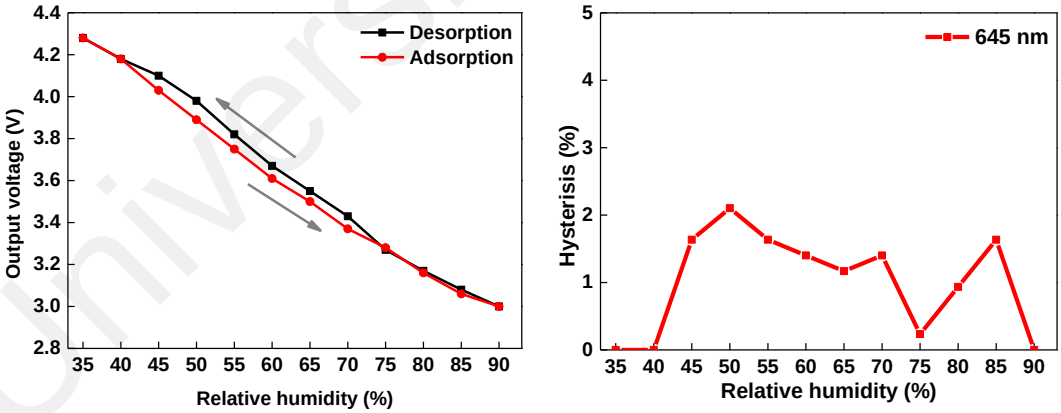

(c)

Figure 4.7: Hysterisis curves obtained at different light source operating wavelengths (a) 470 nm (b) 530 nm and (c) 645 nm

Subsequently, the continuous response and recovery times between 40% and 90% RH were measured by recording the time taken to reach ~90% of the total output power during the adsorption and desorption process (Yu et al., 2021). Referring to Figure 4.8, the

response and recovery times for the wavelength 645 nm were approximately 61 s and 68 s, respectively. Then, the wavelength of 530 nm response and recovery times were around 91 s and 74 s, respectively. And the wavelength at 470 nm response and recovery times were 105 s and 101 s, respectively. Fast adsorption-desorption rates of water molecules on the sensor can be caused by the uniform and highly ordered ZnO nanorods on the surface of the fiber, which enables significant surface interaction of the ZnO nanorods with the humidity (S Azad et al., 2017). However, the absorbance characteristics of the water vapor differed in different spectral bands (H. Wang et al., 2020). Thus, the wavelength of 645 nm produced the fastest response and recovery times, with abrupt changes in RH levels followed by wavelengths of 530 nm and 470 nm.

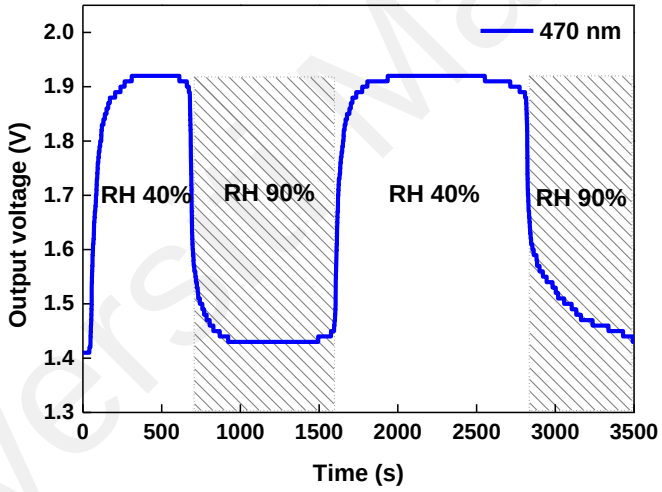

(a)

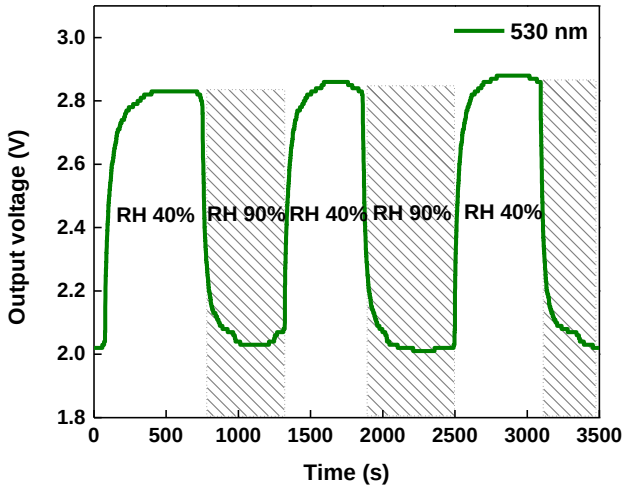

(b)

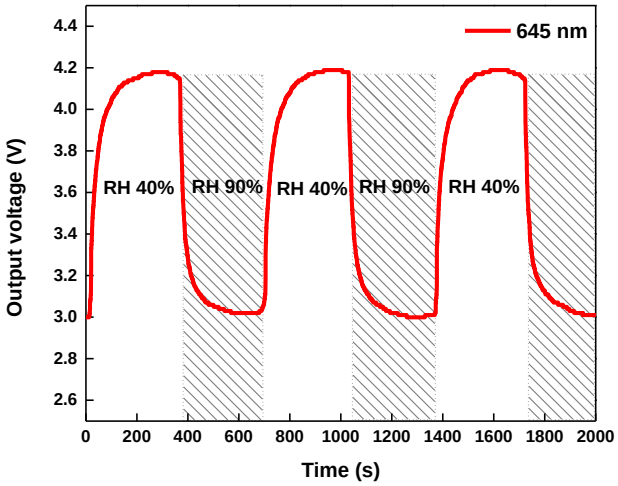

(c)

Figure 4.8: The continuous response and recovery times for different wavelengths; (a) 470 nm (b) 530 nm and (c) 645 nm

Table 4.1 summarizes the characteristics of the sensor tested at three different wavelengths. A wavelength of 645 nm produced the best sensing response compared with wavelengths of 530 nm and 470 nm with a sensitivity of 0.0231 V/%RH. Then, the resolution of the 645 nm wavelength also improved and reached 1.6228%. The wavelength 645 nm also produced the fastest response and recovery times, which were 61 s and 68 s respectively. The average standard deviation of wavelength 470 nm showed the lowest value of 0.0301 V when compared to the other wavelengths. Lower photon energy at 645 nm reduces scattering, which is advantageous for evanescent wave sensors as it allows for deeper penetration into the surrounding medium, enhancing sensitivity to humidity changes (Afsharipour et al., 2023; Mohan & Khijwania, 2024)

Table 4.1: Characteristics of the sensor

Parameters	Wavelengths		
	470 nm	530 nm	645 nm
Average standard deviation (V)	0.0301	0.0363	0.0363
Resolution (%RH)	2.7614	2.4862	1.6228
Sensitivity (V/%RH)	0.0109	0.0143	0.0248
Linearity (%)	99.55	99.10	99.47
Response time (sec)	105	91	61
Recovery time (sec)	101	74	68

4.2.2 Performance Comparison with an Uncoated POF Sensor

In this section, ZnO nanorods were synthesized using hydrothermal methods and coated onto a tapered POF before bending it to a radius of 5 cm for RH sensing. The proposed sensor was inserted into a plastic holder to form the fiber into a U-shape structure. Tapered U-shape POF coated with ZnO nanorods was labeled Z-UPOF, while the tapered U-shape POF without coating was labeled N-UPOF in this work. A red light-emitting diode was used to investigate the sensitivity of the RH sensor. The present work demonstrated the higher sensitivity of the Z-UPOF compared with the uncoated sensor. This approach provides an efficient, easy and cost-effective method for RH sensing. Figure 4.9 shows the image of the Z-UPOF with a bending radius of 5 cm.

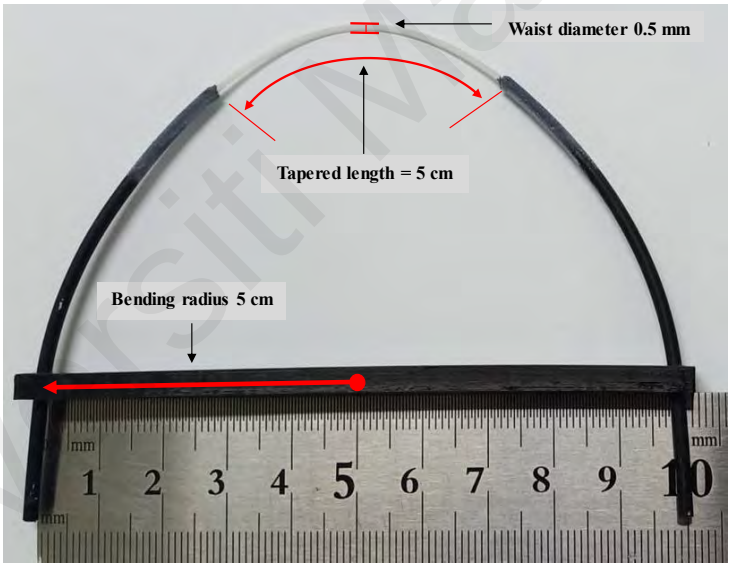

Figure 4.9: The image of prepared U-shape tapered POF with a bending radius of 5 cm.

The experimental setup for RH sensing in this work is shown in Figure 4.2 (a). Throughout the experiment, a temperature and humidity meter was fixed on the controlled chamber (0.13 m x 0.9 m x 0.6 m) wall as a reference to the actual chamber RH level. One tip of the sensor (Z-UPOF/N-UPOF) was connected to the red LED, and the other tip of the sensor was connected to the phototransistor to perform RH sensing. The power

supply Arduino Uno +5 V was used to operate the LED and the phototransistor, while a computer was used to monitor the data of the humidity sensing. The red LED wavelength of 650 nm was used to access the optical fiber effects on light transmission through the fiber, and the optical power was converted into an electrical signal using a phototransistor IF-D92 (from Industrial Fiber Optics, USA). During exposure of the sensor to relative humidity, the temperature inside the controlled chamber was kept constant at 24 ºC. In this work, the N-UPOF and Z-UPOF were exposed to RH in the range of 35% to 90%. To accommodate the lowest RH levels in this measurement, silica gel was used to lower the RH level to 35%. Then wet wipes were substituted inside the chamber to raise the RH level to 90%. This experiment was recorded for every 5% of RH level, starting from 35% RH and repeated three times to ensure the reliability of both sensors.

The repeatability properties of N-UPOF and Z-UPOF are shown in Figure 4.10. This measurement was conducted three times between 35% to 90%RH. It can be observed that the output voltages of the N-UPOF and the Z-UPOF decreased as the RH level increased. The maximum repeatability percentages (MR%) for N-UPOF and Z-UPOF were approximately 16% and 8%, respectively. Hence, the higher MR% in N-UPOF contributed to the irregular output voltage shift (Figure 4.10 (a)), while the output voltages of Z-UPOF showed better consistency (Figure 4.10 (b)). In addition, Z-UPOF produced a higher output voltage range of 1.56 – 2.61 V in comparison with the N-UPOF (2.13 – 2.90 V). This difference can be caused by the variation of effective RI and the changes of light incident on the ZnO nanorods (M. Q. Lokman, H. R. B. A. Rahim, et al., 2016). These results suggest that ZnO nanorods allow more absorption of water particles to induce more changes in the EW with respect to the amount of humidity adsorption in order to achieve good repeatability.

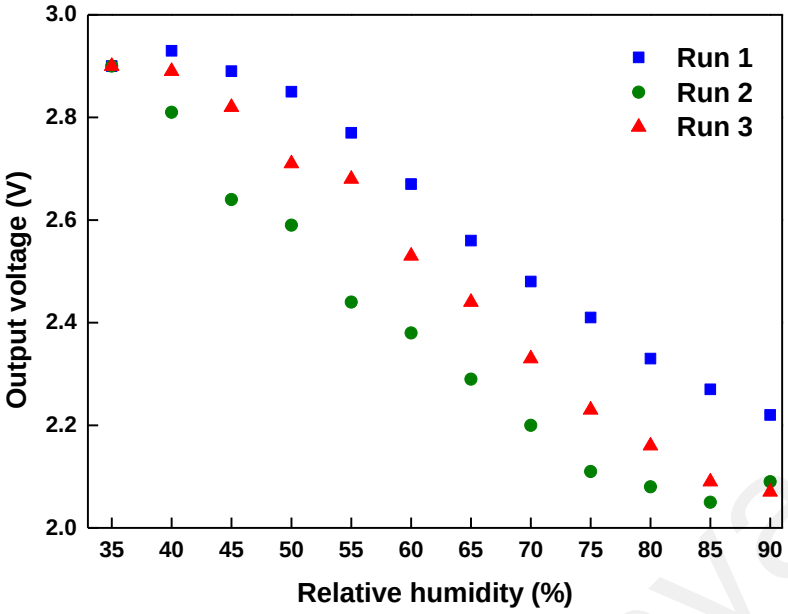

(a)

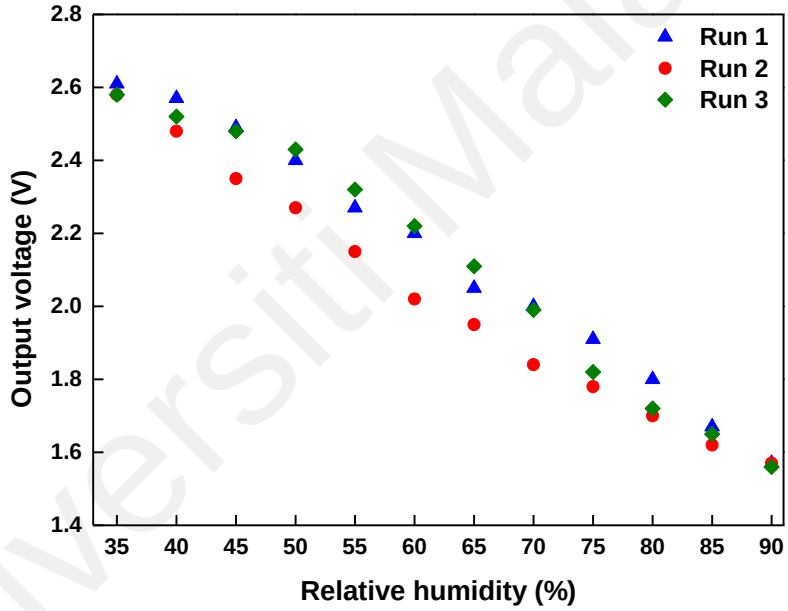

(b)

Figure 4.10: The repeatability properties of (a) N-UPOF and (b) Z-UPOF

Hysteresis curves of N-UPOF and Z-UPOF sensors are displayed in Figure 4.11. This test was carried out by observing the sensing responses for the adsorption and desorption processes of RH in the range of 35 to 90% RH for both sensors. Based on Figures 4.11 (a) and (b), the highest calculated humidity hysteresis (γH) contributed by N-UPOF and Z-UPOF were approximately 11.34% and 6.89%, respectively. The humidity hysteresis

was calculated using Equation (2.7) where small hysteresis produced in a sensor results in higher reliability and measurement consistency (Arunachalam et al., 2019). As seen, Z-UPOF has lower humidity hysteresis thus this sensor produced better measurement consistency in the voltage stability compared to the N-UPOF sensor, due to the coated material on the tapered U-shape POF.

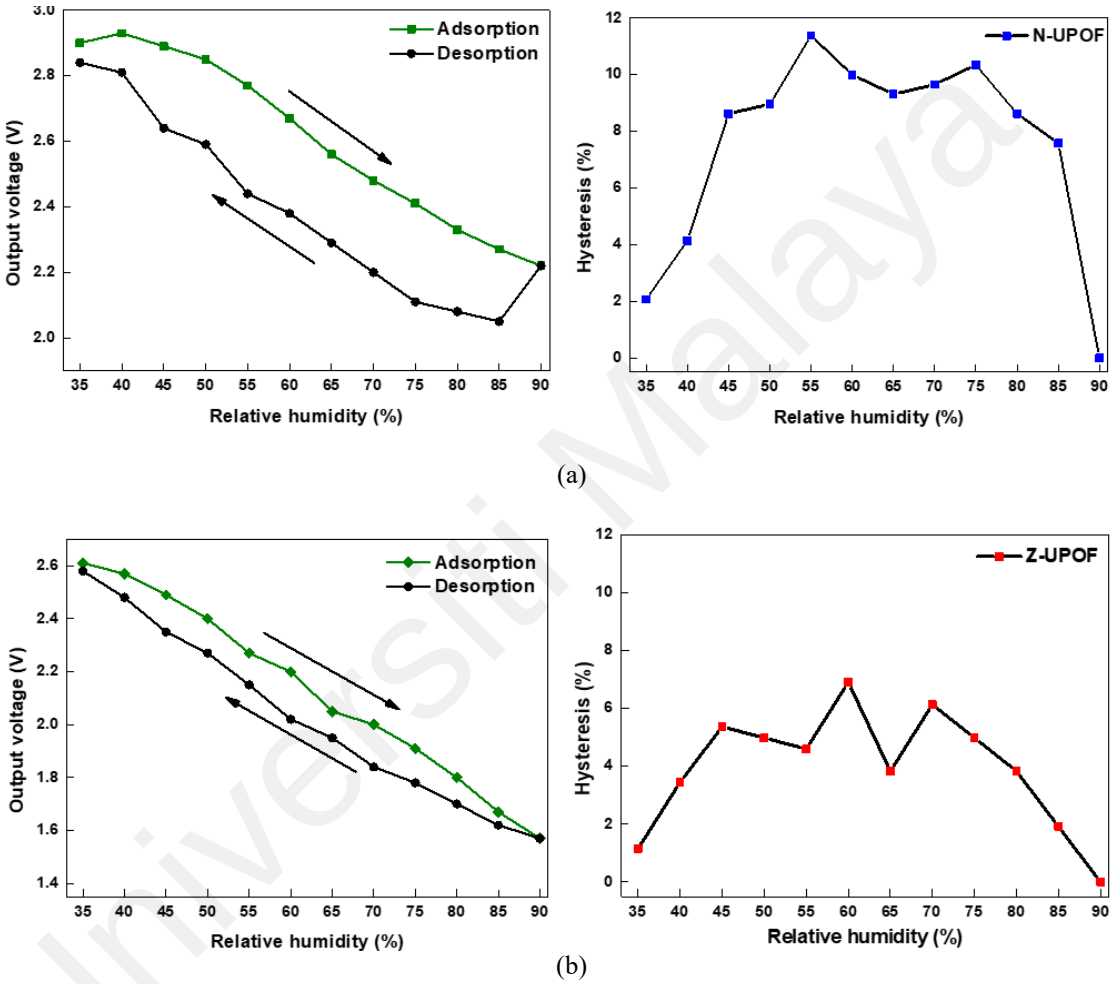

Figure 4.11: Hysteresis curves of; (a) N-UPOF and (b) Z-UPOF

Output voltages plotted against RH for N-UPOF and Z-UPOF sensors are shown in Figure 4.12. The output voltages for both sensors decreased linearly with the increment of RH levels. It can be observed that the sensitivity of the N-UPOF is 0.0158 V/%RH with a linearity of more than 99%, while the sensitivity of Z-UPOF is 0.0194 V/%RH with a linearity of more than 99%. This can be caused by high surface area, high

photosensitivity, catalyst-free growth, large area uniform production and high sensitivity of ZnO nanorods (Harith et al., 2020). Besides that, the rapid adsorption of water molecules on the surface can also be attributed to the porous structure of ZnO nanorods on the POF. This surface adsorption process also modulates the optical properties of the ZnO nanorods. As the RH level increases, additional water molecules on the surfaces of the ZnO nanorods on the Z-UPOF were absorbed. This behavior was also reported by Liu et al., where increasing water molecules lead to an increase in the effective surrounding medium refractive index as well as in the coefficient of absorption of ZnO nanorod surfaces, leading both to a larger leakage and light absorption within the ZnO nanorods structures (Liu et al., 2012).

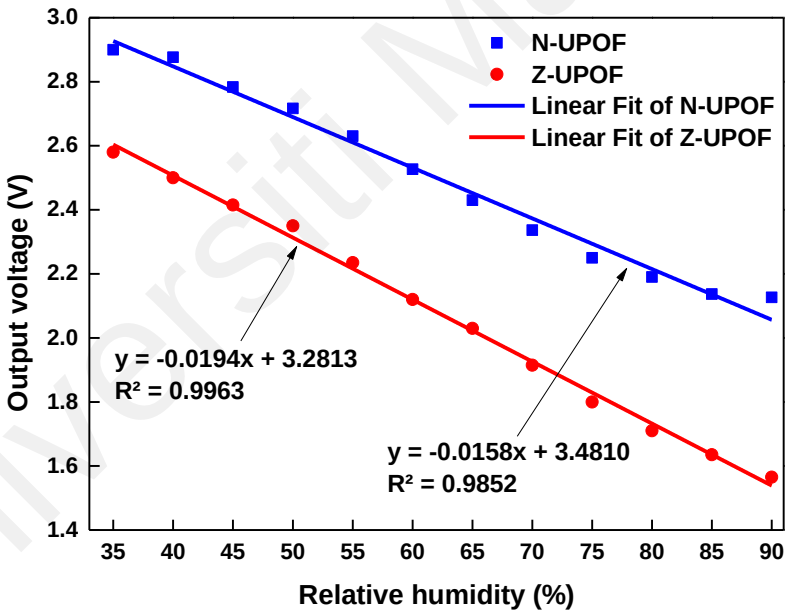

Figure 4.12: Output voltages against relative humidity for N-UPOF and Z-UPOF sensors.

Both sensors (N-UPOF and Z-UPOF) were tested for voltage stability by exposure to 90% RH, where the output voltages were recorded continuously for 60 s on the first day and after 10 days. Figure 4.13 displays N-UPOF and Z-UPOF voltage stability for the 1st and 10th day. It was observed that the output voltage for N-UPOF after 10 days was similar

to the 1st day, while output voltage stability for Z-UPOF was slightly reduced after 10 days. It was revealed that the output voltage of Z-UPOF was slightly reduced because of the degradation of ZnO nanorods after 10 days, where this phenomenon has also been observed in work previously (Huda Adnan Zain et al., 2020).

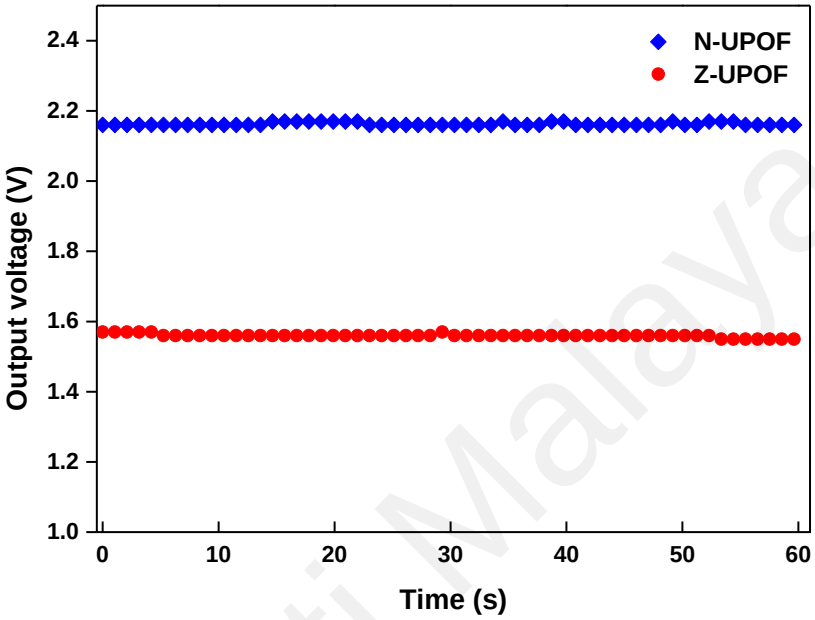

(a)

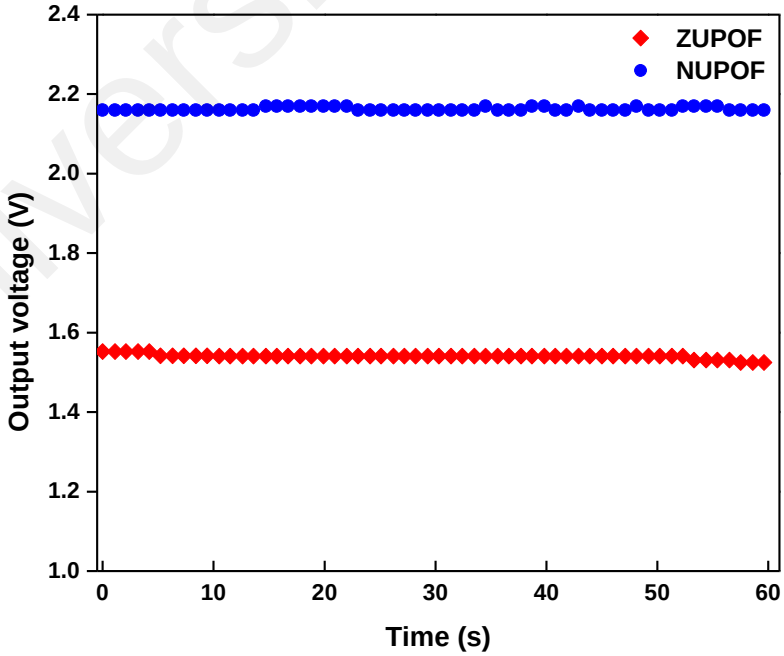

(b)

Figure 4.13: N-UPOF and Z-UPOF voltage stability during (a) the 1st day and (b) 10th day.

Table 4.2 summarizes the characteristics of N-UPOF and Z-UPOF sensors. Both sensors (N-UPOF and Z-UPOF) showed superiority in terms of sensing performance with > 99% linearity. The standard deviation and resolution were found to be 0.0619 V and 3.1958 % RH for the Z-UPOF, while N-UPOF obtained 0.1157 V and 7.3233 % RH respectively. This is because the Z-UPOF enhanced the interaction between the sensing region and the environment, thus significantly increasing the sensing response (Saeed Azad et al., 2017). It was found that the sensitivity and resolution of the Z-UPOF sensor improved by a factor of 1.23 and 2.18, respectively compared to the N-UPOF.

Table 4.2: Characteristics of N-UPOF and Z-UPOF sensors

Parameters	N-UPOF	Z-UPOF
Average standard deviation (V)	0.1157	0.0619
Resolution (%)	7.3233	3.1958
Sensitivity (V/%RH)	0.0158	0.0194
Linearity (%)	>99	>99

4.3 Humidity Sensing using a Tapered U-shape POF Coated HEC/PVDF

HEC/PVDF is a stable, inexpensive, and relatively common composite. It can be utilized as coating to improve RH sensing of fiber sensors due to its absorbent nature which possesses a great ability to absorb water. The coating refractive index changes since the HEC/PVDF gel coating absorbs water, rendering the sensing construction more sensitive to the air RH variations. In this section, the performance of an optimized tapered (500 µm) U-shape POF coated with HEC/PVDF is investigated as a relative humidity sensor. The sensor operation is based on intensity modulation technique, using a tapered POF probe coated with a polymer blend of HEC/PVDF composite that acts as the humidity sensitive cladding or transducer. The tapered POF was coated with HEC/PVDF, via a sol-gel immersion method before it was dried in air for 24 hours forming a coating layer in the U-shape structure, as described in the previous chapter.

In this section, the RH sensing performance is investigated at three different wavelenghts of LED: 645, 530 and 470 nm. The LED was power up by Arduino Uno controller to transmit light through the fiber and detected by phototransitor. The phototransitor converts the output light into electrical quantities in the form of voltages. The output voltages are then amplified by a differential amplifier and the analog signal from the photodetector is converted into a digital signal by the Arduino Uno microcontroller. The working principle of the humidity sensor is based on HEC/PVDF coating onto POF, which functions as a tranducer to change a transmitted light intensity due to the changes of light scattering effects inside the fiber. This is because the HEC/PVDF refractive index changes when it is exposed to changes in humidity levels. Changes in RH levels result from the changes in the refractive index around the sensor. In this experiment, the proposed sensor was exposed to %RH levels from 35% to 90% inside the controlled chamber at a fixed temperature at 24 ºC. The previous method used to lower and higher the RH level inside the chamber was duplicated in this experiment. Figure 4.14 show the experimetal set-up of humidity sensing for the tapered U-shaped POF coated with HEC/PVDF. The proposed setup is similar to that of the ZnO coated sensor described in the previous section.

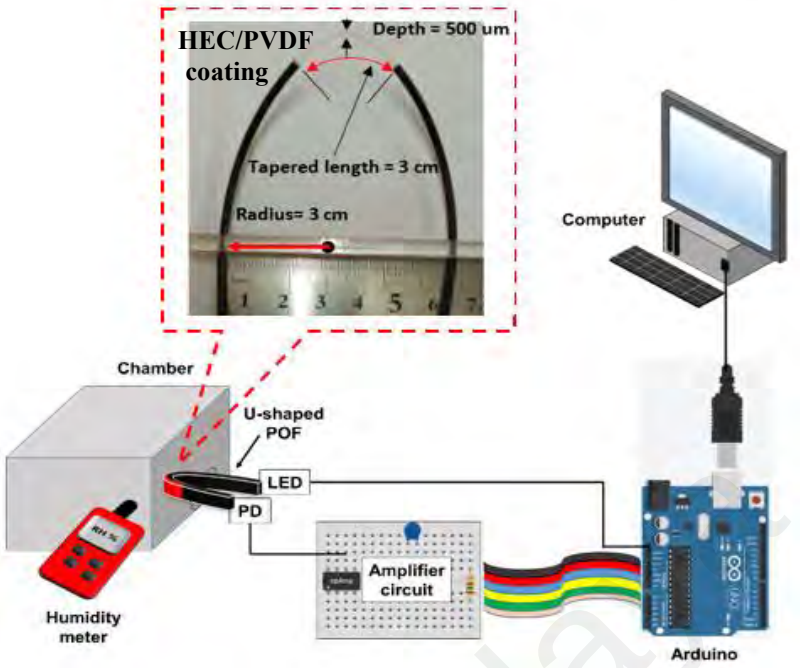

Figure 4.14: Experimental setup for humidity sensing with HEC/PVDF coating

The trendline graphs of the humidity sensor when the RH changes from 35% to 90% at three different wavelengths are presented in Figure 4.15. The output voltage increases exponentially in exposure to humidity levels for all graphs. HEC/PVDF consists of hydroxyethyl cellulose and polyvinylidenefluoride compound, which is a relatively common and inexpensive 3-D mesh gel material with transparent porous structure. These pores absorb water molecules from the air when the relative humidity increases. Thus, the refractive index of the coated area of the POF increases with the exposure of higher RH level to the sensor probe. The increase of index contrast in the POF waveguide structure reduces the propagation loss inside the sensing structure. Consequently, the sensing structure shows a trend of lower losses with increasing relative humidity, as shown in Figure 4.15.

A similar trend was also obtained with previous results of a humidity sensor using HEC/PVDF (Batumalay et al., 2013; A Lokman et al., 2015). It is observed that the intensity of the transmitted light of the HEC/PVDF composite on tapered POF increases

with relative humidity in a quadratic manner. The voltage difference produced by the proposed sensors is 1.58 V, 1.17 V and 0.49 V for wavelengths of 645 nm, 530 nm, and 470 nm, respectively. The 645 nm wavelength showed the highest voltage difference, followed by the 530 nm and 470 nm wavelengths. This indicates that the longer wavelengths provide higher sensitivity compared to the shorter wavelengths. This is attributed to the scattering loss, which is lower at longer wavelengths.

The HEC/PVDF has a higher refractive index than the core of POF when in a dry state, creating a higher light confinement which, in turn, increases the intensity of the light propagating through the U-shape POF (Yeo et al., 2008). As a result, a constant increase of output voltage was obtained at a RH range from 35% to 50%. However, the output voltage starts to increase exponentially when the RH level was further increased from 55% to 90% RH. This could be due to the HEC/PVDF which starts to swell when it is exposed to a humidity higher than 55% RH. When the HEC/PVDF layer hydrates, the refractive index value slightly increases, and it further confines the intensity of light propagating through the POF. The reaction mechanisms that contributed to this trend are the absorption of water vapor, swelling, alteration in coating thickness and change in refractive index (Rao et al., 2021). The adjusted R-squared value or the coefficient of the determination is the measure of the goodness of fit. It was obtained at values of 0.998, 0.998, 0.991 with the use of light source operating at 470 nm, 530 nm, and 645 nm, respectively. The considerably high values of the adjusted R-squared allow the prediction of unknown relative humidity by the model.

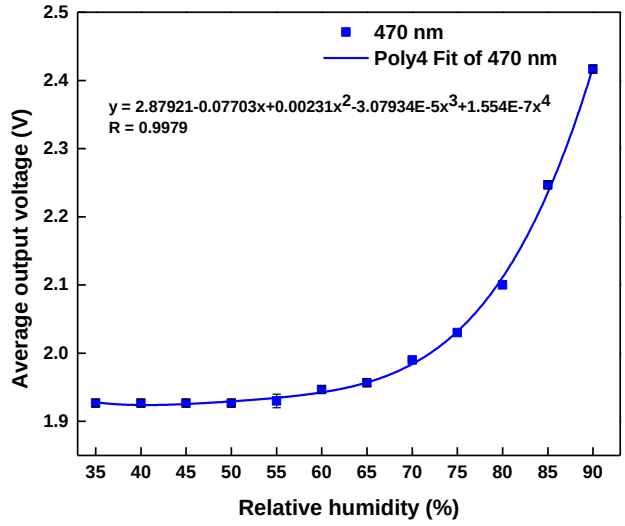

(a)

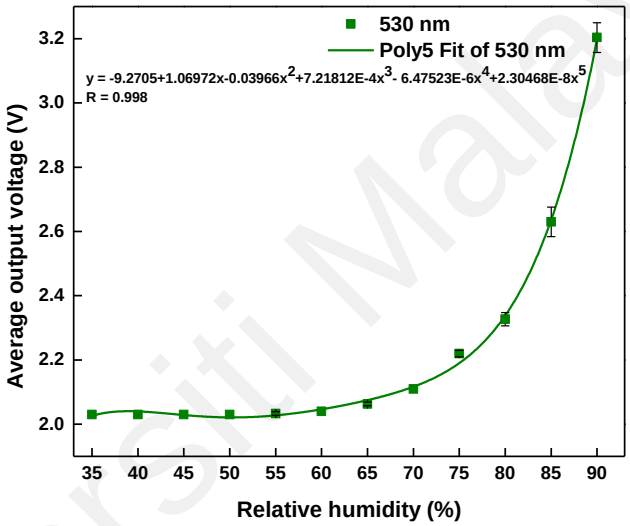

(b)

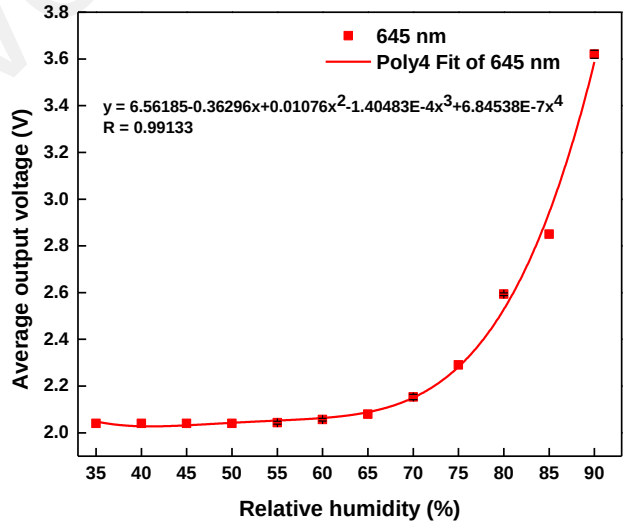

(c)

Figure 4.15: The trendline graphs of the humidity sensor when the RH changes from 35% to 90% at three different wavelengths (a) 470 nm (b) 530 nm and (c) 645 nm.

Based on Figure 4.16, the sensitivity of the sensor is investigated over two different humidity ranges, 40-70 %RH and 70-90 %RH in order to observe the sensitivity characteristic at lower and higher humidity. Within 40 to 70 %RH, the sensor sensitivities were recorded at 0.4 V/%RH, 0.3 V/%RH and 0.1 V/%RH for the use of 645 nm, 530 nm and 470 nm light sources, respectively. Significantly higher sensitivities of 0.0733, 0.0547 and 0.0152 V/%RH were obtained within 70 to 90% at wavelengths of 645 nm, 530 nm, and 470 nm, respectively. This is because the optical properties, such as refractive index and light absorbance, of HEC/PVDF change as it absorbs moisture from the environment (Hirai et al., 2023).

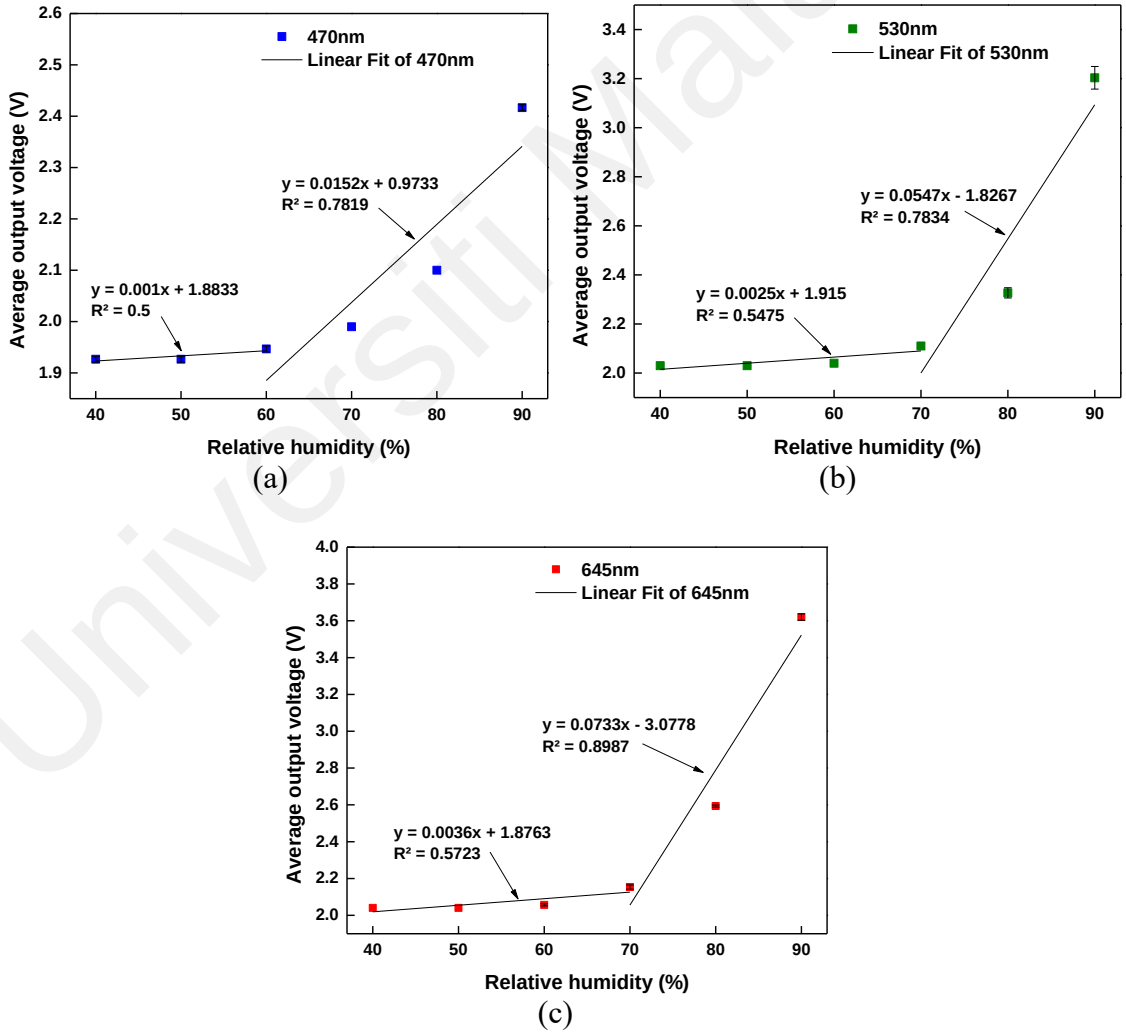

Figure 4.16: Sensitivity of HEC/PVDF based humidity sensor at three different wavelengths (a) 470 nm (b) 530 nm and (c) 645 nm.

Repeatability test of the proposed sensor were evaluated at multiple wavelengths of 470 nm, 530 nm, and 645 nm. The sensor was tested three times continuously at each wavelength, with adsorption procedure and plot the data. The repeatability of the proposed sensor is seen to be excellent, as the output voltage is recorded throughout the RH level as seen in Figures 4.17 (a), (b) and (c) for a signal wavelength at 470 nm, 530 nm, and 645 nm, respectively. The lowest percentage error was recorded at 0.11% when it tested at 645 nm wavelength.

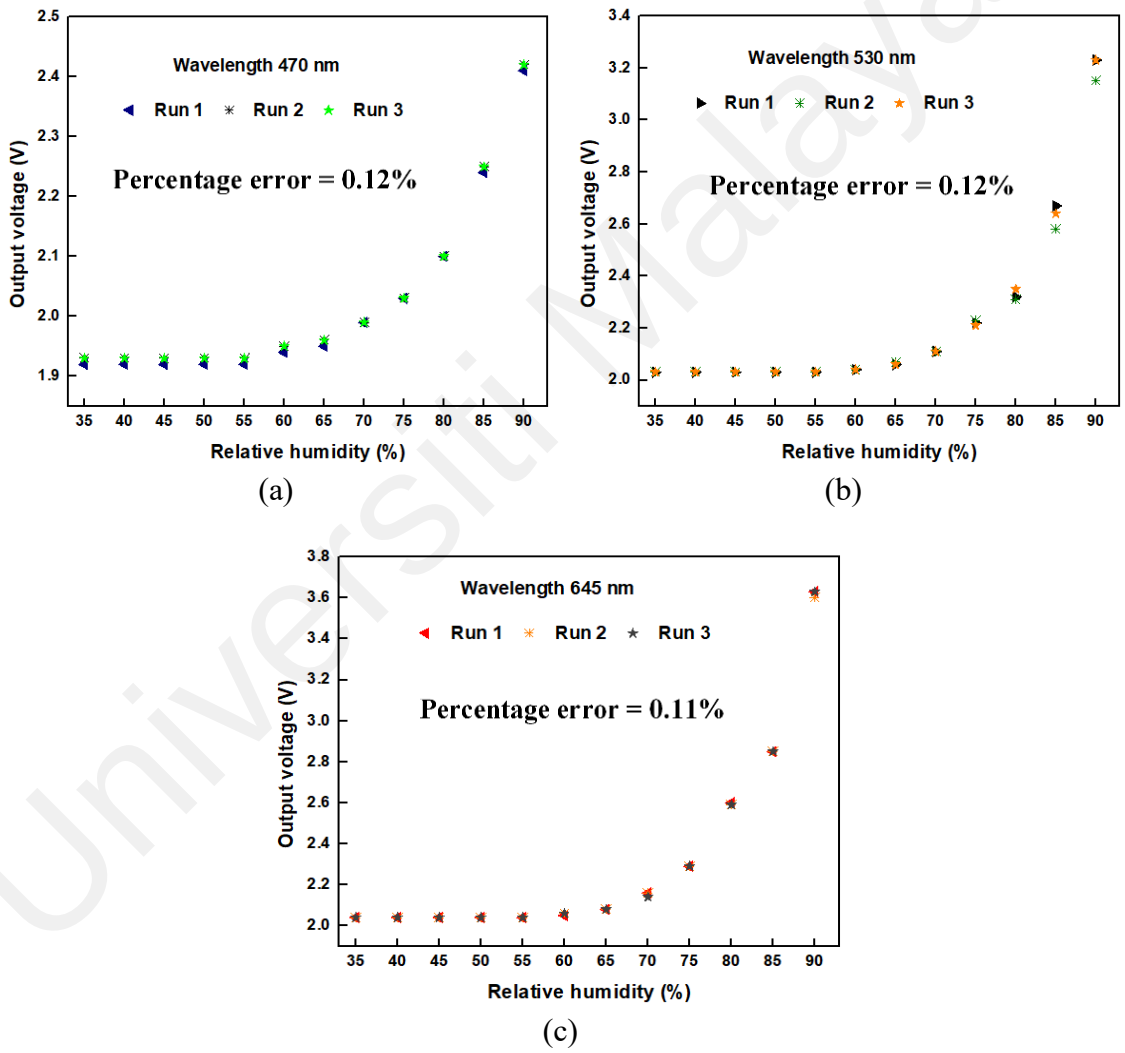

Figure 4.17: Repeatability test results for the HEC/PVDF based humidity sensor.

Figure 4.18 shows the hysteresis of the humidity sensing with tapered U-shape POF coated with HEC/PVDF at three different light source wavelengths. The sensing response was observed as the RH level was increased and then reduced. Based on the Figures 4.18 (a), (b) and (c), the adsorption and desorption of RH graphs for all wavelengths show a good hysteresis pattern. The errors are only observed at high RH levels due to the fast change of humidity levels during the measurements. This indicates that the absorption and outgoing of water characteristics of humidity sensitive material HEC/PVDF at different relative humidity levels remain the same (Xia et al., 2013).

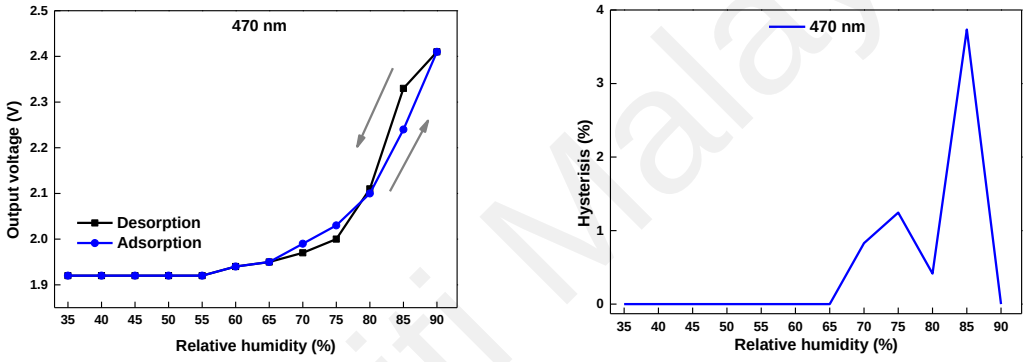

(a)

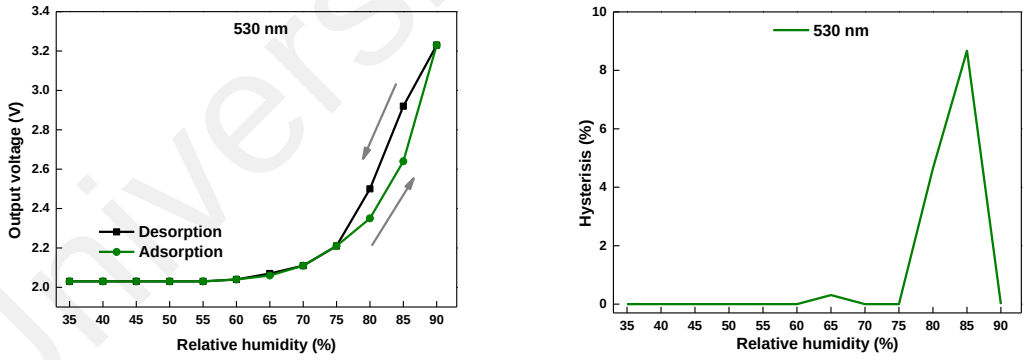

(b)

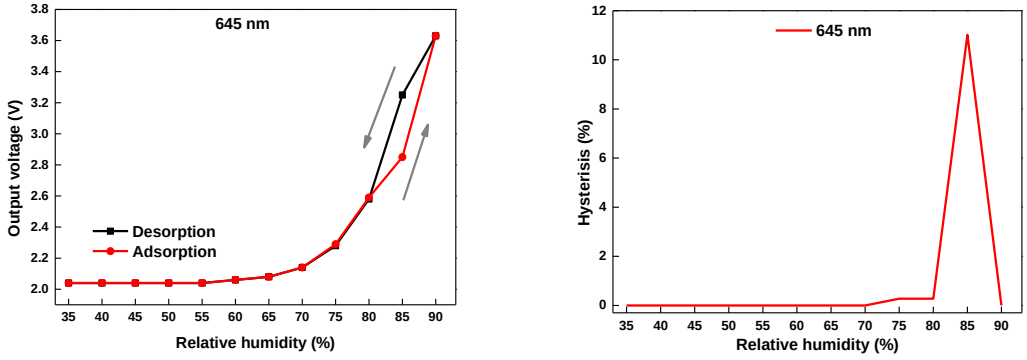

(c)

Figure 4.18: Reversibility test result for the HEC/PVDF based humidity sensor.

The HEC/PVDF based humidity sensor was also tested for voltage stability by exposure to 50% RH, where the output voltages were recorded continuously for 180s. As shown in Figure 4.18, the proposed sensor shows the ability of the sensor to maintain its performance characteristic for a certain period of time at three different light source wavelengths. Table 4.3 summarizes the performance of the HEC/PVDF based humidity sensor at three different LED wavelengths. It is found that the use of a longer wavelength light source (645 nm) exhibits the superior sensing performance. The highest sensitivity of 7.3 V/%RH was recorded with the smallest standard deviation of 0.0034 V.

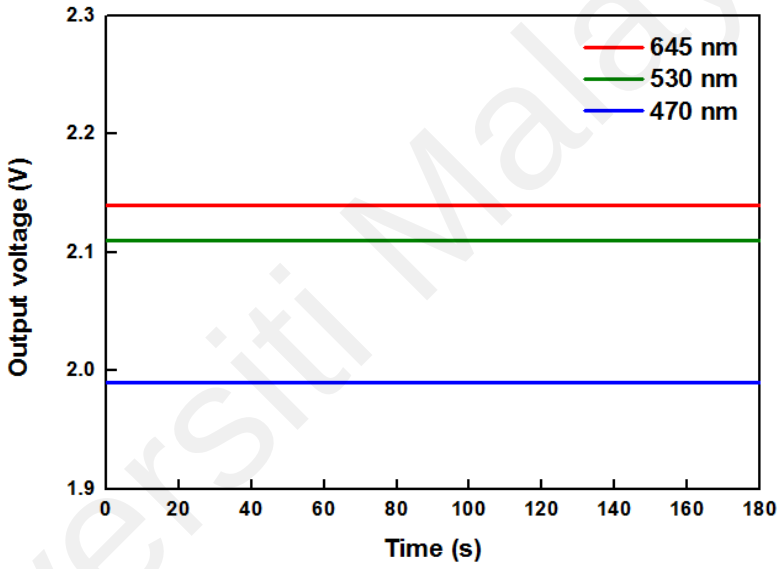

Figure 4.19: Stability test result for the HEC/PVDF based humidity sensor.

Table 4.3: Sensing performance of the HEC/PVDF based humidity sensor configured at three different LED wavelengths.

Parameters	470 nm	530 nm	645 nm
Average standard deviation (V)	0.0043	0.0107	0.0034
Voltage differences (V)	0.49	1.17	1.58
Sensitivity within a range from 40-70 %RH (V/%RH)	0.001	0.0025	0.0036
Sensitivity within a range from 70-90 %RH (V/%RH)	0.0152	0.0547	0.0733

4.4 Summary

A relative humidity (%RH) sensor was successfully developed and optimized using a tapered U-shaped POF coated with zinc oxide nanorods or HEC/PVDF as a sensing probe using relative humidity. By coating ZnO nanorods on tapered POF via a hydrothemal method, the sensor performance greatly improved when compared to the N-UPOF. The sensitivity and resolution of the Z-UPOF sensor improved by factors of 1.23 and 2.18, respectively compared to the N-UPOF. For three source wavelengths of 470 nm, 530 nm and 645 nm, the output voltage of the sensor was inversely proportional to %RH in the range of 35% to 90% RH. The proposed sensor produced the best sensitivity of 0.0231 V/%RH at 645 nm wavelength, with a slope linearity of 99.47% and fast response and recovery times of 61 s and 68 s respectively. On the other hand, the HEC/PVDF based humidity sensor exhibited the highest sensitivity of 0.0733 V/%RH with the smallest standard deviation of 0.0034 V when the LED wavelength of 645 nm was used. This study showed that the proposed sensors were simple to fabricate with the advantages of small size and good repeatability, all of which are useful for %RH sensing applications. The results showed that a wavelength of 645 nm was the best source wavelength. Table 4.4 show the summary of plastic optical fiber towards humidity sensing at recent development and proposed work. The proposed sensor with ZnO nanorods in U- shape structure offers better sensitivity compare to the straight structure but moderate sensitivity, similar to other ZnO coated sensors.

Table 4.4: Summary of plastic optical fiber towards humidity sensing at recent development and proposed work

No	Type	Sensitivity performances	Coating materials	References
1	Proposed sensor	0.0248V/%RH	Zinc oxide (ZnO) nanorods	
2	Straight, centrally decladded POF	0.3041 dB/% RH	Multiwalled carbon nanotube-doped chitosan	(Mohan & Negi, 2024)
3	Single-mode tapered fiber	0.19 dB/% RH	Sodium polyacrylate (SPA)	(Li et al., 2024)
4	Twisted, micro-bend (TMB-1 and TMB-2)	Sensitivity: TMB-1 = 680.8 nW/%RH, TMB-2 = 763.9 nW/%RH;	Chemical coating	(Hussian et al., 2024)
5	Combination of Macro and Micro Bendings	Sensitivity increased 10-fold with combined bending	-	(Kuswanto et al., 2022)
6	Loop, Tapered POF	0.0285 V/%RH at 470 nm	Zinc oxide (ZnO) nanorods	(Hisam et al., 2022)
7	Straight fiber	0.0057 V/%RH	Silicone oil	(Waluyo et al., 2022)
8	U-bent plastic optical fiber	Sensitivity of 0.0316 O.D./ppm	Iron	(Ashraf et al., 2022)
9	U-shaped POF	0.17×10^{-2} % RH^{-1}	Polyimide (PI) and graphene oxide (GO) layers	(Zhong et al., 2020)
10	Straight, Tapered POF	0.0295 %/mV	Zinc oxide (ZnO) nanorods	(Harith et al., 2020)
11	Macro-bending biconical tapered POF	1.60 mV/% (10-45% RH) and 3.40 mV/% (45-90% RH)	Fluorescent moisture-sensitive film	(Guo et al., 2019)

CHAPTER 5: TAPERED U-SHAPE PLASTIC OPTICAL FIBER COATED WITH ZINC OXIDE NANORODS FOR FORMALDEHYDE SENSING APPLICATION

5.1 Introduction

Formaldehyde (HCHO) is a colorless, rapidly polymerized gas at ambient temperature which pollutes both indoor and outdoor air (Y. Wang et al., 2020). Most of us use formaldehyde containing products on a daily basis. It is found in many items; including fabrics, foods, disinfectants, photo processing chemicals, preservatives and even beauty products (Fappiano et al., 2022; Mahmudiono et al., 2022). In addition, some furniture and construction materials containing the resins urea-formaldehyde (UF) and phenol-formaldehyde (PF). Besides being a polymerized gas, formaldehyde is also very easy to dissolve in water (H_2O). As a result, the synthesis of a diol ($CH_2(OH)_2$) was presented, namely formalin, which is an aqueous solution (37% by mass) of formaldehyde.

Formaldehyde is a highly toxic and volatile organic compound (VOC) which becomes dangerous to humans when concentrations are above a certain level. Considering this issue, the World Health Organization (WHO) published a recommendation for safe exposure settings, specifying that a concentration of 0.08 ppm should not be exposed for more than 30 minutes indoors (Aung et al., 2021). The World Health Organization has determined that formaldehyde is teratogenic, and the International Agency for Research on Cancer has classified it as a human carcinogen (IARC) (Faria et al., 2022; Omotayo et al., 2019; Ying Zhang et al., 2022). Dizziness, fatigue, headaches, and irritation of the skin, nose, eyes and throat have all been reported as temporary symptoms. However, if the "sick building syndrome" continues to be exposed in everyday life, major health problems may arise. Furthermore, when combined with protein, it increases the risk of allergy asthma, nausea and edema. Continuous exposure may cause injury to the central

nervous, respiratory, blood and immunological systems, as well as pneumonia, bronchospasm and cancer in humans.

Several formaldehyde detection methods have been proposed and demonstrated in previous studies, including cataluminescence (K.-W. Zhou et al., 2018), spectroscopy (Ge et al., 2021), bio-sniffer (Toma et al., 2021) and chemiresistor (Yun et al., 2021). However, these detection methods necessitate bulky size of equipment, which results in a greater running cost. Some of the methods utilized also need high temperatures to work, which requires more electricity. Due to this disadvantage, a fiber-optic sensor is prefered in recent sensing applications since it can be operated at room temperatures and is immune to EMI (Suhantoro & Yulianti, 2021; Waluyo et al., 2022). In addition, due to low cost sensor fabrication (Cennamo et al., 2011; Ghaffar et al., 2021) and strength in mechanical properties (L. Liu et al., 2021; Yulianti et al., 2021), many works have also been focused on the use of POF.

To date, many researchers have shown interest in nanomaterial based sensor devices by virtue of their mechanical and electrical properties (M. Liu et al., 2021), unique optical qualities (Hassan et al., 2021), and suitability for a wide range of applications including gas sensors, photocatalysis, superconductors and optoelectronic devices (Hassan & Najim, 2021; Sharma et al., 2022; Wu et al., 2019). Owing to this, a variety of nanomaterials from semiconductor metal oxides, including ZnO (Chakrabarti et al., 2020; Jali, Abdul Rahim, et al., 2019; Noorasid et al., 2021), tin oxide (SnO_2) (Keley et al., 2021), titanium dioxide (TiO_2) (Nguyen et al., 2021), indium oxide (In_2O_3) (Devi & Singh, 2021) and nickel oxide (NiO) (John et al., 2022) have been used to fabricate gas sensors. However, ZnO has higher electrical compatibility and biocompatibility (Vijjapu et al., 2020), as well as high chemical stability (Jeong et al., 2020). In addition, ZnO nanorods are a practical material among researchers due to huge advantages such as

simple preparation (Eskikaya et al., 2022) and low-cost (Nataraj et al., 2022). Furthermore, due to its excellent optical transparency and ability to work within the visible range, ZnO is suited for optoelectronic applications (Hassan & Najim, 2021).

In the previous chapter, a tapered U-shape POF coated with ZnO nanorods was developed for humidity sensing. This chapter reports a tapered U-shape POF coated with ZnO nanorods for formaldehyde vapor sensing at 26 ºC. The hydrothermal technique was utilized to grow ZnO nanorods on the 500 µm waist diameter of tapered POF before the fiber was bent into a U-shape, as described in Chapter 3. The variations of output voltage were recorded on the microcontroller as the changes in light intensity were guided in the POF. By enhancing its effectiveness for monitoring in hazardous environments where minimal or abrupt gas leaks may occur (Chen et al., 2019; Jo & Park, 2016), the proposed sensor was exposed to formaldehyde vapor concentrations ranging from 5 to 20% at room temperature utilizing a working wavelength of 645 nm.

5.2 Preparation of Sensor Probe and Formalin Concentration

The standard POF model SH4001 Super Eska was used in this work. It was tapered to reduce the waist diameter to 500 µm. A hydrothermal technique was the used to grow ZnO nanorods on the tapered region. Prior to initiating the growth process, the tapered region was treated with a ZnO nanocrystallites deposition method during the seeding process. The seeding solution was made by mixing zinc acetate dihydrate ($Zn(CH_3COO)_2$) and ethanol. Then, the solution was mixed with pH control solution, which is formed by mixing sodium hydroxide and ethanol. Thus, the deposition of ZnO nanocrystallites begins by immersing the fiber sample in the seeding solution and stirring the solution at a 200 rpm speed. Finally, the seeded fiber was annealed for 3 hours at 70 ºC on the heater before initiating growing activity. Throughout the growth phase, a synthesis solution of 10 mM zinc nitrate hexahydrate ($Zn(NO_3)2H_2O$) and

hexamethylenetetramine ($(CH_2)6N_4$) was utilized. The seeded fiber was immersed in the synthesis solution and then dried for 12 hours at 90 ºC in the oven. The synthesis solution was replaced every 5 hours with a new solution to maintain a uniform rate of ZnO growth. The preparation of tapered POF, seeding and growth processes were thoroughly described in Chapter 3. After the process was completed, both of fiber tips were inserted into a plastic holder to form a U-shape structure with a radius of 3 cm. Figure 5.1 show the tapered U-shape fiber coated with ZnO nanorods, which will be used in formaldehyde vapor sensing.

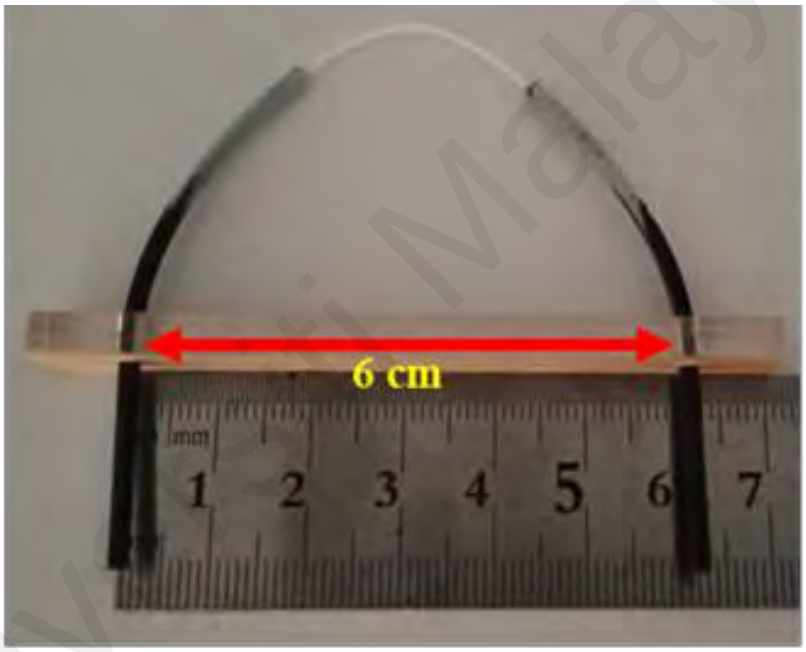

Figure 5.1: Tapered U-shape fiber coated with ZnO nanorods, which was bent at a radius of 3 cm.

The proposed formaldehyde vapor sensing is based on the chemisorption concept. The refractive index exposed to the proposed sensor was higher than pure water vapors (> 1.333). The value of refractive index varies depending on the formalin concentration. Therefore, formalin solutions with various concentrations are prepared in this work.

The formalin concentration was measured by diluting the formaldehyde with DI water. The required concentration was calculated using the following formula (Jali, Abdul Rahim, et al., 2019).

$$M1V1 = M2V2 \tag{5.1}$$

where $M1$ specifies the molarity concentration of the concentrated solution, $V1$ specifies the volume of the concentrated solution, $M2$ specifies the molarity concentration of the dilute solution and $V2$ specifies the volume of the dilute solution. The total concentration volume (100 ml) was fixed for each concentration at 5, 10, 15, and 20% to preserve reliability throughout the test. Then, to confirm the final mixture of DI water and formaldehyde, the refractive index of each concentration was measured using a refractometer (from PAL-RI, Atago, Japan). Table 5.1 shows the refractive index of each formalin concentration. Since formaldehyde has a slightly higher refractive index number, the substance can only be detected when it is fully evaporated at a high humidity level, assuming the environment is fully covered by humidity and formalin vapor.

Table 5.1: Formalin concentration and refractive index

Formalin concentration (%)	Refractive index
0	1.3326
5	1.3382
10	1.3444
15	1.3502
20	1.3558

5.3 Experimental Setup for Formaldehyde Vapor Sensing

Figure 5.2 presents the experiment setup for formaldehyde vapor sensing. The tapered fiber waist diameter of 500 µm was placed inside the controlled chamber with a size of 0.13 m x 0.9 m x 0.6 m. Then, an LED light source (from Industrial Fiber Optics, USA) with a 645 nm wavelength was used to investigate the output voltage of the sensor when

it was exposed to different formalin concentrations. A temperature and humidity meter (Model UT333S, Uni-Trend Technology, China) were mounted within the chamber to provide a reference of formalin spread level. Firstly, the controlled chamber was set at 55 % at a 26 ºC of humidity level to duplicate the real user environment. Following that, 30 ml of formalin was poured into the beaker and allowed it to naturally evaporate and spread throughout the chamber. Then, the mixture of formalin and water will cause the environment to be filled with humidity and formalin concentration when it is fully evaporated. In this case, we use humidity with 0 % formalin concentration as a reference to distinguish between formalin concentrations. Thus, the humidity level will increase regularly throughout this period because water from the solution is readily available. The output voltage was measured when the humidity meter displayed 80, 85 and 90%. This procedure was conducted for formalin concentrations of 5, 10, 15, and 20%, and the results for each concentration were compared to 0% (DI water). A phototransistor (Model IF-D92, Industrial Fiber Optics, USA) was used to detect voltage changes and record in the computer using Arduino platform. During formalin exposure, adsorption, and desorption of formalin vapor on the ZnO surface alters the refractive index of ZnO, which modifies the light scattering pattern inside the fiber and changes the output voltage (Yusof, Harun, et al., 2019; Huda Adnan Zain et al., 2020). The strategy for detecting with ZnO nanorods was based on how the refractive index and electrical conductivity of the area around the rods changed during the absorption process (Samavati et al., 2019).

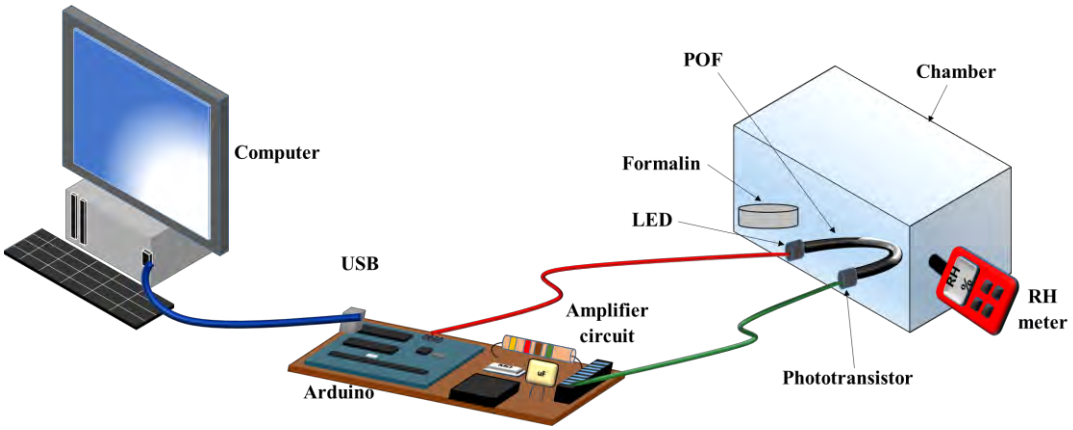

Figure 5.2: Experimental set-up for formaldehyde sensing

5.4 Sensing Performance

The formaldehyde vapor sensing response against humidity for five different formalin concentrations is shown in Figure 5.3. RH values ranging from 80% to 90% were used to examine the distribution of the formaldehyde vapor throughout the chamber. According to the graph, the proposed sensor responded linearly to changes in formaldehyde vapor concentration caused by the ZnO light scattering effect inside the fiber. This is attributed to ZnO, which has good electrical conductivity. It attracts the formalin molecules to increase the effective refractive index in the ZnO coating around the fiber (M. Jali et al., 2021). Therefore, higher light loss leakage at the sensor area and a drop in output voltage were observed when higher formalin concentration was exposed to the sensor. When the sensor was exposed to a separate formaldehyde vapor concentration, the RH level at 90% demonstrated a significant increase in voltage difference, as shown in Figure 5.3. As a result, the chamber was considered completely saturated with vapor at this RH level.

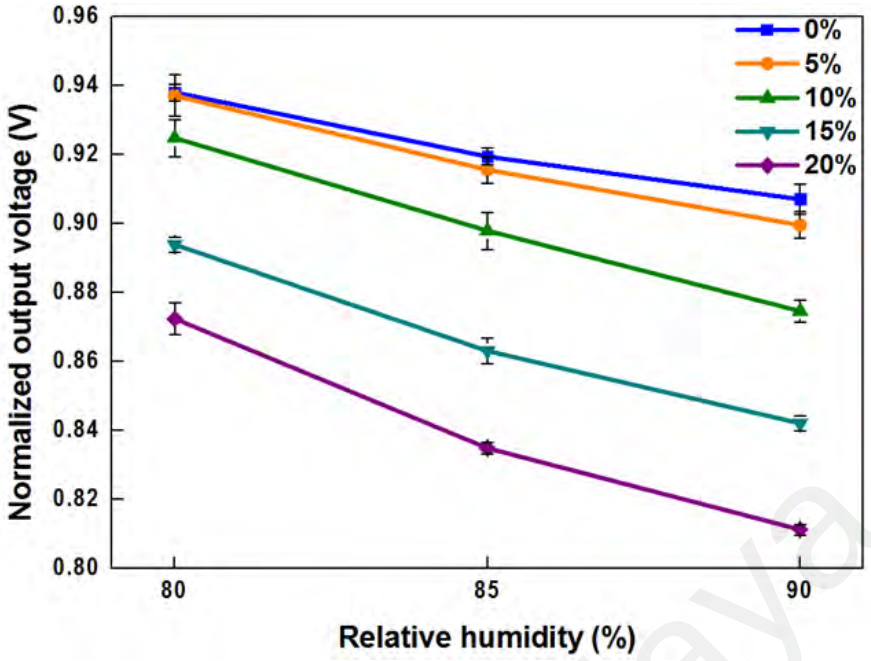

Figure 5.3: Formaldehyde vapor sensing response

Figure 5.4 shows the voltage difference observed for various formalin concentrations ranging from 0% to 20% at three different humidities; 80, 85 and 90% RH. According to the bar graph, the voltage variations do not significantly affect the 0% to 10% formalin concentrations at 80% and 85% RH, respectively. This could be due to the formalin content not entirely changing to formaldehyde vapor. The gas concentration reflected by the change in conductivity is significantly affected by the subsequent desorption of reaction products and the catalytic dopant (Jali, Rahim, Johari, Yusof, et al., 2019). As a result, the voltage difference for 0% to 20% of formalin concentration demonstrated a significant increment when the RH level reach at 90%. At this time, the chamber could be considered to be completely saturated with vapor. Furthermore, natural evaporation of formalin takes a long time, therefore the occurrence of saturated vapor was validated by measuring the drop in output voltage at 90% RH compared to DI water. Table 5.2 shows a significant drop in output voltage for formalin concentrations ranging from 5% to 20%. The total output voltage drop was detected at 0.0958 V when the sensor was exposed to a higher concentration of 20%.

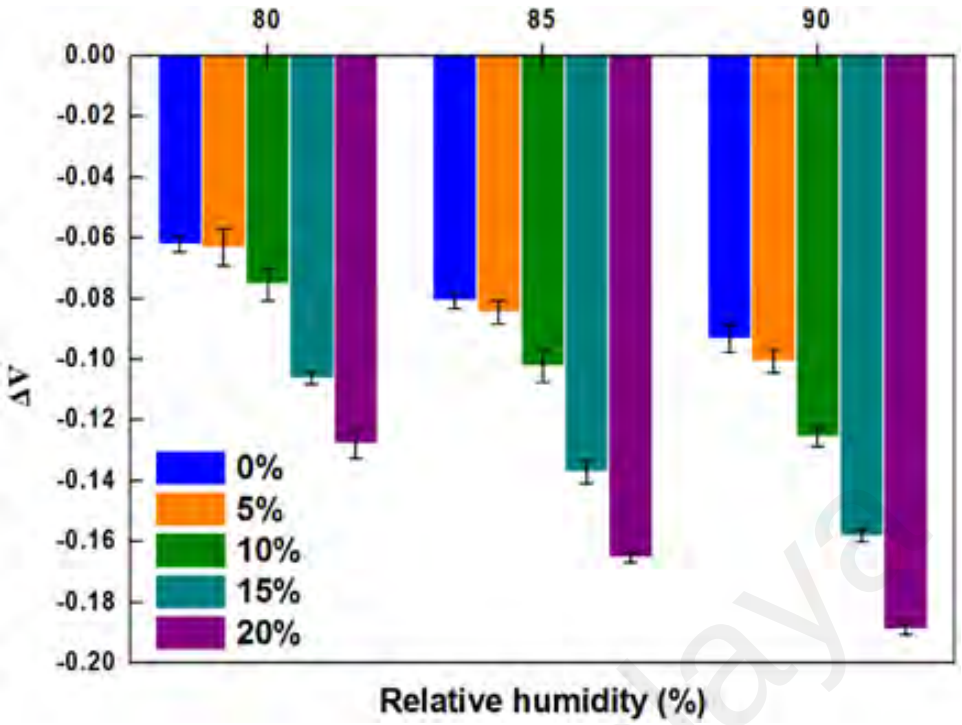

Figure 5.4: Voltage difference of 0% to 20% formalin concentration at 80% to 90% RH

Table 5.2: Reduction of output voltage at 90 % RH

Formalin concentration (%)	ΔV (V)
5	-0.0075
10	-0.0324
15	-0.0650
20	-0.0958

Figure 5.5 illustrates the stability performance of 0% to 20% formalin concentration in 600 s at 90% RH. In this experiment, all the formalin concentrations produce stable output voltage, with the slopes ranging between 8.53975e-9 to 9.50776e-7. These numbers are very small and very reasonable for such a sensor system. As a result, the proposed sensor shows the ability of the optical fiber sensor to maintain its performance characteristic for a certain period of time (Golnabi & Azimi, 2007). The measurement of the separate formalin concentration also revealed excellent stability while the relative humidity remained constant at 90%. It is also worthy of note that the gas sensing response

was enhanced by the high humidity. This meant that the humidity level was saturated when the formalin concentration was fully spread throughout the chamber with a low tendency to the absorption process. This observation on stability further confirms the presence of water in formalin.

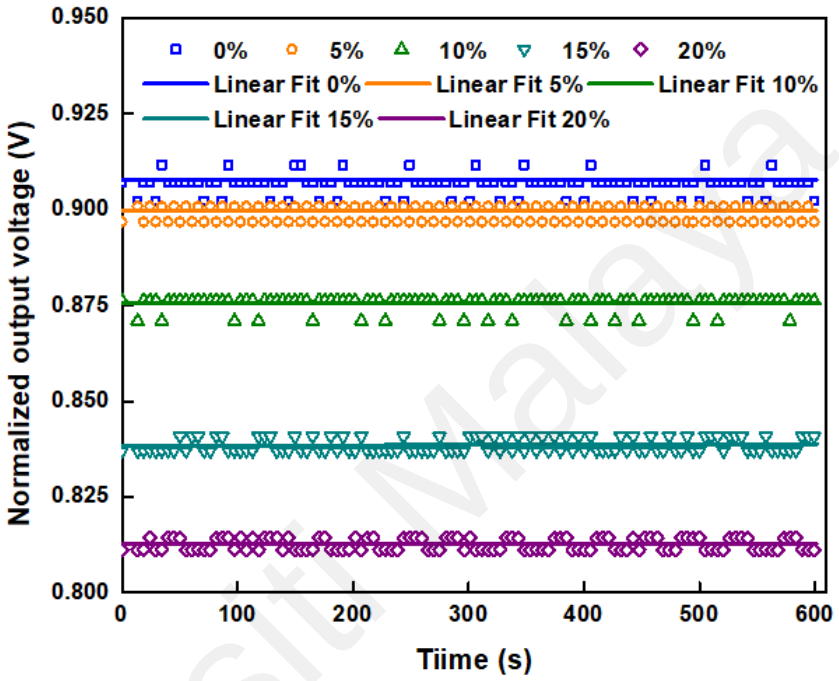

Figure 5.5: Stability performance of 0% to 20% formalin concentration in 600 s at 90% RH

Figure 5.6 presents the proposed sensor performance at 90% of the RH level. According to the graph, the output voltage decreases as the formalin concentration increases. This behaviour is in accordance with findings reported in work done by (Yusof, Jali, et al., 2019). The plot of formalin with 0% concentration was distant from the linear fit line because it operates as a zero reference that is unaffected by formalin. The proposed sensor was determined to have an average linearity of 98.58%, as shown in Table 5.3. Furthermore, the sensor has a sensitivity of 0.00543 V/% and can detect formaldehyde vapor concentrations above 5% with a standard deviation of 0.00746 V.

Due to their high surface-to-volume ratio, zinc oxide nanorods are capable of increasing the adsorption of vapor molecules on their surface (Shooshtari et al., 2022). According to Table 5.1, when the formalin concentration increases, the refractive index value also increases. Therefore, during the adsorption process, the vapor modulates the refractive index around the ZnO nanorods, hence altering their electrical conductivity. The refractive index of ZnO was changed as the electrical conductivity changed, resulting in changes in light scattering patterns on ZnO nanorods. Here, the effects of higher light leakage are observed when the vapor concentration is increased.

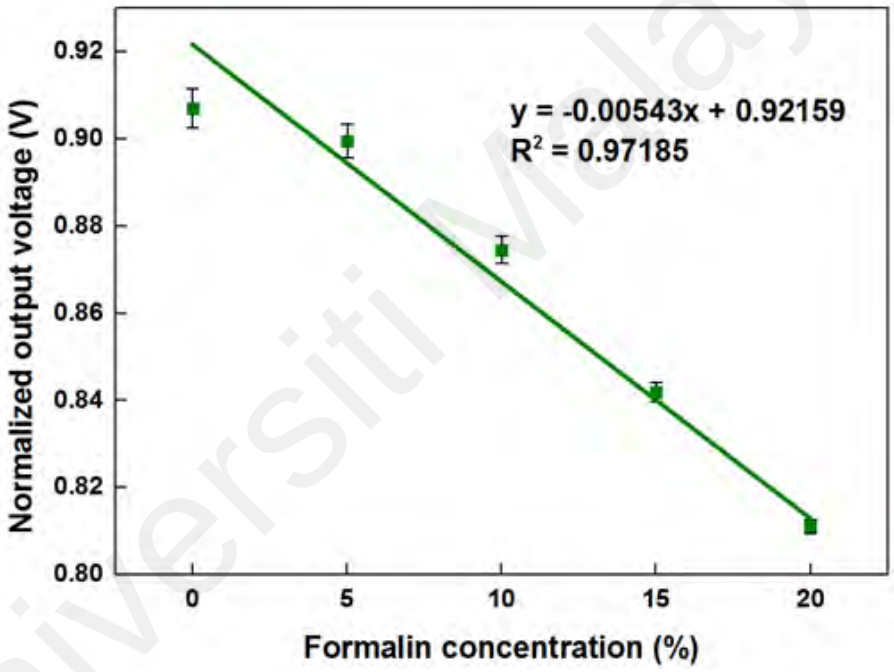

Figure 5.6: Sensor performance at 90% RH

Table 5.3: Characteristics of sensor

Parameters	Performance
Linearity (%)	98.58
Sensitivity (V/%)	-0.00543
Average Standard deviation (V)	0.00746
Resolution (%)	1.37385

5.5 Contributions of Study

The applications of these fiber-optic sensors are wide, including the critical areas of air quality monitoring and physiological condition assessment, among others. In air quality monitoring, fiber optic sensors can detect pollutants and hazardous compounds, offering a reliable tool for environmental protection efforts and public health. In this area of food safety, sensors play a very critical role in detecting contaminants such as formaldehyde in seafood and preservatives in milk, hence maintaining product integrity and protecting consumers. Fiber optic sensors can also be used to monitor vital signs, breath humidity, and biochemical markers in medicine and physiology, which makes them very important in non-invasive health monitoring and in the creation of wearable technology. These technological advances not only make fiber optic sensors more precise and responsive but also increase their adaptability to specific application requirements. These enhancements in accuracy, versatility, and cost-effectiveness enable wide use in the fields of scientific research, industrial monitoring, health care, and consumer product sectors, hence fostering safer and more efficient methodologies within each area.

5.6 Summary

Continuous exposure to formaldehyde may cause injury to the central nervous, respiratory, blood and immunological systems. Tapered U-shape POF coated with zinc oxide nanorods was successfully evaluated at a wavelength of 645 nm for formaldehyde vapor sensing within concentrations ranging from 5% to 20%. The tapered POF with 500 μm waist diameter was prepared using the chemical and mechanical etching techniques. Zinc oxide nanorods were synthesized using the hydrothermal method and grown for 12 hours on the tapered POF. The fabricated sensor exhibited a substantial sensitivity to concentrations ranging from 5% to 20%. The decrease in output voltage was determined to be 0.0958 V for the concentration at 20%, with comparison to 0% which is DI water.

This was due to the increasing scattering effect of ZnO nanorods at 20% of formaldehyde concentration. The sensor response demonstrated an excellent linearity of 98.58% across all vapor concentrations. The sensor sensitivity was measured to be -0.00543 V/%. Finally, when tested continuously for 600 seconds at a 5% concentration variation, the sensor displayed exceptional stability. This proposed sensor might therefore also be used to detect air pollution produced, not just by formaldehyde vapor, but also by other dangerous or poisonous vapors or gases. Table 5.4 summarizes the development of plastic optical fiber for formaldehyde detection and highlights the proposed research efforts. Few comparative studies can be made because of the different experimental arrangements. However, the proposed sensor based on ZnO nanorods with U-shaped exhibits superior sensitivity.

Table 5.4: Summary of plastic optical fiber towards formaldehyde sensing and proposed work

No	Type	Sensitivity performances	Coating materials	References
1	Proposed sensor	0.00543 V/% formaldehyde	Zinc oxide (ZnO) nanorods	
2	Straight plastic optical fiber	5-fold lower detection limit	None (3D printing filament-based waveguide)	(Darder et al., 2022)
3	Plastic optical fiber	Detection limit: 0.03 to 0.20 ppmv formaldehyde	Nafion® cladding doped with Leuco Fuchsin dye	(del Mar Darder et al., 2022)
4	Exposed fiber tip	Limit of detection: 0.2 mg/L formaldehyde	Polyoxometalate salt [(C4H9)4N]4H[PMo10V2O40]	(Veríssimo et al., 2020)
6	Bent plastic optical fiber	Sensitivity to RI changes of <0.4%	-	(Saracoglu & Hayber, 2016)

CHAPTER 6: CONCLUSIONS AND FUTURE WORK

6.1 Conclusions

Plastic optical fibers (POFs) have received substantial attention in constructing various optical sensor devices due to their advantages; including flexibility, ease of handling, low-cost test equipment, high numerical aperture and visible wavelength operating range as compared to the glass optical fiber. To widen the range of applications, the development of a functional POF was also investigated. This thesis aimed to demonstrate a tapered U-shape POF coated with a sensitive material for humidity and formaldehyde vapor sensing. Four objectives have been outlined to achieve this goal.

The first objective is to fabricate a tapered U-shape POF coated with ZnO nanorods (or HEC/PVDF) for humidity and formaldehyde vapor concentrations sensing. Tapered POF has been successfully fabricated in this study, whereby the waist diameter of POF was reduced by using chemical and mechanical etching technique. The tapering process has been conducted by carefully controlling several elements such as sand paper grit used and hand pressure movement to meet the specific waist diameter at the sensing region. Meanwhile, ZnO growth on the tapered POF for 12 hours has been performed via a hydrothermal synthesis technique. The tapered POF coated with ZnO was then bent into U-shape with radius of 3 cm or 5 cm. To summarize, the first objective was successfully achieved as described in Chapter 3.

The second objective was to optically characterize and optimize the sensing performance by controlling the POF waist with different LED wavelengths at various humidity and formaldehyde vapor concentrations. An optimization approach for selecting the optimum POF waist diameter at different wavelengths has been described in this thesis. The sensing performance of the tapered U-shape POF coated with ZnO nanorods was then optimized by investigating several performance parameters such as output

voltage and sensitivity, based on a humidity sensing scheme used as a baseline for a vapor detection system. Based on experimentation, it was found that the POF tapered waist diameter with 500 μm tested at the wavelength of 645 nm provided an optimum result in all these performance parameters. It is also noteworthy to mention that the smaller waist diameter did not produce better output results, due to the higher light leakage causing less sensitivity. Thus, the waist diameter of 500 μm generates a greater evanescent wave at 645 nm that interacts favorably with environmental changes by producing the maximum voltage difference of 1.28 V. To summarize, the second objective was successfully achieved as described in Chapters 3 and 4.

Precise humidity measurements are vital for many applications including food, agriculture and in electronic industries. The third objective was to demonstrate RH sensing using a tapered U-shape POF coated with ZnO nanorods. The humidity sensing performance of the proposed sensor was validated experimentally by exposing the proposed sensor to humidity concentration levels from 35% to 90% RH. A simple fiber-optic sensor for RH sensing application has been successfully demonstrated using ZnO nanorods coated on tapered U-shape POF (Z-UPOF) in Chapter 4. The Z-UPOF structure greatly improved the sensing performance, when compared to the uncoated tapered U-shape POF (N-UPOF). The sensitivity and resolution of the Z-UPOF sensor improved by factors of 1.23 and 2.18, respectively, compared to the N-UPOF. Besides, the Z-UPOF sensor also exhibited better repeatability properties in terms of output voltage when exposed to 35 to 90%RH for three repeated measurements. The results obtained revealed that the newly proposed POF sensor has excellent sensing performance as an RH sensor in terms of sensitivity, repeatability and stability. To summarize, the third objective has been achieved.

Continuous exposure to formaldehyde may cause injury to the central nervous, respiratory, blood and immunological systems. Therefore, the fourth objective was to demonstrate a formaldehyde vapor concentration sensor using a tapered U-shape POF coated with ZnO nanorods. This sensor probe was evaluated at a wavelength of 645 nm for formaldehyde vapor sensing within a concentration range from 5% to 20%. The tapered POF with 500 μm waist diameter was prepared using chemical and mechanical etching techniques. ZnO nanorods were synthesized using the hydrothermal method and grown for 12 hours on the tapered POF. The proposed sensor exhibited a high response to formaldehyde concentration ranging from 5% to 20% with sensitivity and linearity measured to be 0.00543V/% and 98.58%, respectively. Excellent measurement stability was observed when concentrations from 5% and above were maintained over a 600 second period. The highest difference voltage produced was 0.0958V, due to the greater scattering effect of the ZnO nanorods at 20% of formaldehyde concentration. This proposed sensor has the potential to be also used to detect air pollution produced not just by formaldehyde vapor, but also by other dangerous or poisonous vapours or gases. To summarize, the fourth objective has been achieved. In summary, all four objectives set for this work have been achieved.

The novelty of this thesis lies in the development of a dual function sensing device that combines humidity and formaldehyde vapor detection in a single, compact and portable sensor. Unlike traditional single-function sensors, this device utilizes a tapered U-shaped plastic optical fiber (POF) coated with Zinc oxide (ZnO) nanorods and Hydroxyethyl cellulose/polyvinylidene fluoride (HEC/PVDF), which enhances sensitivity and response time through evanescent wave interactions.

Additionally, this design introduces an innovative application of ZnO nanorods for both %RH and formaldehyde vapor sensing, significantly improving sensor performance

across multiple wavelengths (especially at 645 nm). Additionally, the fabrication process, which employs accessible chemical and mechanical etching techniques, is scalable and more cost-effective, thereby distinguishing it from more complex and costly sensor technologies. This unique approach positions the device as more versatile for environmental and industrial monitoring, with potential expansion to other hazardous gas detection applications, thereby addressing the need for more efficient multi-gas sensors.

The contribution of this device offers enhanced sensitivity and performance by utilizing Zinc oxide (ZnO) nanorods and Hydroxyethyl cellulose/polyvinylidene fluoride (HEC/PVDF) coatings. The sensor then achieves higher sensitivity and rapid response times for both humidity (%RH) and formaldehyde vapor, outperforming traditional sensors. This improvement supports real-time, accurate monitoring, which is essential in applications across food safety, agriculture and electronics.

Also, the scalable and cost-effective design sensor fabrication process uses accessible chemical and mechanical etching techniques, making it more practical for large-scale production. This approach offers a simpler, lower-cost alternative to existing sensor technologies potentially broadening access to effective environmental monitoring tools.

Further, versatility in applications make the device's adaptability to different wavelengths and its capacity to detect other hazardous gases positions a valuable tool for diverse air quality and pollution monitoring applications, therefore potentially expanding its utility in both industrial and public health contexts.

Overall, this work provides a more practical, impactful solution for multi-gas sensing therefore meeting industrial needs whilst also setting the foundation for broader environmental applications.

6.2 Recommendation for Future Work

In this thesis, it has been proved that a POF tapered U-shape can be used as a sensor. This sensor showed good performance as a point sensor because of how it was built, especially when used as a relative humidity and formaldehyde sensor. The results obtained have great potential for the tapered U-shaped POF to be used in different types of sensing in the future.

In this study, relative humidity and formaldehyde were used as sensors by applying them to the air medium. In other words, the POF tapered U-shape may work in normal air or air with a mix of gases. The sensing performance in this thesis shows that both air conditions can work well with the POF tapered U-shape. The idea of evanescent wave absorption makes a tapered U-shaped gas sensor more sensitive. Hence, the proposed sensor has strong potential to detect other dangerous or poisonous chemicals or vapors in the air in the future.

REFERENCES

Adouane, A., Ghoumazi, M., Bouchaour, M., & Guermat, A. (2023). Study and simulation of the effects of geometry and materials on the detection potential of tapered fiber sensors. *Physica Scripta*, *98*(7), 075514.

Afsharipour, E., Malviya, K. D., Montazeri, M., Mortazy, E., Soltanzadeh, R., Hassani, A., Rosei, F., & Chaker, M. (2023). Evanescent-field excited surface plasmon-enhanced U-bent fiber probes coated with Au and ZnO nanoparticles for humidity detection. *Processes*, *11*(2), 642.

Ahmad, M., & Hench, L. L. (2005). Effect of taper geometries and launch angle on evanescent wave penetration depth in optical fibers. *Biosensors and Bioelectronics*, *20*(7), 1312-1319.

Amiri, I., Azzuhri, S., Jalil, M., Hairi, H., Ali, J., Bunruangses, M., & Yupapin, P. (2018). Introduction to Photonics: Principles and the Most Recent Applications of Microstructures. *Micromachines*, *9*(9), 452.

Arunachalam, S., Izquierdo, R., & Nabki, F. (2019). Low-hysteresis and fast response time humidity sensors using suspended functionalized carbon nanotubes. *Sensors, 19*(3), 680.

Arzuk, E., Karakuş, F., & Orhan, H. (2021). Bioactivation of clozapine by mitochondria of the murine heart: Possible cause of cardiotoxicity. *Toxicology*, *447*, 152628.

Ascorbe, J., Corres, J. M., Matias, I. R., & Arregui, F. J. (2016). High sensitivity humidity sensor based on cladding-etched optical fiber and lossy mode resonances. *Sensors and Actuators B: Chemical, 233,* 7-16.

Ashraf, M., Beg, M. T., Moin, F., Rajesh, R., & Singhal, G. (2022). U-bent plastic optical fiber sensor for iron in iron supplements. *IEEE Sensors Journal*, *22*(15), 14921-14928.

Aung, W.-Y., Sakamoto, H., Sato, A., Yi, E.-E.-P.-N., Thein, Z.-L., Nwe, M.-S., Shein, N., Linn, H., Uchiyama, S., & Kunugita, N. (2021). Indoor Formaldehyde Concentration, Personal Formaldehyde Exposure and Clinical Symptoms during Anatomy Dissection Sessions, University of Medicine 1, Yangon. *International Journal of Environmental Research and Public Health*, *18*(2), 712.

Azad, S., Sadeghi, E., Parvizi, R., Mazaheri, A., & Yousefi, M. (2017). Sensitivity optimization of ZnO clad-modified optical fiber humidity sensor by means of tuning the optical fiber waist diameter. *Optics & Laser Technology*, *90*, 96-101.

Azad, S., Sadeghi, E., Parvizi, R., & Mazaheri, A. (2017). Fast response relative humidity clad-modified multimode optical fiber sensor with hydrothermally dimension controlled ZnO nanorods. *Materials Science in Semiconductor Processing, 66,* 200-206.

Azman, N. (2022). Development of liquid concentration sensor using optical fiber. *Journal Fotonik*, *3*(1), 26-32.

Ballato, J., & Gibson, U. J. (2021). Core opportunities for future optical fibers. *Journal of Physics: Photonics*, *3*(4), 041001.

Ban, S., & Lian, Y. (2024, April). The Structure and Applications of Fused Tapered Fiber Optic Sensing: A Review. In *Photonics* (Vol. 11, No. 5, p. 414). MDPI.

Bariain, C., Matias, I. R., Arregui, F. J., & Lopez-Amo, M. (2000). Optical fiber humidity sensor based on a tapered fiber coated with agarose gel. *Sensors and Actuators B-Chemical*, *69*(1-2), 127-131. https://doi.org/Doi 10.1016/S0925-4005(00)00524-4

Baruah, S., & Dutta, J. (2009). Hydrothermal growth of ZnO nanostructures. *Science and technology of advanced materials, 10*(1), 013001.

Baruah, S., K Pal, S., & Dutta, J. (2012). Nanostructured zinc oxide for water treatment. *Nanoscience & Nanotechnology-Asia, 2*(2), 90-102.

Batumalay, M., Harun, S., Ahmad, F., Nor, R., Zulkepely, N., & Ahmad, H. (2014). Study of a fiber optic humidity sensor based on agarose gel. *Journal of Modern Optics*, *61*(3), 244-248.

Batumalay, M., Harun, S. W., Irawati, N., Ahmad, H., & Arof, H. (2014). A study of relative humidity fiber-optic sensors. *IEEE Sensors Journal, 15*(3), 1945-1950.

Batumalay, M., Lokman, A., Ahmad, F., Arof, H., Ahmad, H., & Harun, S. W. (2013). Tapered plastic optical fiber coated with HEC/PVDF for measurement of relative humidity. *IEEE Sensors Journal*, *13*(12), 4702-4705.

Beres, C., de Nazaré, F. V. B., de Souza, N. C. C., Miguel, M. A. L., & Werneck, M. M. (2011). Tapered plastic optical fiber-based biosensor–Tests and application. *Biosensors and Bioelectronics, 30*(1), 328-332.

Bernardini, L., Barbosa, E., Charão, M. F., & Brucker, N. (2022). Formaldehyde toxicity reports from in vitro and in vivo studies: a review and updated data. *Drug and Chemical Toxicology*, *45*(3), 972-984.

Bilodeau, F., Hill, K., Faucher, S., & Johnson, D. (1988). Low-loss highly overcoupled fused couplers: Fabrication and sensitivity to external pressure. *Journal of Lightwave Technology*, *6*(10), 1476-1482.

Borysiewicz, M. A. (2019). ZnO as a functional material, a review. *Crystals*, *9*(10), 505.

Cennamo, N., Massarotti, D., Conte, L., & Zeni, L. (2011). Low cost sensors based on SPR in a plastic optical fiber for biosensor implementation. *Sensors*, *11*(12), 11752-11760.

Chakrabarti, S., Banerjee, P., Mitra, P., & Roy, A. (2020). Zinc oxide–based nanomaterials for environmental applications. In *Handbook of Smart Photocatalytic Materials* (pp. 73-107). Elsevier.

Chen, G. Y., Lancaster, D. G., & Monro, T. M. (2017). Optical microfiber technology for current, temperature, acceleration, acoustic, humidity and ultraviolet light sensing. *Sensors*, *18*(1), 72.

Chen, K., Guo, M., Liu, S., Zhang, B., Deng, H., Zheng, Y., Chen, Y., Luo, C., Tao, L., & Lou, M. (2019). Fiber-optic photoacoustic sensor for remote monitoring of gas micro-leakage. *Optics express*, *27*(4), 4648-4659.

Chin, L. C., Whelan, W. M., & Vitkin, I. A. (2010). Optical fiber sensors for biomedical applications. In *Optical-thermal response of laser-irradiated tissue* (pp. 661-712). Springer.

Corres, J. M., Arregui, F. J., & Matías, I. R. (2007). Sensitivity optimization of tapered optical fiber humidity sensors by means of tuning the thickness of nanostructured sensitive coatings. *Sensors and Actuators B: Chemical, 122*(2), 442-449.

Culshaw, B., & Kersey, A. (2008). Fiber-optic sensing: A historical perspective. *Journal of Lightwave Technology*, *26*(9), 1064-1078.

Darder, M. d. M., Serrano, L. A., Bedoya, M., & Orellana, G. (2022). 3D Printing Filaments Facilitate the Development of Evanescent Wave Plastic Optical Fiber (POF) Chemosensors. *Chemosensors*, *10*(2), 61.

Dedova, T., Volobujeva, O., Klauson, J., Mere, A., & Krunks, M. (2007). ZnO nanorods via spray deposition of solutions containing zinc chloride and thiocarbamide. *Nanoscale Research Letters, 2,* 391-396.

del Mar Darder, M., Bedoya, M., Serrano, L. A., Alba, M. Á., & Orellana, G. (2022). Fiberoptic colorimetric sensor for in situ measurements of airborne formaldehyde in workplace environments. *Sensors and Actuators B: Chemical*, *353*, 131099.

Devi, P., & Singh, J. (2021). A Highly Sensitive Colorimetric Gas Sensor Based on Indium Oxide Nanostructures for H 2 S Detection at Room Temperature. *IEEE Sensors Journal*, *21*(17), 18512-18518.

Divagar, M., Gowri, A., John, S., & Sai, V. V. R. (2018). Graphene oxide coated U-bent plastic optical fiber based chemical sensor for organic solvents. *Sensors and Actuators B: Chemical, 262,* 1006-1012.

Domingues, M. d. F. F., & Radwan, A. (2017). Polymer Optical Fiber Sensors. In *Optical Fiber Sensors for loT and Smart Devices* (pp. 61-72). Springer.

Du, H., Zhang, H., Fan, Y., Zheng, Y., Yuan, S., Jia, T.-T., Li, M., Hou, J., Li, Z., & Li, Y. (2023). A novel fluorescent probe for the detection of formaldehyde in real food samples, animal serum samples and gaseous formaldehyde. *Food chemistry*, *411*, 135483.

Elosua, C., Arregui, F. J., Villar, I. D., Ruiz-Zamarreño, C., Corres, J. M., Bariain, C., Goicoechea, J., Hernaez, M., Rivero, P. J., & Socorro, A. B. (2017). Micro and nanostructured materials for the development of optical fibre sensors. *Sensors*, *17*(10), 2312.

Eskikaya, O., Ozdemir, S., Tollu, G., Dizge, N., Ramaraj, R., Manivannan, A., & Balakrishnan, D. (2022). Synthesis of two different zinc oxide nanoflowers and comparison of antioxidant and photocatalytic activity. *Chemosphere*, 135389.

Fallah, H., Chaudhari, M., Bora, T., Harun, S., Mohammed, W., & Dutta, J. (2013). Demonstration of side coupling to cladding modes through zinc oxide nanorods grown on multimode optical fiber. *Optics letters*, *38*(18), 3620-3622.

Fang, Y., Ren, G., Li, M., Yang, Y., Guo, D.-Y., & Pan, Q. (2021). Sensitively liquid and gaseous detection of formaldehyde based on a supramolecular organic framework. *Sensors and Actuators B: Chemical*, *349*, 130726.

Fappiano, L., Carriera, F., Iannone, A., Notardonato, I., & Avino, P. (2022). A Review on Recent Sensing Methods for Determining Formaldehyde in Agri-Food Chain: A Comparison with the Conventional Analytical Approaches. *Foods*, *11*(9), 1351.

Faria, I. D. L., Gouvêa, M. M., Netto, A. D. P., & de Carvalho Marques, F. F. (2022). Determination of formaldehyde in bovine milk by micellar electrokinetic chromatography with diode array detection. *LWT*, *163*, 113473.

Faruki, M. J., Ab Razak, M. Z., Azzuhri, S. R., Rahman, M. T., Soltanian, M. R. K., Brambilla, G., ... & Ahmad, H. (2016). Effect of titanium dioxide (TiO2) nanoparticle coating on the detection performance of microfiber knot resonator sensors for relative humidity measurement. *Materials Express, 6*(6), 501-508.

Fauzi, F., Rianjanu, A., Santoso, I., & Triyana, K. (2021). Gas and humidity sensing with quartz crystal microbalance (QCM) coated with graphene-based materials–A mini review. *Sensors and Actuators A: Physical*, *330*, 112837.

Ferguson, J. A., Boles, T. C., Adams, C. P., & Walt, D. R. (1996). A fiber-optic DNA biosensor microarray for the analysis of gene expression. *Nature biotechnology*, *14*(13), 1681.

Fuke, M. V., Kanitkar, P., Kulkarni, M., Kale, B. B., & Aiyer, R. C. (2010). Effect of particle size variation of Ag nanoparticles in Polyaniline composite on humidity sensing. *Talanta, 81*(1-2), 320-326.

Gaddam, V., Kumar, R. R., Parmar, M., Nayak, M., & Rajanna, K. (2015). Synthesis of ZnO nanorods on a flexible Phynox alloy substrate: influence of growth temperature on their properties. *RSC advances*, *5*(109), 89985-89992.

Ge, K., Yi, L., Wu, Q., Li, Y., Zhang, H., & Gu, Y. (2021). Detection of Formaldehyde by Surface-Enhanced Raman Spectroscopy Based on PbBiO2Br/Au4Ag4 Nanospheres. *ACS Applied Nano Materials*, *4*(10), 10218-10227.

Ghaffar, A., Li, Q., Mehdi, I., Abro, K., Karim, N., Onyekwena, C. C., Mehdi, M., & Chen, B. (2021). A novel sensor design for displacement measurement using plastic optical fiber-based on face-coupling method. *Optical Fiber Technology*, *67*, 102684.

Golnabi, H., & Azimi, P. (2007). Design and performance of a plastic optical fiber leakage sensor. *Optics & Laser Technology*, *39*(7), 1346-1350.

Griffiths, J., & Robinson, S. (1999). The OxyLite: A fibre-optic oxygen sensor. *The British journal of radiology*, *72*(859), 627-630.

Guo, Z., Chu, F., Fan, J., Zhang, Z., Bian, Z., Li, G., & Song, X. (2019). Study of macro-bending biconical tapered plastic optical fiber for relative humidity sensing. *Sensor Review, 39*(3), 352-357.

Hammouche, H., Achour, H., Makhlouf, S., Chaouchi, A., & Laghrouche, M. (2021). A comparative study of capacitive humidity sensor based on keratin film, keratin/graphene oxide, and keratin/carbon fibers. *Sensors and Actuators A: Physical*, *329*, 112805.

Harith, Z., Batumalay, M., Irawati, N., Harun, S. W., Ahmad, H., & Hu, T. (2020). ZnO nanorod-coated tapered plastic fiber sensors for relative humidity. *Optics Communications, 473,* 125924.

Harith, Z., Irawati, N., Rafaie, H. A., Batumalay, M., Harun, S. W., Nor, R. M., & Ahmad, H. (2015). Tapered Plastic Optical Fiber Coated With Al-Doped ZnO Nanostructures for Detecting Relative Humidity. *IEEE Sensors Journal*, *15*(2), 845-849. https://doi.org/10.1109/jsen.2014.2353038

Harun, S. W., Lim, K., Tio, C., Dimyati, K., & Ahmad, H. (2013). Theoretical analysis and fabrication of tapered fiber. *Optik*, *124*(6), 538-543.

Hassan, F. M., & Najim, A. A. (2021). Synthesis and Characterization of Nanocrystalline Co-DOPED ZnO Thin Films Prepared by Chemical Spray Pyrolysis for Optoelectronic Applications. *Surface Review and Letters*, *28*(12), 2150118.

Hassan, M. M., Xu, Y., Zareef, M., Li, H., Rong, Y., & Chen, Q. (2021). Recent advances of nanomaterial-based optical sensor for the detection of benzimidazole fungicides in food: a review. *Critical Reviews in Food Science and Nutrition*, 1-22.

Healey, B. G., Li, L., & Walt, D. R. (1997). Multianalyte biosensors on optical imaging bundles. *Biosensors and Bioelectronics*, *12*(6), 521-529.

Hernaez, M., Acevedo, B., Mayes, A. G., & Melendi-Espina, S. (2019). High-performance optical fiber humidity sensor based on lossy mode resonance using a nanostructured polyethylenimine and graphene oxide coating. *Sensors and Actuators B: Chemical*, *286*, 408-414.

Hernaez, M., Acevedo, B., Mayes, A. G., & Melendi-Espina, S. (2019). High-performance optical fiber humidity sensor based on lossy mode resonance using a nanostructured polyethylenimine and graphene oxide coating. *Sensors and Actuators B: Chemical, 286,* 408-414.

Hirai, Y., Suzuki, Y., & Morisawa, M. (2023). Two-wavelength dye-doped swellable clad POF humidity sensor. *IEEE Sensors Journal*, *23*(8), 8435-8442.

Hisam, M. N., Abdul RAHIM, H. R., Razak, H. A., Azmi, S. N., Johari, S. H., Jali, M. H., Mohd CHACHULI, S. A., Thokchome, S., Muhammd, A. R., & Harun, S. W. (2022). Tapered plastic optical fiber loop coated with ZnO nanorods using multiple channels for relative humidity sensing. *Przeglad Elektrotechniczny*, *98*(4).

Hoffmann, V., Moser, C., & Saak, A. (2019). Food safety in low and middle-income countries: The evidence through an economic lens. *World Development*, *123*, 104611.

Hussain, S., Liu, T., Kashif, M., Cao, S., Zeng, W., Xu, S., Naseer, K., & Hashim, U. (2014). A simple preparation of ZnO nanocones and exposure to formaldehyde. *Materials Letters*, *128*, 35-38.

Hussian, S., Mehdi, M., Ghaffar, A., Lan, K., Hu, Y., Lin, H., Qaisrani, M. A., Ali, S., Lin, J., & Mehdi, R. (2024). Development of a dual point humidity sensor using POF based on twisted fiber structure. *Scientific Reports*, *14*(1), 10735.

Imani, R., & Cuellar, G. H. (2020). Introductory chapter: Optical fibers. *Optical Fiber Applications*, 3.

Irawati, N., Rahman, H. A., Ahmad, H., & Harun, S. W. (2017). A PMMA microfiber loop resonator based humidity sensor with ZnO nanorods coating. *Measurement, 99,* 128-133.

Jagtap, S., Rane, S., Arbuj, S., Rane, S., & Gosavi, S. (2018). Optical fiber based humidity sensor using Ag decorated ZnO nanorods. *Microelectronic Engineering*, *187*, 1-5.

Jali, M. H., Rahim, H. R. A., Johari, M. A. M., Yusof, H. H. M., Johari, S. H., & Ahmad, A. (2021). Effect of ZnO nanomaterials coated glass growth duration to the adjacent microfiber light transmission at room temperature. *Journal Fotonik, 2*(1), 8-14.

Jali, M. H., Abdul Rahim, H. R., Johari, M. A. M., Yusof, H. H. M., Rahman, B. M. A., Harun, S. W., & Yasin, M. (2019). Formaldehyde sensing using ZnO nanorods coated glass integrated with microfiber. *Optics & Laser Technology*, *120*. https://doi.org/10.1016/j.optlastec.2019.105750

Jali, M. H., Johari, M. A. M., Rahim, H. R. A., Yusof, H. H. M., Ahmad, A., Baharom, M. F., & Harun, S. W. (2021). Aligned vertical growth of zinc oxide nanorods on glass substrates using optimum hydrothermal synthesis technique. *Indonesian Journal of Electrical Engineering and Computer Science*, *23*(2), 694-700.

Jali, M. H., Rahim, H. R. A., Johari, M. A. M., Ahmad, A., Yusof, H. H. M., Johari, S. H., Baharom, M. F., Thokchom, S., Dimyati, K., & Harun, S. W. (2021). Integrating microsphere resonator and ZnO nanorods coated glass for humidity sensing application. *Optics & Laser Technology*, *143*, 107356.

Jali, M. H., Rahim, H. R. A., Johari, M. A. M., Hamid, S. S., Yusof, H. H. M., Thokchom, S., Wang, P., & Harun, S. W. (2019). Optical characterization of different waist diameter on microfiber loop resonator humidity sensor. *Sensors and Actuators A: Physical*, *285*, 200-209.

Jali, M. H., Rahim, H. R. A., Johari, M. A. M., Yusof, H. H. M., Rahman, B., Harun, S. W., & Yasin, M. (2019). Formaldehyde sensing using ZnO nanorods coated glass integrated with microfiber. *Optics & Laser Technology*, *120*, 105750.

Jeong, S.-W., Bolortuya, S., Eadi, S. B., & Kim, S. (2020). Fabrication of superhydrophobic surfaces based on PDMS coated hydrothermal grown ZnO on PET fabrics. *Journal of Adhesion Science and Technology*, *34*(1), 102-113.

Jeunhomme, L. B. (1983). Single-mode fiber optics. Principles and applications. *Optical Engineering, New York: Dekker, 1983*.

Jia, Q., Tang, W., Yan, W., & Qiu, M. (2023). Fibre tapering using plasmonic microheaters and deformation-induced pull. *Light: Advanced Manufacturing*, *4*(1), 25-36.

Jiang, H., Yang, R., Tang, X., Burnett, A., Lan, X., Xiao, H., & Dong, J. (2013). Multilayer fiber optic sensors for in situ gas monitoring in harsh environments. *Sensors and Actuators B: Chemical*, *177*, 205-212.

Jiao, S.-x., Zhao, Y., & Gu, J.-j. (2018). Simultaneous measurement of humidity and temperature using a polyvinyl alcohol tapered fiber bragg grating. *Instrumentation Science & Technology*, *46*(5), 463-474.

Jindal, R., Tao, S., Singh, J. P., & Gaikwad, P. S. (2002). High dynamic range fiber optic relative humidity sensor. *Optical Engineering, 41*(5), 1093-1096.

Q. Jing, W. Fu, W. Li, H. Yang, M. Li, J. Ma, X. Zhou, M. Sun, H. Zhao, Y. Zhang, et al. Jing, Q., Fu, W., Li, W., Yang, H., Li, M., Ma, J., Zhou, X., Sun, M., Zhao, H., Zhang, Y., Zhao, W., Zhang, L. & Chen, H. (2012). Synthesis of snowflake-like multi-layered ZnO with controllable pore sizes and its photocatalytic property. *Applied surface science, 258*(8), 3604-3610.

Jo, Y.-D., & Park, K.-D. (2016). Emergency response plane of toxic gas releases with considering ventilation ratio and meteorological conditions. *International Journal of Safety and Security Engineering*, *6*(2), 229-237.

John, R. A. B., Shruthi, J., Reddy, M. R., & Kumar, A. R. (2022). Manganese doped nickel oxide as room temperature gas sensor for formaldehyde detection. *Ceramics International*, *48*(12), 17654-17667.

Keley, M. M., Borghi, F. F., Allil, R. C., Mello, A., & Werneck, M. M. (2021). Cu2-xO-functionalized plastic optical fiber for H2S sensing. *Optical Fiber Technology*, *62*, 102469.

Kind, H., Yan, H., Messer, B., Law, M., & Yang, P. (2002). Nanowire ultraviolet photodetectors and optical switches. *Advanced materials*, *14*(2), 158-160.

Kołodziejczak-Radzimska, A., & Jesionowski, T. (2014). Zinc oxide—from synthesis to application: a review. *Materials, 7*(4), 2833-2881.

Korposh, S., James, S. W., Lee, S.-W., & Tatam, R. P. (2019). Tapered optical fibre sensors: Current trends and future perspectives. *Sensors*, *19*(10), 2294.

Kuk, S. K., Ji, S. M., Kang, S., Yang, D. S., Kwon, H. J., Koo, M. S., Oh, S., & Lee, H. C. (2023). Singlet-oxygen-driven photocatalytic degradation of gaseous formaldehyde and its mechanistic study. *Applied Catalysis B: Environmental*, *328*, 122463.

Kulkarni, S. S., & Shirsat, M. D. (2015). Optical and structural properties of zinc oxide nanoparticles. *International Journal of Advanced Research in Physical Science, 2*(1), 14-18.

Kuswanto, H., Abimanyu, I., & Dwandaru, W. S. B. (2022). Increasing the Sensitivity of Polymer Optical Fiber Sensing Element in Detecting Humidity: Combination of Macro and Micro Bendings. *Trends in Sciences*, *19*(7), 3200-3200.

Li, S., Shi, Y., Zhang, X., Zhou, M., Zhang, B., Zhou, L., Wu, T., & Guo, J. (2024). Weakly coupled photonic flexible sensors based on sodium polyacrylate. *Sensors and Actuators A: Physical*, *377*, 115731.

Liu, L., Deng, S., Zheng, J., Yuan, L., Deng, H., & Teng, C. (2021). An enhanced plastic optical fiber-based surface plasmon resonance sensor with a double-sided polished structure. *Sensors*, *21*(4), 1516.

Liu, M., Su, W., Qin, X., Cheng, K., Ding, W., Ma, L., Cui, Z., Chen, J., Rao, J., & Ouyang, H. (2021). Mechanical/Electrical Characterization of ZnO Nanomaterial Based on AFM/Nanomanipulator Embedded in SEM. *Micromachines*, *12*(3), 248.

Liu, Y., Zhang, Y., Lei, H., Song, J., Chen, H., & Li, B. (2012). Growth of well-arrayed ZnO nanorods on thinned silica fiber and application for humidity sensing. *Optics express*, *20*(17), 19404-19411. https://doi.org/10.1364/OE.20.019404

Lokman, A., Arof, H., & Harun, S. W. (2015). Tapered fiber coated with hydroxyethyl cellulose/polyvinylidene fluoride composite for relative humidity sensor. *Sensors and Actuators A: Physical*, *225*, 128-132.

Lokman, A., Arof, H., Harun, S. W., Harith, Z., Rafaie, H. A., & Nor, R. M. (2015). Optical fiber relative humidity sensor based on inline Mach–Zehnder interferometer with ZnO nanowires coating. *IEEE Sensors Journal*, *16*(2), 312-316.

Lokman, M., Rahim, H., Harun, S., Hornyak, G., & Mohammed, W. (2016). Light Backscattering (eg Reflectance) by Zinc Oxide Nanorods on Tips of Plastic Optical Fibers with Application for Humidity and Alcohol Vapor Sensing. *IET Micro Nano Lett.*

Lokman, M. Q., Bin Abdul Rahim, H. R., Harun, S. W., Hornyak, G. L., & Mohammed, W. S. (2016). Light backscattering (eg reflectance) by ZnO nanorods on tips of plastic optical fibres with application for humidity and alcohol vapour sensing. *Micro & Nano Letters*, *11*(12), 832-836.

Luo, Y., Chen, C., Xia, K., Peng, S., Guan, H., Tang, J., ... & Chen, Z. (2016). Tungsten disulfide (WS 2) based all-fiber-optic humidity sensor. *Optics express, 24*(8), 8956-8966.

Mahmudiono, T., Ramaiah, P., Maleki, H., Doewes, R. I., Shalaby, M. N., Alsaikhan, F., & Mohammadi, M. J. (2023). Evaluation of the impact of different disinfectants on new coronavirus and human health. *Reviews on Environmental Health, 38*(3), 451-460.

Mallik, A. K., Liu, D., Kavungal, V., Wu, Q., Farrell, G., & Semenova, Y. (2016). Agarose coated spherical micro resonator for humidity measurements. *Optics express, 24*(19), 21216-21227.

Maseer, S. Z., Mahdi, B. R., & Abd Aljbar, N. (2023). Hybrid structure of u bent optical fiber local surface plasmon resonance sensor based on graphene. *Indonesian Journal of Electrical Engineering and Computer Science*, *29*(2), 644-651.

Md Johari, M. A., Abdul Khudus, M. I. M., Bin Jali, M. H., Al Noman, A., & Wadi Harun, S. (2018). Effect of Size on Single and Double Optical Microbottle Resonator Humidity Sensors. *Sensors and Actuators A: Physical*, *284*, 286-291. https://doi.org/10.1016/j.sna.2018.10.035

Memon, S. F., Ali, M. M., Pembroke, J. T., Chowdhry, B. S., & Lewis, E. (2017). Measurement of ultralow level bioethanol concentration for production using evanescent wave based optical fiber sensor. *IEEE Transactions on Instrumentation and Measurement*, *67*(4), 780-788.

Miles, D., Cameron, P., & Mattia, D. (2015). Hierarchical 3D ZnO nanowire structures via fast anodization of zinc. *Journal of Materials Chemistry A*, *3*(34), 17569-17577.

Mohan, S., & Khijwania, S. K. (2024). Graphene oxide based optical fiber humidity sensor having a linear response throughout a large dynamic range and optimum sensitivity. *Applied Optics*, *63*(1), 179-185.

Mohan, S., & Negi, M. S. (2024). Carbon nanotube-based Optical Fiber Sensor with Rapid Response for Human Breath Monitoring and Voiceprint Recognition. *IEEE Sensors Letters*.

Mulyanti, B., Abdurrahman, F., Pawinanto, R. E., Heri, A., & Sugandi, G. (2017). Fabrication of polymer optical fiber as intrinsic optical sensor using etching technique. *Advanced Science Letters, 23*(2), 1310-1313.

Naresh, V., & Lee, N. (2021). A review on biosensors and recent development of nanostructured materials-enabled biosensors. *Sensors*, *21*(4), 1109.

Nataraj, N., Chen, T.-W., Gan, Z.-W., Chen, S.-M., Lou, B.-S., Ali, M., & Al-Hemaid, F. (2022). Two-dimensional copper oxide/zinc oxide nanoflakes with three-dimensional flower-like heterostructure enhanced with electrocatalytic activity toward nimesulide detection. *Materials Today Chemistry*, *24*, 100768.

Navale, Y., Navale, S., Ramgir, N., Stadler, F., Gupta, S., Aswal, D., & Patil, V. (2017). Zinc oxide hierarchical nanostructures as potential NO2 sensors. *Sensors and Actuators B: Chemical*, *251*, 551-563.

Nguyen, T. T., Ngo, Q. M., Tran, N. Q., Nguyen, D. K. V., & Phan, T. B. (2021). Enhanced birefringence for refractometric optical fiber sensor with titanium oxide. *Photonics and Nanostructures-Fundamentals and Applications*, *47*, 100973.

Nie, X., Dong, K., Tian, Y., Zong, C., Chen, Z., Wang, X., & Zhao, Y. (2023). A green analysis detection of formaldehyde in grooming products by surface enhanced Raman spectroscopy. *Materials Today Sustainability*, *22*, 100303.

Noorasid, N. S., Arith, F., Alias, S. N., Mustafa, A. N., Roslan, H., Johari, S. H., ... & Ismail, M. M. (2021). Synthesis of ZnO nanorod using hydrothermal technique for dye-sensitized solar cell application. In *Intelligent Manufacturing and Mechatronics: Proceedings of SympoSIMM 2020* (pp. 895-905). Springer Singapore.

Omotayo, O. P., Omotayo, A. O., Mwanza, M., & Babalola, O. O. (2019). Prevalence of mycotoxins and their consequences on human health. *Toxicological research*, *35*(1), 1-7.

Oprea, O., Andronescu, E., Ficai, D., Ficai, A., N Oktar, F., & Yetmez, M. (2014). ZnO applications and challenges. *Current Organic Chemistry*, *18*(2), 192-203.

Orfanakis, M., Tserevelakis, G. J., & Zacharakis, G. (2021). A Cost-Efficient Multiwavelength LED-Based System for Quantitative Photoacoustic Measurements. *Sensors*, *21*(14), 4888.

Parangusan, H., Bhadra, J., Ahmad, Z., Mallick, S., Touati, F., & Al-Thani, N. (2020). Capacitive type humidity sensor based on PANI decorated Cu–ZnS porous microspheres. *Talanta*, *219*, 121361.

Patel, B. C., Sinha, G., & Goel, N. (2020). Introduction to sensors. In *Advances in Modern Sensors: Physics, design, simulation and applications* (pp. 1-1-1-21). IOP Publishing Bristol, UK.

Paul, T., Choudhury, D. R., Ghosh, D., & Saha, C. (2024). Advancements in optical sensors for explosive materials Identification: A comprehensive review. *Results in Chemistry*, 101602.

Peng, Y., Zhao, Y., Chen, M. Q., & Xia, F. (2018). Research advances in microfiber humidity sensors. *Small*, *14*(29), 1800524.

Peterson, A. H., & Sawyer, S. M. (2021). Oxygen adsorption and photoconduction models for metal oxide semiconductors: a review. *IEEE Sensors Journal*, *21*(15), 16409-16427.

Polsongkram, D., Chamninok, P., Pukird, S., Chow, L., Lupan, O., Chai, G., Khallaf, H., Park, S., & Schulte, A. (2008). Effect of synthesis conditions on the growth of ZnO nanorods via hydrothermal method. *Physica B: Condensed Matter*, *403*(19-20), 3713-3717.

Prabu, K., & Malavika, R. (2019). Highly birefringent photonic crystal fiber with hybrid cladding. *Optical Fiber Technology*, *47*, 21-26.

Punjabi, N., Satija, J., & Mukherji, S. (2015). Evanescent wave absorption based fiber-optic sensor-cascading of bend and tapered geometry for enhanced sensitivity. In *Sensing Technology: Current Status and Future Trends III* (pp. 25-45). Springer.

Raghuwanshi, S. K., Kumar, S., & Kumar, R. (2023). Taper fiber-based SPR sensor. In *Geometric Feature-Based Fiber Optic Surface Plasmon Resonance Sensors* (pp. 43-69). Springer.

Rahim, H. R. B. A., Lokman, M. Q. B., Harun, S. W., Hornyak, G. L., Sterckx, K., Mohammed, W. S., & Dutta, J. (2016). Applied light-side coupling with optimized spiral-patterned zinc oxide nanorod coatings for multiple optical channel alcohol vapor sensing. *Journal of Nanophotonics*, *10*(3), 036009.

Rahim, H. R. B. A., Manjunath, S., Fallah, H., Thokchom, S., Harun, S. W., Mohammed, W. S., Hornyak, L. G., & Dutta, J. (2016). Side coupling of multiple optical channels by spiral patterned zinc oxide coatings on large core plastic optical fibers. *Micro & Nano Letters*, *11*(2), 122-126.

Rahman, H. A., Harun, S. W., Yasin, M., Phang, S. W., Damanhuri, S. S. A., Arof, H., & Ahmad, H. (2011). Tapered plastic multimode fiber sensor for salinity detection. Sensors and Actuators A: *Physical, 171*(2), 219-222.

Rajan, G., Mathews, S., Farrell, G., & Semenova, Y. (2010). A liquid crystal coated tapered photonic crystal fiber interferometer. *Journal of Optics, 13*(1), 015403.

Rakha, A., Fatima, M., Bano, Y., Khan, M. A., Chaudhary, N., & Aadil, R. M. (2022). Safety and quality perspective of street vended foods in developing countries. *Food Control*, *138*, 109001.

Rao, X., Zhao, L., Xu, L., Wang, Y., Liu, K., Wang, Y., Chen, G. Y., Liu, T., & Wang, Y. (2021). Review of Optical Humidity Sensors. *Sensors*, *21*(23), 8049.

Rianjanu, A., Julian, T., Hidayat, S. N., Yulianto, N., Majid, N., Syamsu, I., Wasisto, H. S., & Triyana, K. (2020). Quartz crystal microbalance humidity sensors integrated with hydrophilic polyethyleneimine-grafted polyacrylonitrile nanofibers. *Sensors and Actuators B: Chemical*, *319*, 128286.

Sabri, N., Aljunid, S. A., Salim, M. S., Ahmad, R. B., & Kamaruddin, R. (2013, April). Toward optical sensors: Review and applications. In *Journal of Physics: Conference Series* (Vol. 423, No. 1, p. 012064). IOP Publishing.

Salah, G., Azzedine, T., & Chahra, B. (2014). Fabrication and characterization of zinc oxide (ZnO) thin films based humidity sensor with fast response by sol-gel method. *Journal of New Technology and Materials*, *277*(1748), 1-4.

Samavati, Z., Samavati, A., Ismail, A. F., Othman, M. H. D., & Rahman, M. A. (2019). Comprehensive investigation of evanescent wave optical fiber refractive index sensor coated with ZnO nanoparticles. *Optical Fiber Technology*, *52*, 101976.

Saracoglu, O. G., & Hayber, S. E. (2016). Bent fiber sensor for preservative detection in milk. *Sensors*, *16*(12), 2094.

Shan, C., Liu, Z., & Hark, S. (2008). Temperature dependent photoluminescence study on phosphorus doped ZnO nanowires. *Applied physics letters*, *92*(7), 073103.

Sharma, A., Manocha, D., Arora, A., Kumar, A., Srivastava, C. M., Rawat, V., Kim, H., Verma, M., & Rao, G. K. (2022). Applications of green nanomaterials in electronic and electrical industries. In *Green Nanomaterials for Industrial Applications* (pp. 397-421). Elsevier.

Shooshtari, M., Pahlavan, S., Rahbarpour, S., & Ghafoorifard, H. (2022). Investigating Organic Vapor Sensing Properties of Composite Carbon Nanotube-Zinc Oxide Nanowire. *Chemosensors*, *10*(6), 205.

Sikarwar, S., & Yadav, B. (2015). Opto-electronic humidity sensor: A review. *Sensors and Actuators A: Physical*, *233*, 54-70.

Soge, A. O., Dairo, O. F., Sanyaolu, M. E., & Kareem, S. O. (2021). Recent developments in polymer optical fiber strain sensors: A short review. *Journal of Optics*, *50*(2), 299-313.

Stewart, G., Jin, W., & Culshaw, B. (1997). Prospects for fibre-optic evanescent-field gas sensors using absorption in the near-infrared. *Sensors and Actuators B: Chemical*, *38*(1-3), 42-47.

Suhantoro, M., & Yulianti, I. (2021, June). Back scattering method based-plastic optical fiber coupler viscosity sensors. In Journal of Physics: *Conference Series* (Vol. 1918, No. 2, p. 022014). IOP Publishing.

Syuhada, A., Shamsudin, M. S., Daud, S., Krishnan, G., Harun, S. W., & Aziz, M. S. A. (2020). Single-Mode Modified Tapered Fiber Structure Functionalized With GO-PVA Composite Layer for Relative Humidity Sensing. *Photonic Sensors*, 1-11.

Tan, A. J. Y., Ng, S. M., Stoddart, P. R., & Chua, H. S. (2020). Theoretical model and design considerations of U-shaped fiber optic sensors: A review. *IEEE Sensors Journal*, *20*(24), 14578-14589.

Teng, C., Jing, N., Yu, F., & Zheng, J. (2016). Investigation of a macro-bending tapered plastic optical fiber for refractive index sensing. *IEEE Sensors Journal*, *16*(20), 7521-7525.

Toma, K., Iwasaki, K., Zhang, G., Iitani, K., Arakawa, T., Iwasaki, Y., & Mitsubayashi, K. (2021). Biochemical Methanol Gas Sensor (MeOH Bio-Sniffer) for Non-Invasive Assessment of Intestinal Flora from Breath Methanol. *Sensors*, *21*(14), 4897.

Tulliani, J.-M., Inserra, B., & Ziegler, D. (2019). Carbon-based materials for humidity sensing: A short review. *Micromachines*, *10*(4), 232.

Udd, E., Blom, R. G., Tralli, D. M., Saaski, E. W., & Dokka, R. (1994, May). Application of the Sagnac interferometer-based strain sensor to an earth movement detection system. In Smart Structures and Materials 1994: *Smart Sensing, Processing, and Instrumentation* (Vol. 2191, pp. 126-136). SPIE.

Udd, E., & Spillman Jr, W. B. (2011). *Fiber optic sensors: an introduction for engineers and scientists*. John Wiley & Sons.

Venketeswaran, A., Lalam, N., Wuenschell, J., Ohodnicki Jr, P., Badar, M., Chen, K. P., Lu, P., Duan, Y., Chorpening, B., & Buric, M. (2022). Recent advances in machine learning for fiber optic sensor applications. *Advanced Intelligent Systems*, *4*(1), 2100067.

Veríssimo, M. I., Gamelas, J. A., Fernandes, A. J., Evtuguin, D. V., & Gomes, M. T. S. (2020). A new formaldehyde optical sensor: Detecting milk adulteration. *Food chemistry*, *318*, 126461.

Vijayan, A., Fuke, M., Hawaldar, R., Kulkarni, M., Amalnerkar, D., & Aiyer, R. C. (2008). Optical fibre based humidity sensor using Co-polyaniline clad. *Sensors and Actuators B: Chemical, 129*(1), 106-112.

Vijjapu, M. T., Surya, S. G., Yuvaraja, S., Zhang, X., Alshareef, H. N., & Salama, K. N. (2020). Fully integrated indium gallium zinc oxide NO2 gas detector. *ACS sensors*, *5*(4), 984-993.

Waluyo, B. D., Sari, R. D., & Januariyansah, S. (2022, February). Testing and development of plastic optical fiber as humidity and temperature sensor. In *Journal of Physics: Conference Series* (Vol. 2193, No. 1, p. 012071). IOP Publishing.

Wandermur, G., Rodrigues, D., Allil, R., Queiroz, V., Peixoto, R., Werneck, M., & Miguel, M. (2014). Plastic optical fiber-based biosensor platform for rapid cell detection. *Biosensors and Bioelectronics, 54*, 661-666.

Wang, D., Li, W., Zhang, Q., Liang, B., Peng, Z., Xu, J., Zhu, C., & Li, J. (2021). High-performance tapered fiber surface plasmon resonance sensor based on the graphene/Ag/TiO2 layer. *Plasmonics*, *16*(6), 2291-2303.

Wang, H., Bai, J., Dai, M., Liu, K., Liu, Y., Zhou, L., Liu, F., Liu, F., Gao, Y., & Yan, X. (2020). Visible light activated excellent NO2 sensing based on 2D/2D ZnO/g-C3N4 heterojunction composites. *Sensors and Actuators B: Chemical*, *304*, 127287.

Wang, N., Tian, W., Zhang, H., Yu, X., Yin, X., Du, Y., & Li, D. (2021). An easily fabricated high performance Fabry-Perot optical fiber humidity sensor filled with graphene quantum dots. *Sensors*, *21*(3), 806.

Wang, Y., Zhou, Y., & Wang, Y. (2020). Humidity activated ionic-conduction formaldehyde sensing of reduced graphene oxide decorated nitrogen-doped MXene/titanium dioxide composite film. *Sensors and Actuators B: Chemical*, *323*, 128695.

Wang, Z. L. (2004). Zinc oxide nanostructures: growth, properties and applications. *Journal of physics: condensed matter*, *16*(25), R829.

Wolfbeis, O. S. (2004). Fiber-optic chemical sensors and biosensors. *Analytical chemistry*, *76*(12), 3269-3284.

Wu, C.-M., Naseem, S., Chou, M.-H., Wang, J.-H., & Jian, Y.-Q. (2019). Recent advances in tungsten-oxide-based materials and their applications. *Frontiers in Materials*, *6*, 49.

Xia, L., Li, L., Li, W., Kou, T., & Liu, D. (2013). Novel optical fiber humidity sensor based on a no-core fiber structure. *Sensors and Actuators A: Physical*, *190*, 1-5.

Yang, T. (2023). Ultra-compact fiber tapering: plasmonics and structural bending as new combination of heat and pull. *Light: Science & Applications*, *12*(1), 163.

Yasin, M., Zulkarnaen, M., Yhuwana, Y. G. Y., Zaidan, A. H., & Harun, S. W. (2020). Bundled plastic optical fiber based sensor for ECG signal detection. *Optik*, *203*, 164077.

Yeo, T., Sun, T., & Grattan, K. (2008). Fibre-optic sensor technologies for humidity and moisture measurement. *Sensors and Actuators A: Physical*, *144*(2), 280-295.

Yoo, W. J., Heo, J. Y., Jang, K. W., Seo, J. K., Moon, J. S., Park, J.-Y., Park, B. G., Cho, S., & Lee, B. (2011). Measurements of spectral responses for developing fiber-optic pH sensor. *Optical review*, *18*, 139-143.

Yu, D., Li, J., Wang, T., She, X., Sun, Y., Li, J., Zhang, L., Yu, X.-F., & Yang, D. (2020). Black phosphorus all-fiber sensor for highly responsive humidity detection. *physica status solidi (RRL)–Rapid Research Letters*, *14*(4), 1900697.

Yu, S., Chen, C., Zhang, H., Zhang, J., & Liu, J. (2021). Design of high sensitivity graphite carbon nitride/zinc oxide humidity sensor for breath detection. *Sensors and Actuators B: Chemical*, *332*, 129536.

Yulianti, I., Putra, N. D., Rumiana, H., Latif, Z. A. F., Kurniansyah, K. E., & Maimanah, S. (2021, June). Characterization of Mach Zehnder interferometer plastic optical fiber for intensity-based temperature sensor. In *Journal of Physics: Conference Series* (Vol. 1918, No. 2, p. 022010). IOP Publishing.

Yun, G., Koo, K. M., & Kim, Y. (2021). Chemiresistor type formaldehyde sensor using polystyrene/polyaniline core-shell microparticles. *Polymer*, *215*, 123389.

Yusof, H. H. M., Harun, S. W., Dimyati, K., Bora, T., Mohammed, W. S., & Dutta, J. (2018). Optical dynamic range maximization for humidity sensing by controlling growth of zinc oxide nanorods. *Photonics and Nanostructures-Fundamentals and Applications, 30*, 57-64.

Yusof, H. H. M., Harun, S. W., Dimyati, K., Bora, T., Sterckx, K., Mohammed, W. S., & Dutta, J. (2019). Low-Cost Integrated Zinc Oxide Nanorod-Based Humidity Sensors for Arduino Platform. *IEEE Sensors Journal*, *19*(7), 2442-2449. https://doi.org/10.1109/jsen.2018.2886584

Yusof, H. H. M., Jali, M. H., Johari, M. A. M., Dimyati, K., Harun, S. W., Khasanah, M., & Yasin, M. (2019). Detection of formaldehyde vapor using glass substrate coated with zinc oxide nanorods. *IEEE Photonics Journal*, *11*(1), 1-9.

Zain, H. A., Batumalay, M., Rahim, H. R. A., Yasin, M., & Harun, S. W. (2021). HEC/PVDF coated microbottle resonators for relative humidity detection. *Optik*, *232*, 166534.

Zain, H. A., Jali, M. H., Rahim, H. R. A., Johari, M. A. M., Yusof, H. H. M., Thokchom, S., Yasin, M., & Harun, S. W. (2020). ZnO nanorods coated microfiber loop resonator for relative humidity sensing. *Optical Fiber Technology*, *54*, Article 102080. https://doi.org/10.1016/j.yofte.2019.102080

Zain, H. A., Jali, M. H., Rahim, H. R. A., Johari, M. A. M., Yusof, H. H. M., Thokchom, S., Yasin, M., & Harun, S. W. (2020). ZnO nanorods coated microfiber loop resonator for relative humidity sensing. *Optical Fiber Technology*, *54*, 102080.

Zepp, R. G., Hoigne, J., & Bader, H. (1987). Nitrate-induced photooxidation of trace organic chemicals in water. *Environmental science & technology*, *21*(5), 443-450.

Zhang, H., Yang, D., Ma, X., Ji, Y., Xu, J., & Que, D. (2004). Synthesis of flower-like ZnO nanostructures by an organic-free hydrothermal process. *Nanotechnology, 15*(5), 622.

Zhang, Y., Ding, L., Zhang, H., Wang, P., & Li, H. (2022). A new optical fiber biosensor for acetylcholine detection based on pH sensitive fluorescent carbon quantum dots. *Sensors and Actuators B: Chemical*, *369*, 132268.

Zhang, Y., Yang, Y., Ju, H., He, X., Sun, P., Tian, Y., Yang, P., Song, X.-x., Yu, T., & Jiang, Z. (2022). Comprehensive profile of circRNAs in formaldehyde induced heart development. *Food and Chemical Toxicology*, *162*, 112899.

Zhao, Y., Zhao, J., & Zhao, Q. (2020). Review of no-core optical fiber sensor and applications. *Sensors and Actuators A: Physical*, *313*, 112160.

Zhong, N., Xin, X., Liu, H., Yu, X., Chang, H., Tang, B., Zhong, D., Zhao, M., Zhang, H., & Zhao, J. (2020). Plastic optical fiber sensor for temperature-independent high-sensitivity detection of humidity. *Applied optics*, *59*(19), 5708-5713.

Zhou, K. W., Gu, C. X., Peng, Z. K., & Liu, B. N. (2018). Identification and determination of formaldehyde and sulfur dioxide based on cross sensitivity of cataluminescence. In Mechanics and Materials Science: *Proceedings of the 2016 International Conference on Mechanics and Materials Science (MMS2016)* (pp. 911-916).

Zhou, X., Li, X., Cheng, T., Li, S., & An, G. (2018). Graphene enhanced optical fiber SPR sensor for liquid concentration measurement. *Optical Fiber Technology*, *43*, 62-66.

Zhu, L., & Zeng, W. (2017). Room-temperature gas sensing of ZnO-based gas sensor: A review. *Sensors and Actuators A: Physical*, *267*, 242-261.

Zuo, X., Wang, L., He, J., Li, Z., & Yu, S. (2014). SEM-EDX studies of SiO2/PVDF membranes fouling in electrodialysis of polymer-flooding produced wastewater: Diatomite, APAM and crude oil. *Desalination*, *347*, 43-51.